The Characterization of ABL Tyrosine Kinase-Regulated Transcriptional Networks

by

Benjamin Jacob Mayro

Department of Pharmacology and Cancer Biology
Duke University

Date:_____

Approved:

_____
Ann Marie Pendergast, Supervisor

_____
Donald McDonnell

_____
Colleen Wu

_____
Xiao-Fan Wang

_____
Gerard Blobe

Thesis submitted in partial fulfillment of
the requirements for the degree of Doctor
of Philosophy in the Department of
Pharmacology & Cancer Biology in the Graduate School
of Duke University

2022

ABSTRACT

The Characterization of ABL Tyrosine Kinase-Regulated Transcriptional Networks
by

Benjamin Jacob Mayro

Department of Pharmacology & Cancer Biology
Duke University

Date:_____
Approved:

_____
Ann Marie Pendergast, Supervisor

_____
Donald McDonnell

_____
Colleen Wu

_____
Xiao-Fan Wang

_____
Gerard Blobe

An abstract of a thesis submitted in partial
fulfillment of the requirements for the degree
of Doctor of Philosophy in the Department of
Pharmacology & Cancer Biology in the Graduate School of
Duke University

2022

Copyright by
Benjamin Jacob Mayro
2022

Abstract

The ABL family of tyrosine kinases are multifaceted signaling molecules that link diverse extracellular stimuli to intracellular signaling pathways that control cell growth, survival, migration, and invasion during development and normal cellular homeostasis. In recent years, it has been established that multiple solid tumor types hijack ABL kinase signaling to support tumor progression and metastasis. The ABL kinases often potentiate these processes by inducing the stability and/or transactivation of transcriptional regulators. Using *in vivo* mouse models of solid tumor metastasis combined with mechanistic cell signaling and biochemistry, the studies presented herein uncovered multiple transcriptional networks modulated by the ABL kinases through the regulation of their key transcriptional regulators. First, we report on the discovery of an actionable signaling pathway utilized by brain metastatic tumor cells whereby the transcriptional regulator Heat Shock Factor 1 (HSF1) drives a transcriptional program, divergent from its canonical role as the master regulator of the heat shock response, leading to enhanced expression of a subset of E2F transcription factor family gene targets. We find that HSF1 is required for survival and outgrowth by metastatic lung cancer cells in the brain parenchyma. Further, we identify the ABL2 tyrosine kinase as an upstream regulator of HSF1 protein expression and show that the SRC-Homology 3 (SH3) domain of ABL2 directly interacts with HSF1 protein at a noncanonical, proline-

independent SH3 interaction motif. Importantly, knockdown as well as pharmacologic inhibition of ABL2 using allosteric inhibitors impairs expression of HSF1 protein and HSF1-E2F transcriptional gene targets.

We have recently identified that expression of the master transcriptional regulator of the cellular response of hypoxia, HIF-1α, as well as expression of the oncogenic transcription factor MYC are dependent on ABL kinase activity. The hypoxia inducible factor 1-α (HIF-1α) enables cells to adapt and respond to hypoxia, and the activity of this transcription factor is regulated by several oncogenic signals and cellular stressors. While the pathways controlling normoxic degradation of HIF-1α are well understood, the mechanisms supporting the sustained stabilization and activity of HIF-1α under hypoxia are less clear. We report that ABL kinase activity protects HIF-1α from proteasomal degradation during hypoxia. Using a FACS-based CRISPR/Cas9 screen we identified HIF-1α as a substrate of the Cleavage and Polyadenylation Specificity Factor-1 (CPSF1), an E3-ligase which targets HIF-1α for degradation whose activity is regulated by ABL kinases. Interestingly, MYC was also shown to be a substrate of CPSF1, and its expression was decreased upon ABL inhibition. These studies highlight the importance of the ABL kinases in the activation of oncogenic transcriptional networks driven by HSF1, HIF-1α, and MYC.

Dedication

To Sadie, Claire, & George

Contents

List of Tables

List of Figures

Acknowledgements

My graduate training has benefited from the opportunity to learn from and work with a myriad of spectacular scientists that covered the spectrum of career positions.

The individual to whom I owe my greatest gratitude is Dr. Ann Marie Pendergast. It was her passion for science that led me to choose Duke University for my graduate training. It was her generosity that led me to choose her as my mentor. Under her tutelage, I have matured as an experimentalist and critical thinker. I will continue to hold her as my scientific gold standard. I know that I will fondly reference her to my future trainees as she referenced her mentors to me.

My mentorship community extended to include the members of my thesis committee. I am grateful to Drs. Donald McDonnell, Colleen Wu, Xiao-Fan Wang, and Gerard Blobe. In addition to providing critical insights and advice on my research endeavors, these individuals have tirelessly advocated for me. Without their support, my successes would be decreased in both magnitude and quantity.

The Pendergast lab provided me with a haven of scientific colleagues that provided mentorship, friendship, and the opportunity to grow as a mentor. Drs. Jing Jin Gu, Aaditya Khatri, Courtney McKernan, and Jacob Hoj provided me with a supportive environment to anchor myself when I joined the Pendergast lab.

My gratitude towards Jacob Hoj nearly reaches that of Dr. Pendergast. When I joined the lab, Jacob provided daily mentorship and support. The scientific comradery

that subsequently emerged is the highlight of my graduate training. Our divergent technical skillset and scientific interests synergized into a collaboration that improved and hastened the progress of the multiple projects that we undertook. Jacob has set my standards for what a mentor, lab-mate, and friend should be, and I will continue to aspire to reach these.

Luckily after Jacob transition to his next career phase, Ashley Colemon, Michael Caminear and Hannah Scheaffer joined our group. Having the opportunity to mentor Michael and Hannah provided me an opportunity to grow as a mentor and gain two cherished friendships. I hope I provided them the support that Jacob provided to me.

I also owe gratitude towards Dr. Kris Wood. In spite of never filling an official mentorship role, I frequently found myself in his laboratory space interacting with his spectacular trainees. These includes Kevin Lin, Justine Rutter, Gray Anderson, Christian Cerda-Smith, Haley Hutchinson, Chris Bassil, Shane Killarney, Jude Raj, Caroline Bridgwater, and Ann Liu. Beyond the memorable conversations and scientific debate I shared with all-listed Wood Lab members, I owe additional gratitude towards Christian and Haley for their experimental assistance that was critical for the hypoxia project.

1. Introduction

1.1.1 Tyrosine kinases

There are estimated to be at least 566 protein kinases encoded in the human genome (1). These enzymes transfer a phosphate group from ATP onto serine, threonine, and tyrosine amino acids located in substrate proteins. Despite its importance in cell signaling and disease, the phosphotyrosine signal has the lowest relative abundance of the three canonical phosphorylation marks (~1-5% of total cellular phospho-amino acids) (2). Correspondingly, only 90 of the 566 protein kinases are tyrosine kinases (1). The 90 tyrosine kinases can be subdivided into two major classes: receptor tyrosine kinases (RTKs) and non-receptor tyrosine kinases (nRTKs) (2).

The more abundant RTK class contains 58 members that are grouped into 20 distinct families (3). Every RTK shares a conserved protein architecture consisting of four major features: 1) an extracellular domain commonly utilized to bind ligands, 2) a single transmembrane helix, 3) an intracellular kinase a domain, and 4) a carboxy (C)-terminal regulatory region (**Figure 1**) (4). RTKs can be activated through a variety of signals and protein-protein interactions, however the classical model described in 1988 by Schlessinger consists of ligand binding inducing RTK dimer formation and trans-phosphorylation (4, 5). This ligand-induced activation of RTKs allows for the transduction of extracellular signals to intracellular signaling pathways (3).

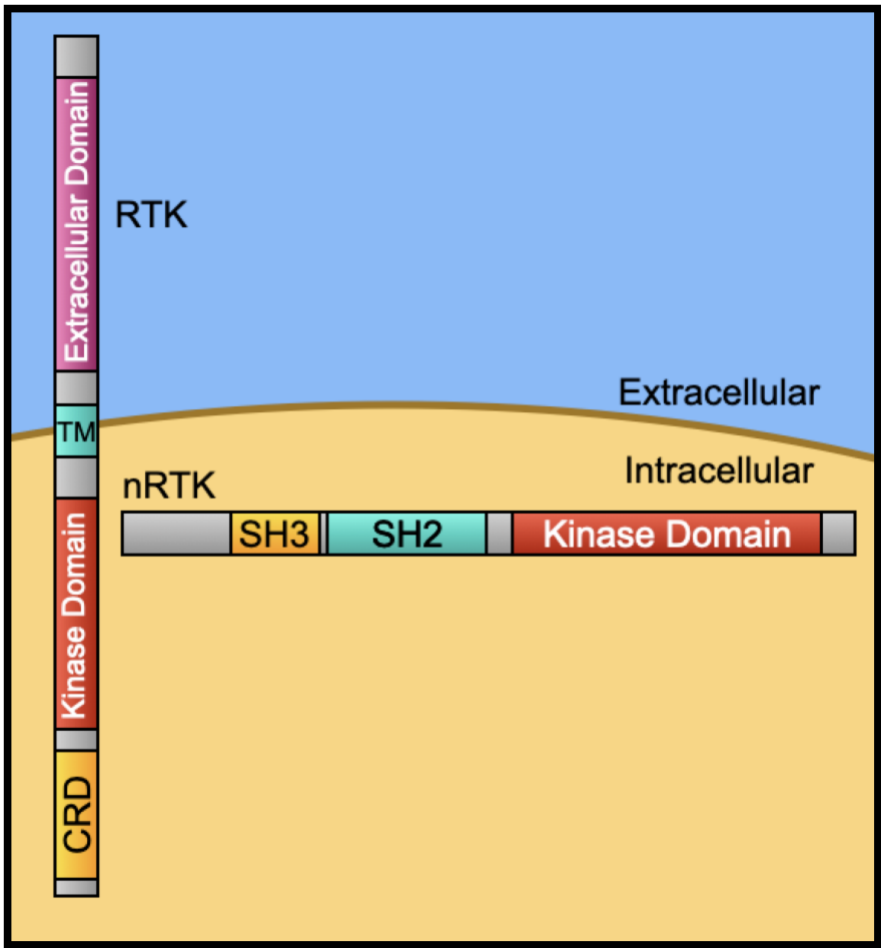

Figure 1: Schematic of general architectures of RTKs and nRTKs. The common architecture of receptor tyrosine kinases includes an extracellular domain, a transmembrane domain (TM), a kinase domain, and a c-terminal regulator domain (CRD). The common architecture of non-receptor tyrosine kinases (nRTKs) includes a SRC homology 3 (SH3) domain, a SRC homology 2 (SH2) domain, and a kinase domain.

The remaining 22 tyrosine kinases are non-receptor tyrosine kinases, which are grouped into 9 families (1). The first non-receptor tyrosine kinase discovered was SRC, with Collett and Erikson uncovering that the SRC gene encoded a protein with intrinsic kinase activity in 1978 (6). Two years later, Tony Hunter and Bart Sefton identified that SRC phosphorylated tyrosine amino acids and not threonine amino acids as was reported previously (6, 7).

SRC is a 60 kDA protein that consists of three major modular domains. The most amino- domain of SRC is the SH3 (SRC Homology 3) domain (**Figure 1**). SH3 domains have a barrel-shape structure formed from two small antiparallel β-sheets packed together (8). This domain binds polyproline rich motifs and was identified by Mayer in 1988 (9). The polyproline rich target sequence of the SH3 domains often forms left-handed polyproline type II helices (10). The middle domain of SRC is referred to as the SH2 (SRC Homology 2) domain (**Figure 1**). This domain is formed by a central antiparallel β-sheet flanked by two α- helices (11). SH2 domains were identified to interact with phosphotyrosine containing peptide sequences in 1986 (12). The biochemical mechanism of SH2 domain- phosphotyrosine binding is that the two α-helices divide the central β-sheet in half resulting in two pockets. One pocket contains a key positively charged arginine residue that electrostatically interacts with the negatively charged phosphotyrosine residue. The other pocket has a binding preference that varies with each SH2 domain (13). The most carboxy domain of SRC is the tyrosine kinase domain, which is also referred to as the SH1 (SRC Homology 1) domain (**Figure 1**). Interestingly, 19 of the 22 nRTKs share this SH3-SH2-SH1 domain architecture which is known as a SRC cassette or SRC module (**Figure 1**) (1, 14).

Unlike RTKs which are transmembrane proteins, nRTKs are intercellular kinases that transduce signals throughout the cytoplasm and organelles (15). The nRTKs modulate signal transduction by interacting with and phosphorylating specific protein

substrates at specific locations using modular domains such as the SH3 and SH2 domains (16). The divergent function and substrate specificity of the nRTKs is partially explained by differences in ligand preference within the SH3 and SH2 domains of the nRTK family members (14). While all SH2 domains bind a phosphotyrosine residue containing peptide, the amino acid sequence flanking the phosphotyrosine residue impacts binding affinity and the consensus target sequence varies for each SH2 domain (11, 17, 18). The SH3 domains tend to bind substrates containing PxxP motifs, where x can be any amino acid. The ligand specificities of the SH3 domains can be broadly divided into two major classes, where class 1 SH3 domains bind a (K/R)xxPxxP motif and class 2 SH3 domains bind a PxxPx(K/R) motif (10, 19). Additionally, some SH3 domains have specificities that diverge from the canonical class 1 and 2, such as the ABL1 SH3 domain. This domain has a consensus target sequence of PPx(F/W/Y)xPPP(A/G/I/LV) (19).

1.2.1 The Abelson family of non-receptor tyrosine kinases

The Abelson family of nonreceptor tyrosine kinases are a family of nRTKs consisting of two paralogues in vertebrate metazoans, ABL1 and ABL2. These kinases link diverse extracellular stimuli to intracellular signaling pathways that control cell growth, survival, migration, and invasion during development and normal cellular homeostasis (**Figure 2**) (20, 21). ABL1 was first discovered as the cellular homolog of the transforming factor co-opted by the Abelson murine lymphosarcoma virus (A-MuLV)

(22). The cellular *ABL1* (*c-ABL*) gene was later identified in 1986 as a component of the fusion oncoprotein BCR-ABL1, which drives distinct human leukemias (23). *ABL2* also known as ABL-related gene (*ARG*) was subsequently identified in 1990 using a sequence homolog search (24).

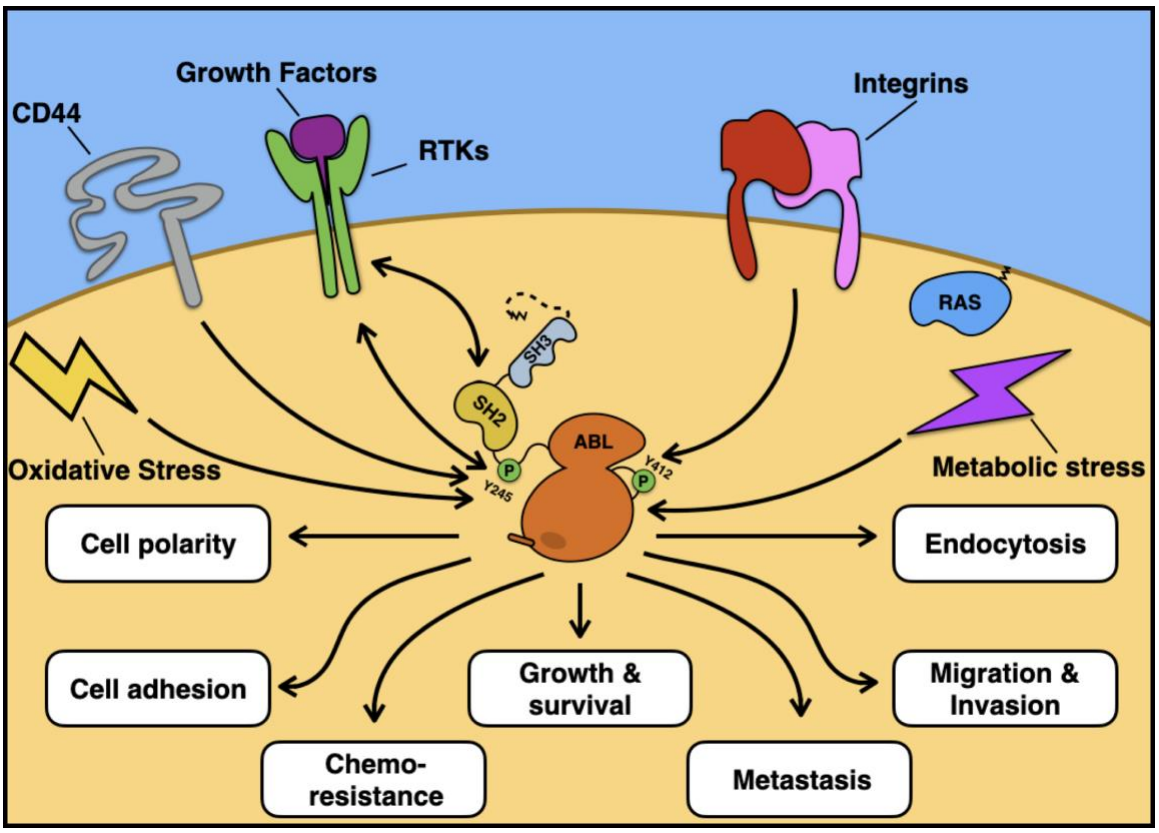

Figure 2: Signaling mechanisms and cellular responses mediated by ABL kinase pathway activation. The ABL kinases are activated by numerous extracellular and intracellular signaling pathways. ABL activation subsequently results in the propagation of a multitude of cellular responses.

1.2.2 Structure, autoinhibition, and activation of the ABL kinases

The ABL kinases contain a canonical SRC cassette followed by a multiple domain containing carboxy tail encoded by a single exon (**Figure 3**). The SH3-SH2-SH1 domains

of human ABL1 and ABL2 are more highly conserved (92%) to each other than the corresponding SRC cassette of any other nRTKs and their closest respective paralog or ortholog (25). This high sequence similarity coupled with conserved intron-exon boundaries suggest that vertebrate *ABL1* and *ABL2* resulted from a gene duplication of a progenitor *Abl* gene (25). The genomes of invertebrate metazoans, such as *Caenorhabditis elegans* and *Drosophila melanogaster*, encode a single *Abl* gene. The *ABL* SRC cassettes of vertebrate and invertebrate metazoans are highly conserved while conservation of the c-terminal tail is variable (25) (**Figure 3**).

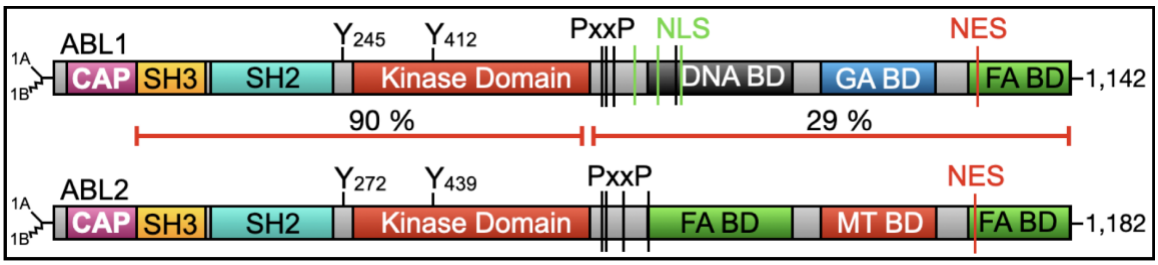

Figure 3: Linear schematic of ABL1 and ABL2 structures. The ABL kinases have a highly homologous n-terminal domain, and a divergent c- terminal domain. The ABL kinases have two main splice variants (1A and 1B), which result from two alternative start codons. ABL1 and ABL2 both contain a CAP domain, SRC homology 3 (SH) domain, SRC homology 2 (SH2) domain, kinase domain, filamentous (F) -actin binding domain (FA BD), nuclear export sequence (NES), and four PxxP SH3-binding motifs. ABL1 contains a DNA binding domain, globular actin binding domain (GA BD), and three nuclear localization sequences (NLS). ABL2 contains an additional F-actin binding domain and a microtubule binding domain (MT BD).

The structures of the ABL SH3, SH2, and SH1 domains have been solved and provided important insights into the ABL kinases and nRTKs in general. In 1992, the ABL SH2 domain was the first SH2 domain to be structurally characterized (11). Subsequently in 1994, the ABL1 SH3 domain was the first SH3 domain to be crystallized

bound to a substrate (8). Almost a decade later, a crystal structure of the ABL SRC cassette was solved providing insights into the previously elusive mechanism of ABL kinase autoinhibition (26, 27).

The activity of nRTKs is tightly regulated in cells. All nRTKs with a SRC cassette have been shown to possess an autoinhibited state that must be relieved to phosphorylate substrates (14). The kinases in the SRC and ABL nRTK families have been shown to adopt similar active and inactive confirmations (**Figure 4**) (14, 26, 28). The interaction between the SH3 domain and sequences in the SH2-SH1 linker plays a conserved role in stabilizing the inactive state of both SRC and ABL family kinases (26, 28).

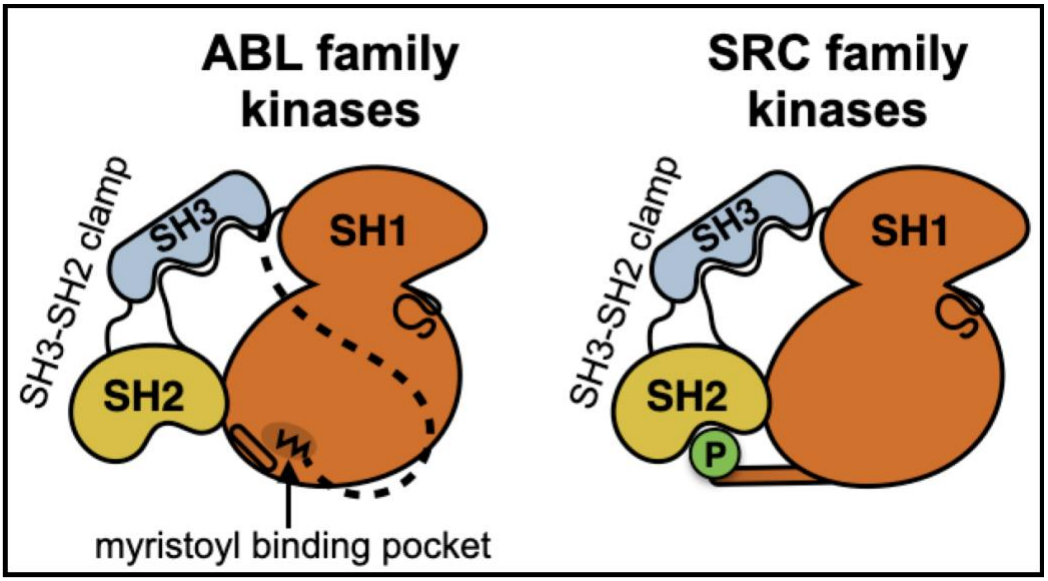

Figure 4: Structure of autoinhibited ABL and SRC family kinases. Schematic showing the similar autoinhibited structures of ABL and SRC family kinases. Notably, the autoinhibited structure of the ABL family of kinases utilizes the binding of a myristoylated glycine into the myristoyl binding pocket located in the c-terminal kinase

lobe. Divergently, the autoinhibited structure of the SRC family of kinases utilizes an intramolecular SH2-phosphotyrosine interaction.

Early domain analysis of ABL1 determined that deletion of the ABL1 SH3 domain was sufficient to activate the kinase (29). Further, mutations in the SH2-SH1 linker led to activation of ABL kinase activity (30). Structural analysis of the inactive ABL1 SRC cassette revealed that a section of the SH2-SH1 linker adopts a polyproline type II helix, which is bound by the SH3 domain (**Figure 4**). The unbound sequences of the SH2-SH1 linker are then clamped against the amino (N)-terminal lobe of the kinase domain. The SH3 domain-SH2-SH1-linker interaction holds ABL and SRC family kinases in an inactive confirmation (26, 28). The PxxP motif in the SH2-SH1 linker of ABL and SRC both differ from the canonical PxxP motif and from each other. SRC contains a PxxQ motif, while ABL contains a PxxY motif (26, 28). Phosphorylation on ABL tyrosine 245 (Y245) (all amino acid numbers correlate with the ABL1 1b isoform) in the inter-linker region was previously shown to be sufficient to elevate ABL1 kinase activity (31). The accepted model is that in the inactive state Y245 forms critical interactions with the N-terminal lobe of the kinase domain. Subsequent phosphorylation of this residue weakens the interaction, destabilizing the inactive state (26, 31).

In SRC family kinases, the SH3-SH2 clamp functions to inhibit the kinase domain, a model that is supported by 1) interaction of the SH3 domain with the SH2-SH1 linker as described above and 2) an intramolecular interaction between the SH2 domain with a phosphotyrosine residue located carboxy to the kinase domain (**Figure 4**)

(28). The interaction between the SRC SH2 domain with the tyrosine phosphorylated tail induces interaction between the SRC SH2 and the C-terminal kinase lobe (28). The ABL kinases lack a homologous carboxy tyrosine residue, and as a result, unlike SRC, inactivation mutations of the ABL SH2 domain are not sufficient to increase kinase activity (29, 32).

The divergent mechanism that the ABL kinases utilize to support the SH3-SH2 clamp was uncovered in 2003 when the inactive structure of the ABL1 SH3-SH2-SH1 domain was solved (**Figure 4**) (26, 27). The ABL SRC cassette is downstream of an 80 amino acid long N-terminal CAP region that contains two alternative start codons for the ABL kinases (**Figure 3**). As a result, the ABL kinases exist as two major splice variants that differ by 19 amino acids in length (1A- short isoform 61 amino acids long, 1B- long isoform 80 amino acids long) (25). In the 2003 structure, Nager et al. uncovered that glycine 2 in the 1B isoform is myristoylated. The myristoyl moiety binds in a hydrophobic pocket in the C-terminal-lobe of the kinase domain (**Figure 4**) that is exclusively found in the ABL kinases (26, 27). The insertion of the myristoyl moiety allosterically induces a 90 degree turn in the αI helix of the C-terminal kinase lobe. When the myristoyl moiety is unbound, the αI helix displaces the ABL1 SH2 domain from docking onto the kinase domain. Conversely, the allosterically induced bend of the αI helix allows for the SH2 domain to bind onto the ABL kinase domain covering a surface area double of what is found between the SRC SH2 and SRC kinase domain (26-28, 33).

Upon activation, the SH3-SH2-SH1 domains of the ABL kinases undergo a drastic conformational drift. The SH2 domain moves from contacting the C-terminal kinase lobe and instead docks onto the N-terminal kinase lobe in a "top hat" position (**Figure 5**) (34, 35). The docking of the SH2 domain onto the N-terminal kinase lobe induces an allosteric activation of the kinase domain (35).

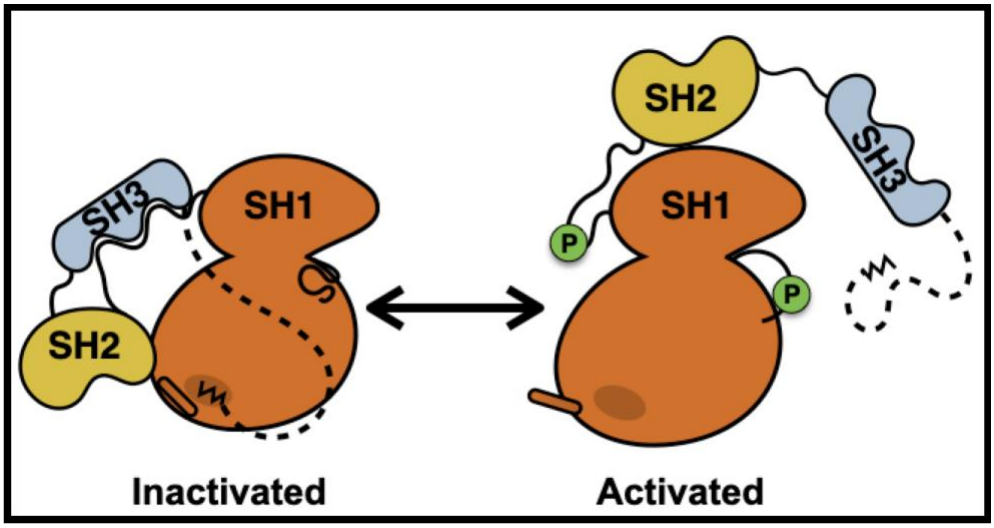

Figure 5: Structure of active and inactive ABL family kinases. The ABL kinases occupy inactive and active confirmations. The inactive confirmation possesses a SH3-SH2 clamp and the binding of the myristoylated glycine into the myristoyl binding pocket. In the active confirmation, the ABL kinases undergo a drastic conformation rearrangement with the SH2 domain adopting a "top hot" conformation.

The ABL kinases are known to processively phosphorylate multiple tyrosine residues in a single substrate and mutation of the SH2 domain impairs this ability (**Figure 6**) (36, 37). Additionally, multiple ABL1 substrates have ABL1 phosphorylation sites that are dependent on the phosphorylation of a previous site by ABL1 (38, 39). Further, the ABL1 kinase and SH2 domains share a consensus target sequence of YxxPP

(36, 40, 41). These data support the working model that the ABL kinase and SH2 domains allow for processive phosphorylation. Here, the SH2 domain often docks onto a tyrosine residue phosphorylated by the ABL kinase domain (**Figure 6**). This docking event lengthens the interaction between the ABL kinases and their substrate allowing for the successive phosphorylation events to occur even at tyrosine residues that poorly match the ABL consensus sequence.

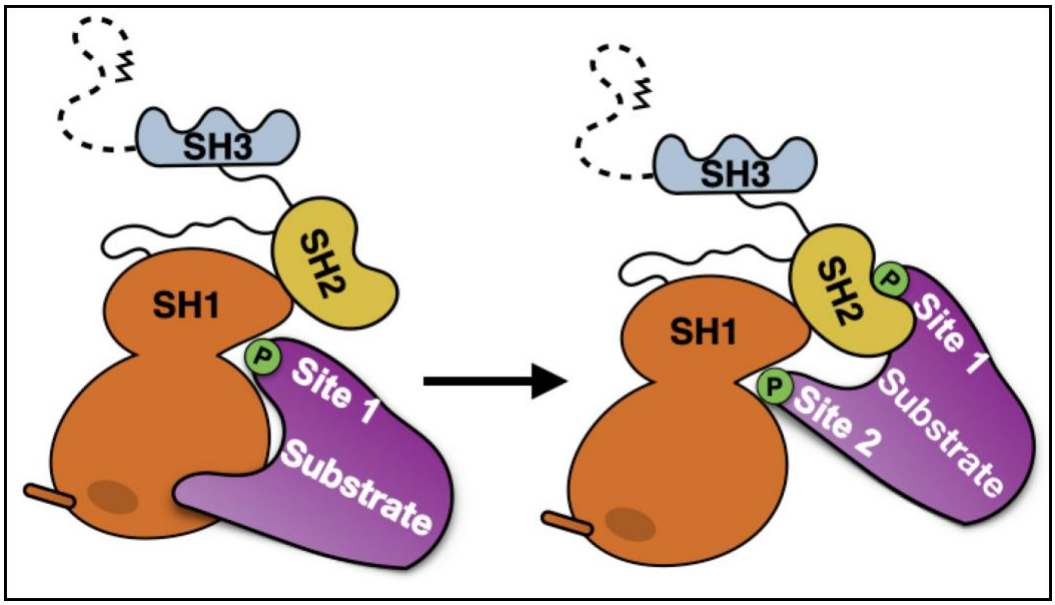

Figure 6: Schematic of the processivity model of ABL kinase phosphorylation. The ABL kinases often utilize processive phosphorylation, where multiple tyrosine residues are phosphorylated in a single substrate.

While the ABL SRC cassette is highly conserved between ABL1 and ABL2 (90%), the C-terminal tails are more divergent (29%) (**Figure 4**). This suggests that the ABL kinases evolved both overlapping and unique functions after gene duplication (25). Both ABL1 and ABL2 contain four PxxP SH3-domain binding motifs located carboxy to the

kinase domain that allow docking of SH3-domain containing proteins, such as CRKL and the ABL-interactor protein 1 (ABI1). Three of these are class 2 (PxxPx(K/R)) SH3 binding motifs found in both ABL1 and ABL2 (10, 25). The fourth PxxP in ABL1 is an additional class 2 motif, while ABL2 possesses a single class 1 ((K/R)xxPxxP) motif (10, 25). Further, both ABL kinases have a WW domain binding (PPxY) motif located within the kinase domain (42).

The C-terminal tail of the ABL kinases encodes multiple domains that mediate additional protein-protein interactions (**Figure 4**). Both ABL1 and ABL2 kinases have a filamentous (F) -actin binding domain (FA BD) located at the most carboxyl end of the kinase (25, 43). ABL2 has additional cytoskeletal binding domains not found in ABL1, namely, an additional F-actin binding domain and a microtubule binding domain (MT BD) (25, 43). ABL2 is predominantly a cytoplasmic protein, while ABL1 occupies both the cytoplasm and nucleus. In this regard, ABL1 has three lysine and arginine amino acids rich nuclear localization signals (NLS) (44, 45). Both ABL1 and ABL2 have a leucine, isoleucine, and valine rich nuclear export signal (NES) (44, 45).

1.2.3 Post-translational modifications of the ABL kinases

The ABL kinases undergo multiple post-translational modifications that impact function and activity. As described above the autoinhibited state of the ABL kinases relies on myristoylation at glycine 2 and dephosphorylation of Y245 in the SH2-SH1 linker region (26, 27, 31). Phosphorylation of Y245 has been shown to be mediated by

members of the SRC family of nRTKs and the platelet derived growth factor receptor (PDGFR) (31, 46-48). The major site of autophosphorylation is Y412 located on the activation loop of the kinase domain. Autophosphorylation of this residue is essential for the adoption of the active confirmation (31, 49). Mechanistically when the activation loop is unphosphorylated, it inserts in between the two kinase lobes. This blocks access of substrates to the SH1 active site and misorients critical residues on the C helix relative to the rest of the residues of the active site. However, upon phosphorylation of Y412, the activation loop no longer occupies the SH1 catalytic cleft, and the C helix reorients to allow for the proper coordination of the catalytic residues (26, 34, 50, 51).

The ABL kinases are also regulated by serine and threonine phosphorylation. ABL1 has been shown to be phosphorylated on T754, which creates a consensus binding site for 14-3-3 proteins (52, 53). The interaction between ABL1 and 14-3-3 proteins promotes the cytoplasmic retention of ABL1 (52). Multiple kinases, such as CLK1, CLK2, MST1, MST2, and TTK, can phosphorylate T754 on ABL1 (54). ABL1 can also become phosphorylated on S637 and S638 by PAK2. These residues are located downstream of the third PxxP motif in ABL1 and impacts interaction with SH3-domin containing interactors. Interestingly, phosphorylation of S637 and S638 reduces interaction with ABI1, but increases interaction with CRK (55).

The ABL kinases also have been shown to be post-translationally regulated on lysine residues. Acetylation of K730 located in the second ABL1 nuclear localization

signal motif by EP300 inhibits ABL1 nuclear translocation (56). ABL1 and ABL2 are both polyubiquitination on lysine residues and subsequently degraded by the proteasome. (57-59). While CBL has been identified as an ABL targeting-E3-ligase (58), the E3-ligase complex that polyubiquitinates and promotes the degradation of activated ABL1 has yet to be uncovered (59).

1.2.4 The ABL kinases as regulators of transcriptional networks

The ABL kinases are central signal transducers that tyrosine phosphorylate numerous, functionally diverse substrates involved in a wide range of cellular pathways and disease states (25, 60). The majority of the ABL substrates can be divided into two major categories 1) proteins involved in cytoskeleton dynamics and signaling, and 2) proteins that regulate transcription (25, 60). A review on the role of ABL kinases in cytoskeleton dynamics and regulation was recently published (61). The role of the ABL kinases as transcriptional regulators is complex and continues to be expanded.

An early discovered transcriptionally-involved substrate of ABL1 is RNA polymerase II (RNAPII) (62). ABL1 was shown to phosphorylates Y1 of the RNAPII C-terminal repeated domain (62). Phosphorylation of this tyrosine residue alongside neighboring threonine and serine residues regulates the recruitment of transcription co-regulators (63). Phosphorylation of Y1 was reported to impair the recruitment of termination factors to RNAPII (64).

The ABL kinases can function as positive and negative regulators of several transcription factors and transcriptional co-activators (20, 25, 60). Some of these interactions are highlighted below. The ABL kinases have been shown to regulate the activity and stability of p53 through direct and indirect mechanisms (65, 66). ABL1 binds to the C-terminal regulatory domain of p53 and promotes p53 DNA binding (65). This interaction with ABL1 stabilizes the p53 tetramer and promotes formation of the p53 tetramer-DNA complex. Interestingly, this function is independent of ABL kinase activity (65). The protein stability of p53 is negatively regulated by the E3-ligase MDM2 (67). ABL1 supports p53 accumulation basally and in response to DNA damage by directly phosphorylating MDM2 on Y394 (66). This phosphorylation event impairs MDM2 E3-ligase activity (66). The p53 paralogue p73 is also regulated by the ABL kinases. In response to DNA damage, ABL1 binds to the C-terminal regulatory domain of p73 in an SH3 domain dependent manner and subsequently phosphorylates p73 on Y99 leading to enhanced p73 transcriptional activity and activation of the apoptosis pathway (68).

ABL was reported to regulate the JUN transcription factor (69, 70). In response to macrophage colony-stimulating factor exposure, ABL1 phosphorylates JUN, which promotes JUN dimerization with FOS, which leads to the formation of the active AP-1 complex (69). ABL1 subsequently interacts with AP-1 in the promoter regions of target genes (69). In T-Cells, ABL1 phosphorylates JUN on Y170. This phosphorylation event

decreases the interaction between JUN and the E3-ligase ITCH (70), which results in decreased JUN ubiquitination and protein turnover (70).

The ABL kinases have been uncovered in several cell contexts to be regulators of the Hippo transcriptional co-activators YAP1 and TAZ. In response to DNA damage, ABL1 phosphorylates YAP1 on Y357 (71). This phosphorylation event increases YAP1 stability and promotes interaction with p73 (71). Phosphorylated YAP1 forms a complex with p73 that activates the cell death pathway (71). Phosphorylation of YAP1 on Y357 by ABL1 has also been linked to activation of YAP1 by oscillatory shear stress (72).

Notably, it was demonstrated that an ABL-regulated TAZ transcriptional network is essential for solid tumor metastasis, and that the ABL kinases stabilize TAZ to promote lung cancer metastasis to multiple organ sites (73). More recently, Wang et al. and Hoj et al. showed that the ABL kinases promote TAZ stabilization and gene transactivation to drive organ-tropic breast cancer metastasis to the bone and lung cancer metastasis to the brain (74, 75). Hoj et al. further demonstrate that ABL2 and TAZ engage in a feed forward signaling loop (75). ABL2 phosphorylates TAZ on Y321, which promotes TAZ nuclear accumulation (75). Nuclear TAZ then drives the expression of multiple target genes, including *ABL2* and other targets that promote brain metastasis (75).

1.2.5 ABL kinase fusions as drivers of leukemia

The most abundant and well characterized role of the ABL kinases in health and disease is as kinase partner of the fusion oncoprotein BCR-ABL1. While the first reference to chronic myelogenous leukemia (CML) in the literature occurred in 1845, it was not until 1960 that the signature chromosomal abnormality of CML was identified (76, 77) Nowell and colleagues observed that leukemic cells taken from their patients with CML always contained the same small abnormal chromosome, while none of their patients with other types of leukemia possessed this abnormal chromosome (77). The christened "Philadelphia chromosome" was identified in 1973 to result from a reciprocal translocation between chromosome 9 and 22 t(9;22)(q34;q11) (78). This truncated chromosome 22 arises as a result of a chromosomal translocation event that produces a fusion gene resulting from the *ABL1* gene on chromosome 9 being translocated onto the *BCR* gene on chromosome 22 at the breakpoint (23). The initial observation from Nowell et al. that nearly all CML patients have leukemic cells containing the Philadelphia chromosome was confirmed over the following decades with over 90 % of CML patients having the BCR-ABL1 fusion oncoprotein present on the Philadelphia chromosome (79). It was later identified that the BCR-ABL1 oncoprotein is the causative driver in 25 % of adult acute lymphoblastic leukemia (ALL), ~1 % of Acute Myeloid Leukemia (AML), and small fraction of myelomas (80-82). The second common ABL1 fusion oncoprotein is NUP214-ABL1, which is observed in 7% of patients with T-cell acute lymphoblastic

leukemia (T-ALL) (83). Rarer ABL fusion oncoproteins have also been identified in multiple leukemias, these include ETV6-ABL1, ETV6-ABL2, RCSD1-ABL1, and ZMIZ1-ABL1 (84-87).

1.2.6 The role of ABL kinases in solid tumors

In contrast to leukemia where the ABL kinases are activated through the generation of oncogenic chimera proteins, the ABL kinases become activated in solid tumors through a complex series of events (20, 21, 60). These events include point mutations, gene amplification, and kinase activation through oncogenic signaling networks. Somatic mutations in ABL1 occur in just 1.5 % of non-small cell lung cancer patients (NSCLC) (88). However, Ewelina et al. uncovered that NSCLC cell lines with somatic mutations in the ABL1 kinase domains are sensitive to ATP-competitive ABL inhibitors *in vivo (88)*. This work provides a proof of principle that even though somatic mutations in the ABL kinases are relatively rare in solid tumors, patients with cancers harboring these mutations may benefit from the use of an ABL kinase inhibitor. Even though somatic mutations in the ABL kinases are relatively rare, multiple solid tumors types demonstrate gene amplification and increased mRNA expression of *ABL1* and *ABL2* (89). Patient data from The Cancer Genome Atlas (TCGA) and other studies have demonstrated gene amplification or increased mRNA expression of *ABL1* and/or *ABL2* in patients with colon, breast, kidney, lung, pancreatic, and ovarian cancer (89-91).

In addition to somatic mutations and increased gene expression, the ABL kinases are often critical signal transducers downstream of oncogenic RTKs. The ABL kinases have been shown to be activated downstream and potentiate the effects of the epidermal growth factor receptor (EGFR), insulin-like growth factor 1 receptor (IGF1R), platelet-derived growth factor receptor (PDGFR), receptor tyrosine-protein kinase erbB-2 (HER2), and tyrosine-protein kinase receptor UFO (AXL) in multiple cancer types and models (46, 75, 92-96).

The ABL kinases have been shown to regulate growth and survival in multiple cell types and xenograft tumor models of melanoma, triple negative breast cancer, HER2 positive breast cancer, non-small cell lung cancer (NSCLC), gastric cancer, and liver cancer (20). In recent years, the ABL kinases have been shown to drive multiple transcriptional and translational programs critical for solid tumor metastasis. Gu et al. uncovered that both ABL-TAZ and ABL-β-catenin transcriptional programs are required for multi-organ metastasis by lung cancer cells, while Wang et al. and McKernan et al. uncovered ABL-regulated programs essential for organ-tropic metastasis of triple negative breast cancer to the bone (ABL-TAZ/STAT5) and HER2 mutated breast cancer to the brain (ABL-YB1) (73, 74, 92).

1.2.7 Pharmacological targeting of the ABL kinases

There has been a long history of success in the development of small molecule inhibitors of BCR-ABL1 and the ABL kinases (20, 97). Work in the 1990s led to the

develop of imatinib, which became the first FDA-approved small molecule targeted therapy in 2002 (98). The initial experiment that led to the development of imatinib was a chemical screen for protein kinase C inhibitors, which led the development of a lead compound was optimized with the potential for diverse chemical modifications (99). The lead compound was optimized and resulted in a compound selective for BCR-ABL1, ABL2, PDGFR, and KIT (99, 100). Subsequently, it was shown that imatinib also has high specificity for receptor tyrosine kinase DDR1 and the oxidoreductase NQO2 (101). Imatinib has been designated the founding member of the Type II kinase inhibitors. These inhibitors occupy a large hydrophobic pocket that is only present in the inactive kinase confirmation where the DFG-motif on the activation loop is in the out position, and sometimes these inhibitors extend into the ATP-binding pocket (102). These inhibitors can be, but are not always, ATP-competitive (102-105). Approximately 33% of patients with CML fail on imatinib due to 1) the evolution of increase drug efflux, 2) gene amplification/ over-expression of BCR-ABL1,or 3) point mutations in the BCR-ABL1 kinase domain (106, 107). The mechanism of resistance in ~20 % of patients with CML on imatinib is specifically the development of the T315I "gate-keeper mutation" (108). The mutation of T315 to I315 decreases the affinity of imatinib for BCR-ABL1 by 1) removing the hydroxyl oxygen on T315 that forms a hydrogen bond interaction imatinib, which is important for proper positioning of imatinib, 2) sterically blocking imatinib from accessing the hydrophobic pocket located behind I315 due to the large

isoleucine residue, and 3) stabilizing the active form of the kinase, which does not bind imatinib (109-111).

To address these resistance mechanisms, second generation ABL kinase inhibitors were developed. A second Type II inhibitor, nilotinib, was approved in 2007 (112). Nilotinib 1) has the same selective target profile as imatinib, 2) has higher affinity for BCR-ABL1, 3) is not a substrate for the transporter p-glycoprotein efflux pump, and 4) is effective against the majority of BCR-ABL1 point mutations that lead to imatinib resistance (97, 113). However, it is not effective against the T315I mutation for the same reasons as imatinib (97). Dasatinib is another second generation ABL kinase inhibitor that received FDA-approval in 2006 (114). Unlike imatinib and nilotinib, dasatinib is a Type I inhibitor that was designed to target both ABL and SRC. This class of inhibitors bind the active form of kinase where the DFG-motif on the activation loop is in the in-position. Type I inhibitors occupy the ATP-binding pocket and, therefore, are ATP-competitive (102, 104). In spite of this, dasatinib is still ineffective against BCR-ABL1 T315I (101). Patients on dasatinib experienced a quicker and more durable response compared to patients on imatinib (115). Dasatinib has been shown to have high affinity for a much larger number of targets than imatinib or nilotinib, binding over 70 kinases at pharmacologically relevant concentrations (101). This characteristic of dasatinib may contribute to the elevated toxicities observed compared to imatinib and nilotinib (101). Ponatinib is a third generation ABL and SRC kinases inhibitor that specifically was

designed to target BCR-ABL T315I. Structurally, ponatinib adopts a similar confirmation as nilotinib in the ABL kinase domain with slight alterations avoiding any steric interference with I315 (116). Patients with CML that have develop resistance to another ABL inhibitor experience an initial complete response to ponatinib (117). However, ponatinib treatment is associated with toxicity, likely due to its ability to target multiple kinases other than BCR-ABL including VEGFR, FGFR, RET, and SRC family kinases(20).

To find novel small molecule inhibitors of BCR-ABL1, Nathanael Gray's group performed a chemical screen looking for compounds with the ability to decrease the proliferation of a BCR-ABL1 driven cell line (118). The screen yielded an initial lead compound that was further optimized to have potent and selective inhibitory properties exclusively in BCR-ABL1 driven cell lines (118). Mutagenesis assays and structural work demonstrated that this compound, unlike other ABL kinase inhibitors, bound the myristate binding site (119). This compound, named GNF-2, inhibited BCR-ABL1 allosterically through a similar mechanism as the binding of the myristoylated glycine of the ABL 1B isoform described above (119). The pharmacokinetics of GNF-2 was improved in GNF-5, but neither of these compounds were clinically successful (120). GNF-2 and GNF-5 are the founding members of the Specifically Targeting the ABL Myristoyl Pocket (STAMP) inhibitors. Because of the potential benefits of generating an ABL inhibitor that is selective to a pocket unique to the ABL kinases, other groups attempted to generate STAMP inhibitors with improved inhibitory properties and

pharmacokinetics (121). Furet's team at Novartis undertook a chemical screen using an NMR based approach (121). Aiming to find compounds that only bound the myristate binding pocket, they utilized an ABL1 kinase domain prebound to imatinib (121). Their initial hits were verified to bind the ABL myristate binding pocket, but did not effectively inhibit ABL kinase activity in cellular assays (121). Crystallization of their initial hits on a ABL1:imatinib complex revealed that even though the drugs bound the myristate binding pocket, they sterically clashed with the αI helix preventing the allosterically induced reorientation from occurring (121). Additional rounds of structural optimization and utilizing known information about the GNF-2:ABL1 interaction resulted in the development of the STAMP inhibitor ABL001 (Asciminib) (121). Importantly, ABL001 had activity against all Type I and Type II ABL inhibitor resistant mutants, including T315I (121). Resistance mechanisms of ABL001 that have emerged center on point mutations in the myristate binding pocket that impact hydrogen bonding with or sterically clashes with ABL001 (122). In 2021, the FDA approved ABL001 as a monotherapy for patients with CML that have been previously treated with two other ABL inhibitors and have the T315I mutation (123). Another exciting potential treatment modality of ABL001 is the co-administration of ABL001 alongside a classical Type I or Type II ABL kinase inhibitor as they occupy distinctive pockets in the ABL kinase domain. This combination with ABL001 was shown to 1) avoid the development of resistance clones when co-administered with nilotinib *in vitro* and *in vivo* and 2) to

restore sensitivity to ponatinib *in vitro* and *in vivo* (122, 124). Multiple clinical trials are currently undergoing assessing the combination of ABL001 with nilotinib, imatinib, and dasatinib in patients with CML.

2. The ABL2 kinase regulates an HSF1-dependent transcriptional program required for lung adenocarcinoma brain metastasis

Material from this chapter was originally published in *PNAS*, 2020;117 (52) 33486-33495doi/10.1073/pnas.2007991117. This was published as a co-first author manuscript alongside Dr. Jacob Hoj.

2.1 Introduction

Brain metastases stemming from primary tumors of the lung are a major health challenge for patients and often result in devastating neurologic impairments and increased mortality (125-127). Despite numerous studies focused on dissecting genetic and non-genetic molecular mechanisms employed by metastatic tumor cells to survive and colonize the unique microenvironment of the brain (128-132), there is a lack of effective therapies to treat this disease (133). Therefore, there is an urgent need to gain additional insights into the mechanisms employed by metastasizing tumor cells for colonization and survival in the brain, which might lead to new rational approaches for pharmacologic intervention.

The transcriptional activator Heat Shock Transcription Factor 1 (HSF1) is a master regulator of protein homeostasis (134, 135). Under normal physiologic conditions, HSF1 monomers are held inactive in the cytoplasm through intramolecular interactions and a regulatory complex consisting of protein chaperones and the chaperonin TCP1 ring complex (TRiC) (136-138). In response to a diverse array of

proteotoxic stresses including heat shock, monomeric HSF1 sheds its inhibitory regulatory complex, translocates to the nucleus, and oligomerizes into transcriptionally active HSF1 trimers (134, 139-141). Active HSF1 then induces transcription of genes encoding molecular chaperones by binding to DNA motifs known as heat shock elements (HSEs) (**Figure 7**) (140).

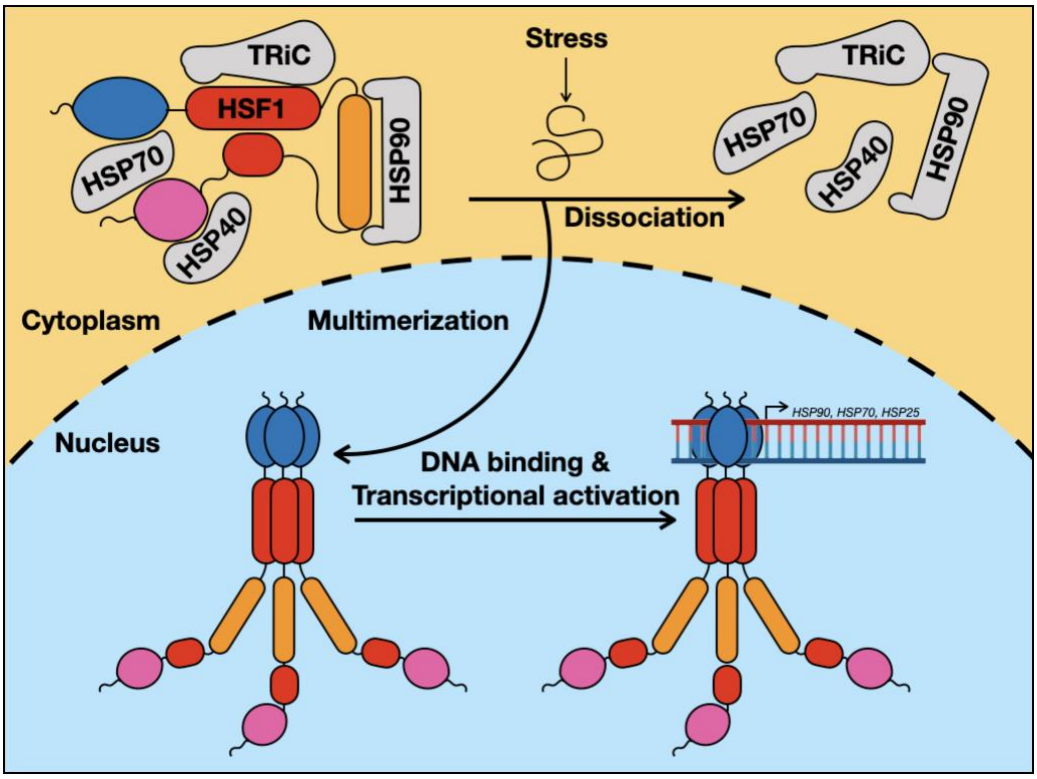

Figure 7: Schematic of the mechanism of HSF1 activation.

Although the role of HSF1 in the context of protein homeostasis is well established, an emerging body of evidence in recent years has shown that HSF1 also functions to drive transcriptional programs implicated in tumor progression and malignancy independent of the canonical heat shock response (142-149). Previous work

identified a divergent cancer-specific transcriptional program driven by HSF1 in highly malignant mammary epithelial cells and tumor cell lines from the lung, breast, and colon (142). Central to this work was the discovery that genome occupancy of HSF1 in the context of tumor malignancy is distinct from that of heat shock and drives expression of target genes implicated in cell cycle, translation and DNA repair. More recently, HSF1 expression was also identified in T-cell acute lymphoblastic leukemia as critical for tumor cell survival by regulating NOTCH1 transcriptional activity (143). Although these studies provide evidence in support of heat shock-independent functions of HSF1, little is known regarding the upstream modulators of HSF1 protein expression as well as the role of HSF1-driven transcriptional programs in the context of tumor metastasis.

In *C. elegans,* HSF1 was recently shown to function with E2F transcription factors to drive a transcriptional program required during larval stages of development, independent of its role in the cellular response to heat shock and proteotoxic stress (**Figure 8**) (150). In this context, HSF1 binds DNA at "degenerate" heat shock elements adjacent to GC-rich E2F binding domains (**Figure 8**). We now show that HSF1 protein levels are upregulated in brain-metastatic lung cancer cells, and that HSF1 regulates expression of E2F gene targets in this setting. Genetic inhibition of HSF1 ablates E2F target gene expression and dramatically impairs survival of lung cancer brain metastases both *in vitro* and in mouse models.

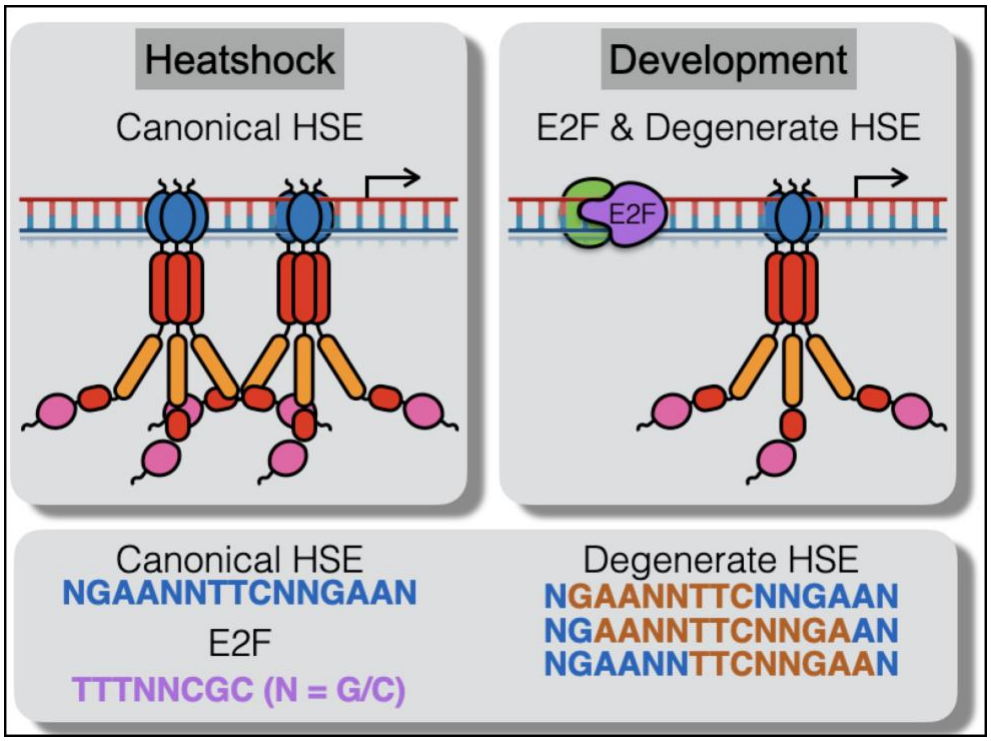

Figure 8: Schematic of HSF1 DNA-binding elements in heatshock and development.

Because therapeutic targeting of transcription factors such as HSF1 and E2F is challenging, we sought to identify actionable upstream regulators of this HSF1-E2F transcription network. We recently characterized a TAZ-AXL-ABL2 feed-forward signaling axis that is activated in brain-metastatic lung cancer cell lines and which is required for successful colonization of these cells in the brain (75). We now show that ABL2 modulates expression of the HSF1 and E2F transcription factors, and that knockdown or allosteric inhibition of ABL2 impairs expression of HSF1- and E2F-dependent transcription programs. We report that HSF1 protein is upregulated in brain-metastatic cancer cells downstream of the ABL2 tyrosine kinase and is required for their

survival both *in vitro* and *in vivo*. Importantly, we show that HSF1-E2F target gene expression is pharmacologically targetable with ABL kinase allosteric inhibitors (75). These data support a critical role for an actionable ABL2-HSF1-E2F pathway in promoting brain metastasis.

2.2 Results

2.2.1 Expression of HSF1 is upregulated in brain-metastatic lung adenocarcinoma cells

HSF1 expression was previously shown to be upregulated during progression of normal epithelial cells towards a malignant, tumorigenic state (142). Thus, we questioned whether HSF1 might be differentially expressed in brain-metastatic cells compared to the parental tumor cell lines from which they were derived. Immunoblot analysis of HSF1 protein expression in EGFR mutant (PC9 and HCC4006) and KRAS mutant (H2030) human lung adenocarcinoma cells compared to their respective brain-metastatic variants PC9-BrM3, HCC4006-BrM and H2030-BrM3, revealed elevated levels of HSF1 protein in the brain-metastatic derivatives **(Figure 9A**). Further, immunofluorescence staining of PC9-BrM3 cells revealed high levels of HSF1 in the nucleus, indicative of transcriptionally active HSF1 (**Figure 9B**).

HSF1 was previously shown to be essential for T cell acute lymphoblastic leukemia cell survival (143). Therefore, we sought to investigate whether the elevated expression of HSF1 in brain-metastatic cells was required for their survival and growth. To examine this possibility, we transduced cells with doxycycline (dox)-inducible

lentiviral shRNAs against either non-targeting control (shNTC) or HSF1 and measured cell viability across multiple time points after induction of shRNA expression. Immunofluorescence and immunoblot analysis demonstrated the effectiveness of HSF1 knockdown (**Figures 9B-C**). Knockdown of HSF1 with multiple shRNAs resulted in a robust decrease in cell viability starting 48 hours post-shRNA induction which correlated with the loss of HSF1 protein (**Figure 9E-J**). This loss corresponded with an increase in G2/M cell cycle arrest as revealed by FACS analysis (**Figure 9D**) and decreases in Cyclin B1 protein expression (**Figure 9C**). Knockdown of HSF1 also resulted in increased levels of cleaved PARP, indicative of apoptotic induction **(Figure 9C**). Parental lung cancer cells exhibited decreased survival upon HSF1 knockdown, but to a lesser extent than the brain-metastatic variants (**Figures 9E-J**). These data show that brain-metastatic lung cancer cells are highly dependent on HSF1 for growth and survival.

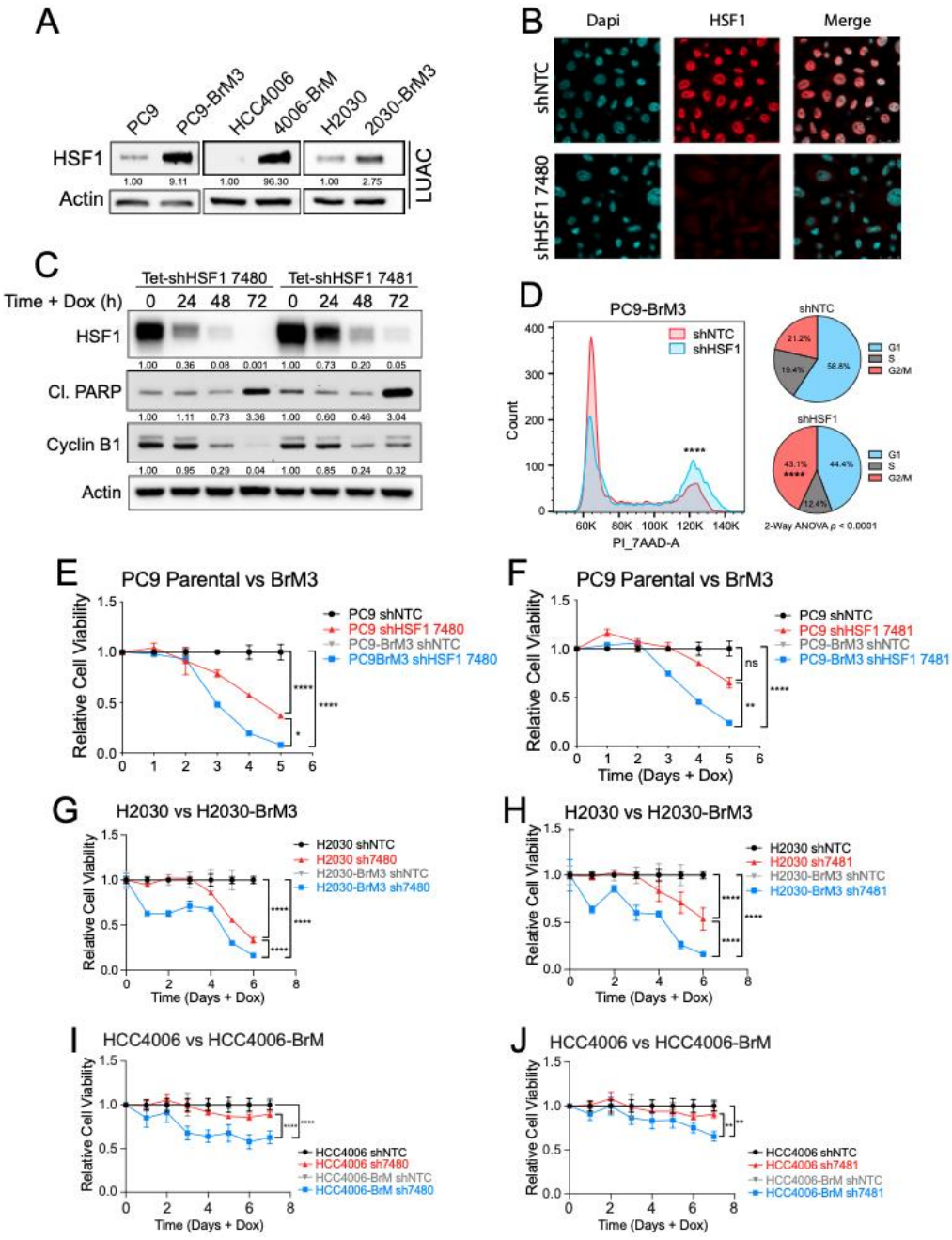

Figure 9: HSF1 protein is upregulated in brain-metastatic lung adenocarcinoma cells and is required for cell survival *in vitro*. A) Immunoblot analysis of HSF1 protein expression in parental vs brain-metastatic lung adenocarcinoma (LUAC) cell lines. Protein quantification data for brain-metastatic lines were normalized to actin loading control and corresponding parental cell line expression. B) Immunofluorescence staining and imaging of HSF1 protein (red) in PC9-BrM3 cells transduced with dox-inducible

lentiviral shRNAs against non-target control (shNTC) or HSF1 (shHSF1 7480). Dapi = nuclear stain (blue). C) Immunoblot analysis of HSF1 protein expression in PC9-BrM3 cells transduced with distinct dox-inducible shRNA clones targeting HSF1 (7480 or 7481) and treated +/- 500 ng/mL doxycycline for the indicated timepoints (h). Protein quantification data were normalized to actin loading control and to corresponding 0 h (untreated) timepoint. D) A) FACS analysis of propidium iodide staining in fixed PC9-BrM3 cells transduced with inducible shNTC or shHSF1 treated with 500 ng/mL doxycycline for 48 h. Pie chart percentages for each cell cycle phase (G1, S, G2/M) are provided as the average of 3 biological replicates per condition, and statistical analysis performed using 2-way ANOVA followed by Tukey's multiple comparison posthoc testing. **** p-value < 0.0001. E-J) Cell-Titer Glo assay measuring cell viability of indicated parental vs brain metastatic cells transduced with shRNAs against non-target control or HSF1 clone 7480 or clone 7481 and treated with doxycycline for the indicated timepoints. For all experiments, n=3 biological replicates per condition. Statistical analysis performed by two-way ANOVA followed by Fisher's multiple comparison post-hoc testing. * p-value < 0.05, ** p-value < 0.01, **** p-value < 0.001, ns = not significant. *Acknowledgment: Experiments from Figures 9B, 9G, and 9H were performed by Dr. Jacob Hoj.*

2.2.2 HSF1 knockdown impairs metastatic outgrowth and tumor cell survival *in vivo*

Given that loss of HSF1 robustly impairs survival of brain-metastatic lung cancer cells *in vitro*, we next evaluated whether HSF1 expression might be required during metastatic colonization and outgrowth of lung cancer cells in an *in vivo* model of brain metastasis. To examine this hypothesis, we performed intracardiac injections of PC9-BrM3 cells transduced with dox-inducible tet-shNTC or tet-shHSF1 shRNAs and co-expressing a luciferase-Tomato (pFuLT) lentiviral reporter. Mice were injected with brain metastatic PC9-BrM3 cells in the left cardiac ventricle and after assessing colonization of the brain at day 10 post-injection with bioluminescent imaging (BLI), mice were administered 3 mg/mL doxycycline water to induce shRNA expression. The 10-day time point was selected as previous studies have shown that metastasizing tumor

cells in circulation complete extravasation into the brain parenchyma within 7 days post-injection (131, 151). We found that the growth rate of metastases in mice injected with PC9-BrM3 cells expressing shRNA against HSF1 was markedly impaired compared to mice injected with non-target shRNA control cells (**Figure 10A**). Metastatic disease burden within the brain was significantly decreased in the HSF1 knockdown group as measured one month after induction with dox water (**Figure 10B**). The rate of whole-body metastatic burden was similarly delayed in the HSF1 knockdown cells (**Figures 10 C-D**). Together, these results show that HSF1 is necessary for the colonization and outgrowth of metastatic tumor cells in an *in vivo* model of lung cancer brain metastasis. Notably, analysis of human lung adenocarcinoma patient microarray datasets correlating mRNA expression with patient survival showed that high expression of *HSF1* correlates with poor overall survival (**Figure 10E**).

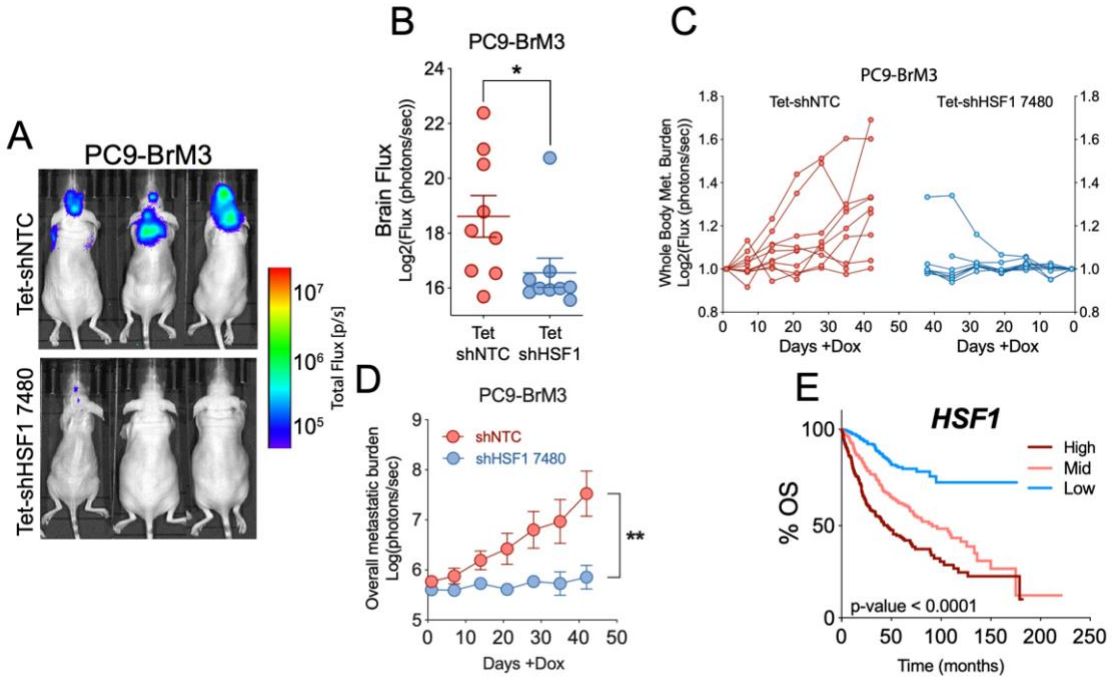

Figure 10: HSF1 knockdown impairs metastatic outgrowth and tumor cell survival *in vivo*. A) Representative bioluminescent images (BLI) and B) quantification of brain metastasis burden in mice injected with PC9-BrM3 cells transduced with dox-inducible shRNAs against non-target control (NTC) or HSF1 (clone 7480). Mice were treated with 3 mg/mL dox water for shRNA induction starting on day 10 post-intracardiac injection. After 28 days on dox water, mice were subjected to BLI analysis. Statistical analysis performed by unpaired two-tailed t-test. * p-value < 0.05. H-I) Individual spider plots (H) and quantification (I) of whole-body metastatic burden in mice as described in Figures 1F-G. Statistical analysis was performed using a mixed-effects model in GraphPad Prism 8 software to account for missing values due to premature animal death. ** p-value < 0.01. J) Kaplan-Meier survival analysis correlating overall survival with mRNA expression of *HSF1* in human lung adenocarcinoma patients. Survival groups were separated by tertile based on mRNA expression (n = 720 total patients), and statistical analysis was performed using Log-Rank Mantel Cox test. *Acknowledgment: Experiments from Figure 10 were performed by Dr. Jacob Hoj.*

2.2.3 HSF1 regulates transcriptional expression of E2F gene targets in brain-metastatic lung cancer cells in a heat shock-independent manner.

To investigate the mechanism by which HSF1 promotes survival of metastatic lung cancer cells, we employed unbiased transcriptional profiling of these cells with or without HSF1 knockdown in order to gain insights into the transcriptional target gene signatures altered by loss of HSF1. We performed RNA-sequencing (RNA-seq) on PC9-BrM3 cells transduced with dox-inducible non-target control shRNA or shHSF1 constructs and treated with doxycycline for 48 hours, a time point at which HSF1 protein is depleted but prior to loss in cell viability observed at longer time points (**Figures 9C-D**). Gene set enrichment analysis (GSEA) was used on an expanded list of gene signatures from the mSigDB database from The Broad Institute to identify pathways affected by HSF1 loss (152). The signatures most depleted upon HSF1 knockdown corresponded to E2F family gene targets and G2/M cell cycle checkpoint targets, consistent with the observed increase in G2/M cell cycle arrest (**Figure 9D, Figures 11A-E**), and loss of Cyclin B1 expression upon HSF1 knockdown (**Figure 9C**). Interestingly, signatures related to the unfolded protein response, while slightly depleted under knockdown conditions, scored relatively poorly despite the known role for HSF1 in this process (**Figure 11A**). Similarly, expression of gene targets representative of a canonical heat shock response remained relatively stable despite HSF1 depletion in these cells (**Figure 11F**). A list of conserved E2F target genes from a number of E2F gene signatures

identified by GSEA, which we confirmed by RT-qPCR to be regulated by E2F family members, was used to generate an HSF1-dependent E2F gene panel (**Figures 11F-H**).

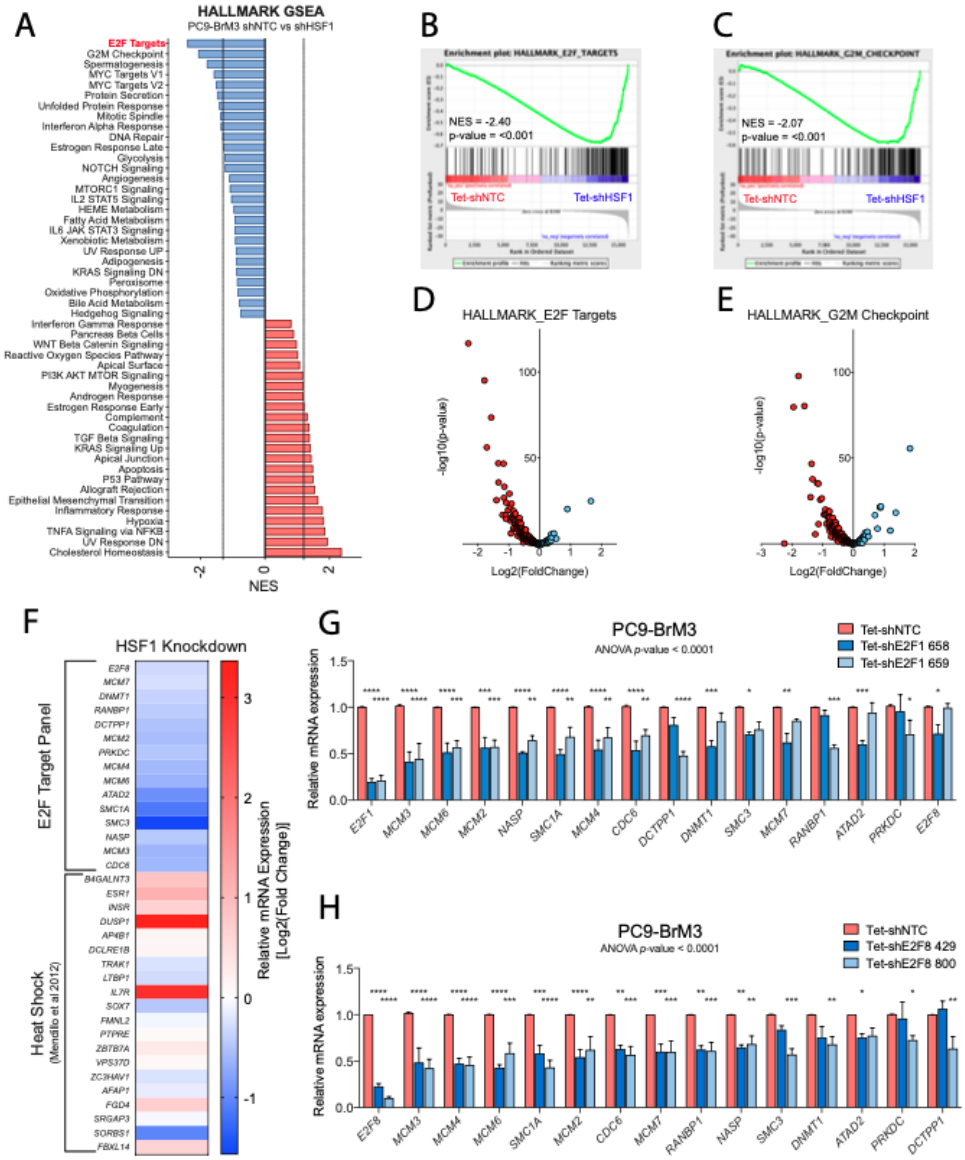

Figure 11: HSF1 regulates transcriptional expression of E2F gene targets in brain-metastatic lung cancer cells in a heat shock-independent manner. A) Waterfall plot of Hallmark GSEA signatures from RNA-seq data ranked by normalized

enrichment score (NES) for PC9-BrM3 cells with inducible expression of shNTC or shHSF1. Negative NES = depleted signature, positive NES = enriched signature. Dotted line represents p-value cutoff < 0.05. B-C) GSEA plots showing B) E2F targets or C) G2M checkpoint signatures depleted in PC9-BrM3 Tet-shHSF1 knockdown cells. D-E) Volcano plots showing relative depletion vs enrichment of target genes within the hallmark E2F Targets (D) or G2M Checkpoint (E) gene sets. F) Heatmap depicting relative expression of the E2F target gene panel and representative heat shock gene panel. G-H) RT-PCR analysis of E2F target gene expression in PC9-BrM3 cells transduced with inducible shRNAs against non-target control (shNTC), and two independent shRNAs against either E2F1 (shE2F1) (G) or E2F8 (shE2F8) (H). Cells were treated with 500 ng/mL doxycycline for 72 h. n = 3 biological replicates. Statistical analysis performed by ANOVA followed by Tukey's multiple comparison posthoc testing. * p-value < 0.05, ** p-value < 0.01, *** p-value < 0.001, **** p-value < 0.0001, ns = not significant. *Acknowledgment: Experiments from Figure 11A, 11B, 11C, and 11D were performed by Dr. Jacob Hoj.*

We next reasoned that if HSF1 promoted transcription of a subset of E2F target genes, then expression of these target genes might also be increased in brain-metastatic cells expressing high HSF1 levels relative to parental cells. RNA-sequencing analysis and GSEA comparing PC9-BrM3 cells with PC9 parental cells revealed enrichment for E2F target gene expression as well as G2M checkpoint targets in the PC9-BrM3 cells (**Figures 12A-C**). RT-qPCR analysis was used to validate increased expression of the HSF1-E2F gene panel in PC9-BrM3 and HCC4006-BrM cells relative to parental PC9 and HCC4006 cells, respectively (**Figures 12D-E**). Notably, RT-qPCR analysis also revealed that E2F family members themselves were differentially expressed in brain-metastatic cells with increased expression of *E2F1*, *E2F2*, *E2F7* and *E2F8*, whereas expression of other E2F family members remained unchanged (**Figure 12F**). Further, immunoblot analysis of brain-metastatic cells revealed enrichment of E2F1 and E2F8 relative to the

varied expression of other E2F family members, implying a potential role for E2F1 and E2F8 in regulating expression of E2F target genes in this system (**Figure 12G**). Of note, analysis of human lung adenocarcinoma patient microarray data revealed that high expression of *E2F1* and *E2F8* was each individually correlated with poor overall survival (**Figures 12 H-I**). Taken together, these data show that loss of HSF1 in brain-metastatic lung cancer cells results in decreased expression of select E2F target genes with minimal impact on expression of canonical heat shock gene targets.

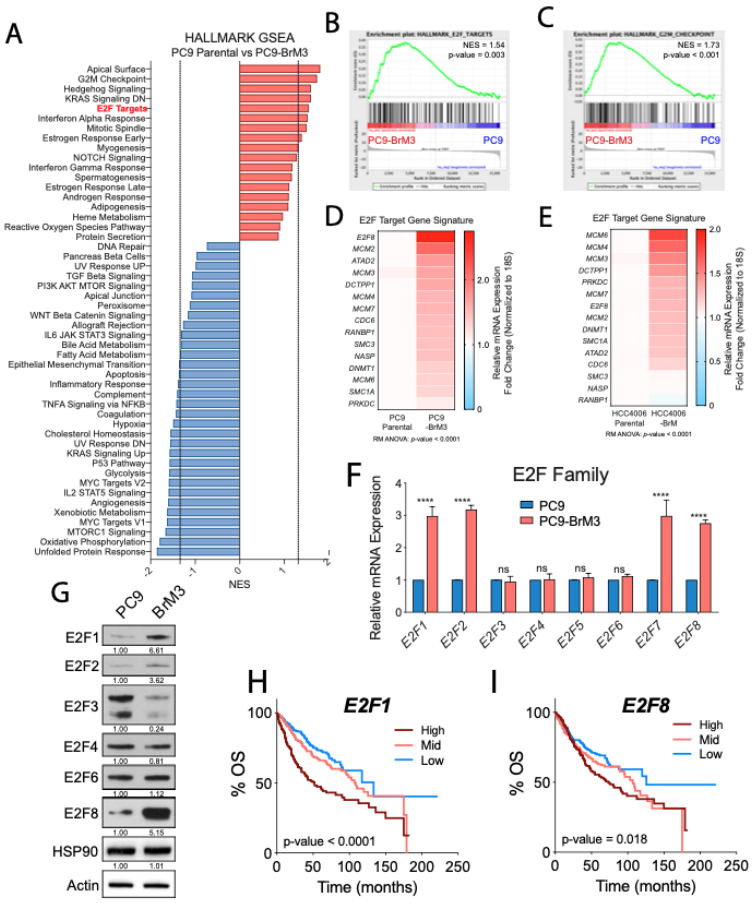

Figure 12: Brain-metastatic lung cancer cells exhibit increased expression of E2F target gene signatures. A) Waterfall plot of Hallmark GSEA signatures from RNA-

seq data ranked by normalized enrichment score (NES) for PC9 parental vs PC9-BrM3 cells. Negative NES = depleted signature, positive NES = enriched signature. Dotted line represents p-value cutoff < 0.05. B-C) GSEA plots showing E2F Target (B) and G2M Checkpoint (C) enrichment signatures in PC9-BrM3 compared to PC9 parental cells. D-E) Heatmaps of mRNA expression (RT-qPCR) for E2F target genes in D) PC9 parental vs PC9-BrM3 cells or E) HCC4006 parental vs HCC4006-BrM cells. F) RT-qPCR analysis of mRNA expression of E2F family genes in PC9 parental vs PC9-BrM3 cells. n=3 biological replicates. n=3 biological replicates. Statistical analysis of RT-qPCR data performed using two-way ANOVA followed by Fisher's multiple comparison post-hoc testing. G) Immunoblot analysis of the indicated proteins expressed in PC9 parental vs PC9-BrM3 cells. Quantification of protein expression was normalized to actin loading control and parental expression. H-I) Kaplan-Meier survival analysis correlating overall survival with mRNA expression for E2F1 or E2F8 in human lung adenocarcinoma patients. Survival groups were separated into tertiles based on mRNA expression (n = 720 total patients), and statistical analysis was performed using Log-Rank Mantel Cox test. For all experiments, * p-value < 0.05, ** p-value < 0.01, *** p-value < 0.005, **** p-value < 0.001, ns = not significant. *Acknowledgment: Experiments from Figure 12A, 12B, 12C, 12D, 12H, and 12I were performed by Dr. Jacob Hoj.*

HSF1 was recently shown to function with E2F transcription factors in *C. elegans* to drive a developmental transcriptional program divergent from the canonical heat shock response (150). Central to this work was the observation that in the context of development, HSF1 occupies genomic loci containing a "degenerate" or partial HSE nearby E2F DNA binding motifs. The canonical DNA element recognized by trimeric HSF1 in response to heat shock consists of triple tandem inverted *nGAAn* repeats (e.g., *nTTCnnGAAnnTTCn* or derivations thereof) (135). E2F family members bind DNA sequences at GC-rich motifs consisting of *TTTnnCGC* (where "*n*" is either C or G) (**Figure 13A**) (153). Given that loss of HSF1 impairs mRNA expression of E2F family target genes in brain metastatic cells, we hypothesized direct HSF1 binding may occur at degenerate HSEs located near promoter regions of known E2F transcriptional targets. To

investigate this possibility, we analyzed the promoter regions of various E2F targets from the E2F target gene panel and found *TTTnnCGC* motifs upstream of their respective transcriptional start sites (**Figures 13 B-D**). We then searched for partial permutations of the canonical HSE sequence containing varying segments of this DNA motif (**Figure 13A**). We detected a significant number of predicted degenerate HSEs which were primarily found immediately downstream of the E2F binding motif and upstream of the transcriptional start site, consistent with the report of E2F-HSF1 co-regulated DNA binding in *C. elegans* (**Figures 13 B-D**). In contrast, analysis of the promoter regions of *HSP90AB1* and *HSPA6*, both known target genes of HSF1 during the canonical heat shock response, showed the presence of expected canonical HSEs upstream of the TSS (**Figures 13E-F**), but no E2F DNA binding motifs were found near the transcriptional start sites of *HSP90AB1* and *HSPA6*. Importantly, ChIP-qPCR analysis in PC9-BrM3 and HCC4006-BrM cells revealed empirically that HSF1 occupancy is enriched at predicted degenerate HSEs upstream of E2F target genes (**Figures 13 G-H).** Collectively, these findings reveal the presence of degenerate HSF1-binding sequences, occupied by HSF1 and distinct from the canonical HSE motif, near a subset of E2F transcriptional targets.

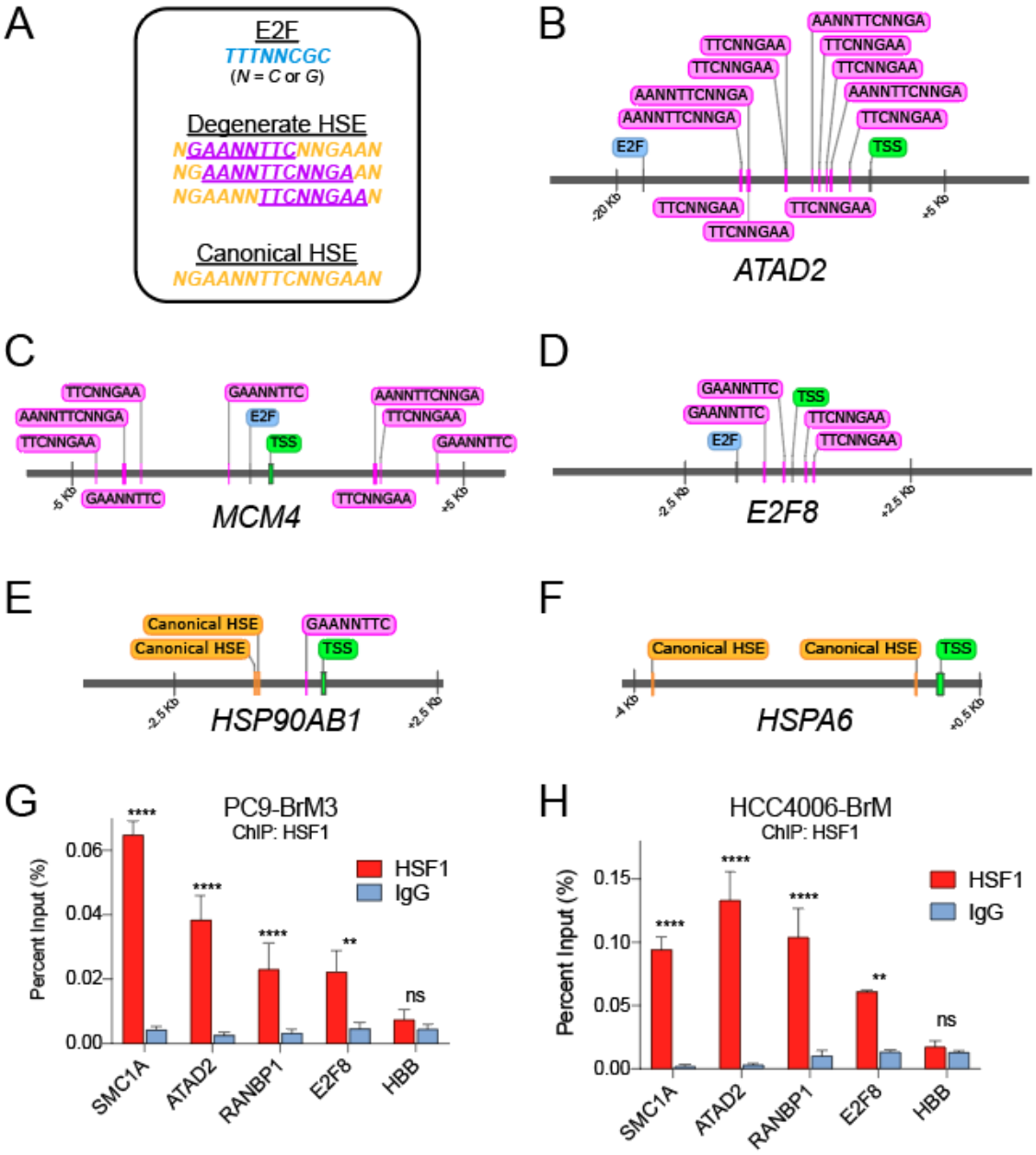

Figure 13: Brain-metastatic lung cancer cells exhibit HSF1 binding at E2F target genes. A) Sequence motifs used for promoter analysis of genes containing E2F binding sites, degenerate HSEs and canonical HSEs. B) Promoter analysis of the E2F target gene ATAD2 with E2F (blue) and predicted degenerate HSE (purple) binding motifs highlighted. TSS = transcriptional start site. C-D) Promoter analysis of the E2F target genes MCM4 and E2F8 with E2F (blue) and predicted degenerate HSE (purple) binding

motifs highlighted. E-F) Promoter analysis of the heat shock responsive target genes HSP90AB1 (E) or HSPA6 (F) with canonical HSE sequences indicated in yellow. For HSP90AB1 and HSPA6 promoters, no E2F binding motifs were identified. G-H) ChIP-qPCR analysis of HSF1 occupancy at degenerate HSEs nearby the indicated E2F target genes in G) PC9-BrM3 or H) HCC4006-BrM cells. HBB (Hemoglobin) gene included as negative control. n = 3 biological replicates. For all experiments, * p-value < 0.05, ** p-value < 0.01, *** p-value < 0.005, **** p-value < 0.001, ns = not significant. *Acknowledgment: Experiments from Figure 13A and 13B were performed by Dr. Jacob Hoj.*

2.2.4 ABL2-dependent regulation of HSF1 protein expression in brain-metastatic lung cancer cells.

Our data reveal that HSF1 is required for survival of brain-metastatic cancer cells and suggest that targeting of HSF1 could be exploited as a potential therapeutic strategy to treat this disease. The structure of HSF1 is not readily amenable to inhibition by small molecules, however HSF1 expression and activity might be impaired through inhibition of upstream HSF1 regulators. As our previous work (75) showed that loss of ABL2 in lung cancer cells impaired brain metastasis outgrowth, similar to the phenotype induced by loss of HSF1 *in vivo*, we evaluated whether ABL2 might also regulate HSF1 expression required for survival and colonization of brain-metastatic cells. Notably, knockdown of ABL2 in PC9-BrM3 cells *in vitro* resulted in a near complete loss of measurable HSF1, E2F1, and E2F8 proteins (**Figure 14A**). Consistent with a heat shock-independent role for HSF1 in brain metastasis, protein expression of HSP90 was not altered by the loss of HSF1 induced by ABL2 knockdown (**Figure 14A**). Interestingly, reciprocal co-immunoprecipitation of endogenous HSF1 and ABL2 in PC9-BrM3 cells showed a strong interaction between these two molecules (**Figures 14 B-C**). In contrast to HSF1 which shuttles between the cytoplasm and the nucleus, ABL2 is a cytoplasmic

protein and lacks a nuclear localization sequence. Co-immunoprecipitation and immunoblot analysis between nuclear and cytoplasmic fractions in cells co-transfected with ABL2-GFP and Flag-tagged HSF1 (Flag-HSF1) revealed that the interaction between these two molecules is restricted to the cytoplasm (**Figure 14D**).

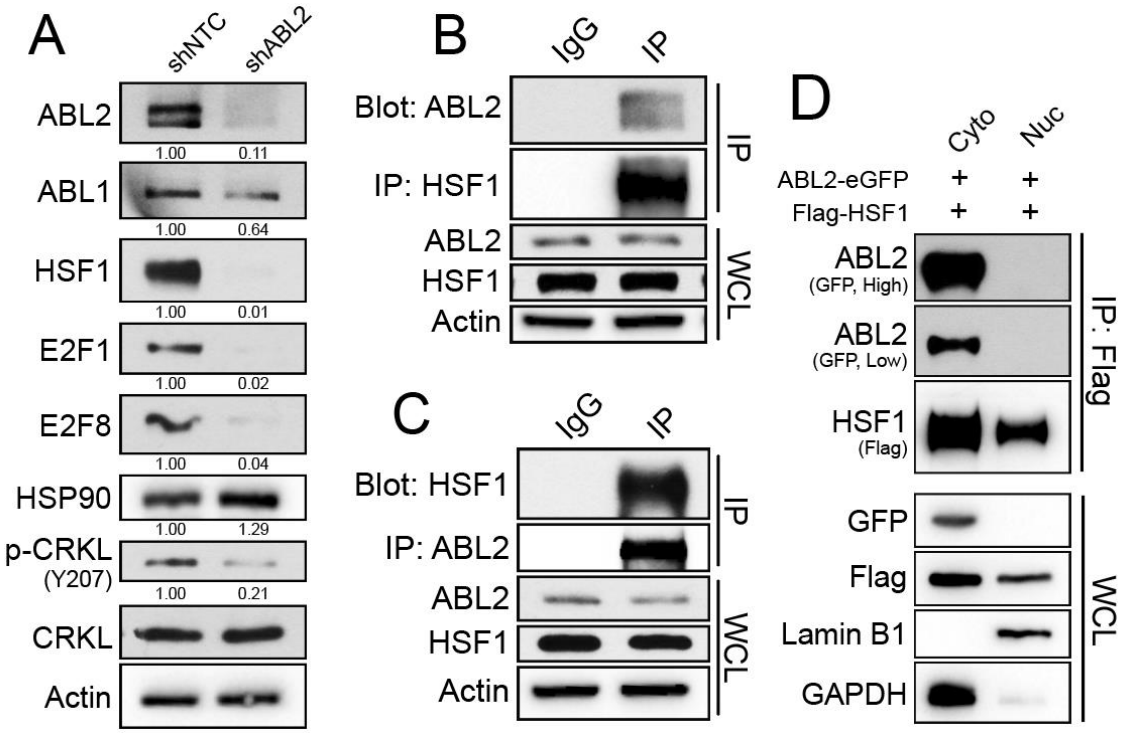

Figure 14: ABL2 kinase regulates HSF1 and E2F protein expression, and interacts with HSF1. A) Immunoblots of the indicated proteins in PC9-BrM3 cells transduced with lentiviral shRNAs against non-target control or ABL2. Quantification was normalized to actin loading control and shNTC, with the exception of phospho-CRKL which was normalized to total CRKL. B) Co-immunoprecipitation pulldown assay for endogenous HSF1 protein and immunoblots of indicated proteins in PC9-BrM3 cells. WCL = whole cell lysate. C) Co-immunoprecipitation pulldown assay for endogenous ABL2 protein and immunoblots of indicated proteins in PC9-BrM3 cells. D) Co-immunoprecipitation pulldown assay of Flag-HSF1 and immunoblots of indicated proteins in nuclear vs cytoplasmic subcellular fractions harvested from 293T cells.

To characterize the interaction between ABL2 and HSF1, we employed wild type (WT), kinase-inactive (K317M), SH2-inactive (R198K), or SH3-inactive (P158L) ABL2-GFP-tagged proteins (**Figure 15A**). Co-transfection of GFP-tagged ABL2 WT or ABL2 mutant proteins with His-tagged HSF1 followed by co-immunoprecipitation assays revealed that expression of the ABL2 P158L mutant resulted in a complete loss of the interaction with HSF1 (**Figure 15B**). Further, GST *in vitro* pulldown assays of purified His-HSF1 and GST-ABL2 SH2 or SH3-SH2 domains revealed a direct interaction between HSF1 and ABL2 that is dependent on the presence of the ABL2 SH3 domain (**Figure 15C**).

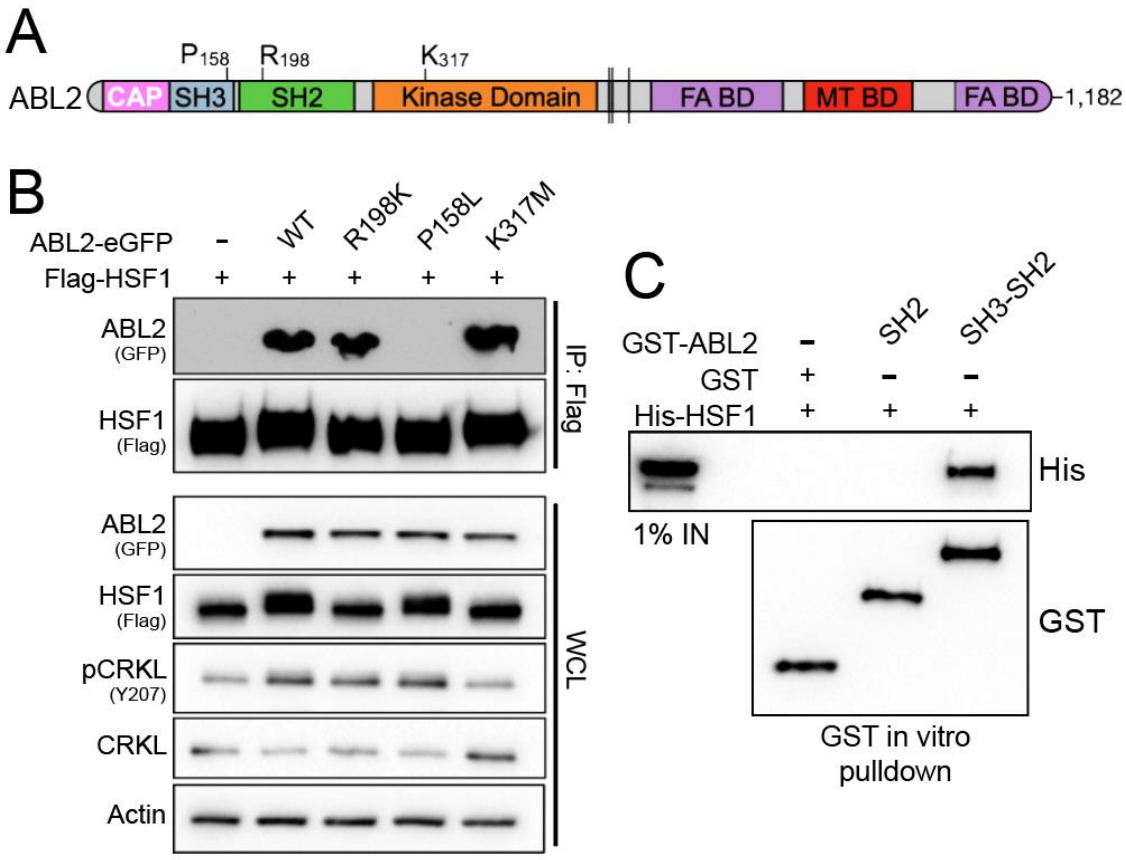

Figure 15: ABL2 interacts with HSF1 in a SH3-dependent, kinase-independent manner. A) Linear protein structures for ABL2. B) Co-immunoprecipitation pulldown assay of HSF1 (Flag) in 293T cells transiently transfected with Flag-tagged HSF1 and GFP-tagged ABL2 WT, ABL2 R198K, ABL2 K317M or empty vector control. C) GST in vitro pulldown assay of purified HSF1 (His) incubated with purified ABL2 SH2 or ABL2 SH3-SH2 protein domains.

Reciprocally, to identify the region of HSF1 responsible for its interaction with ABL2, we generated HSF1 truncation mutants by site-directed mutagenesis (Figure 16A). Co-immunoprecipitation of the HSF1 truncated proteins in cells co-transfected with ABL2-GFP revealed a loss in the interaction between HSF1 and ABL2 upon removal of the LZ1-LZ3 domains (amino acids 130-206) in the HSF1 1-129 truncation mutant (**Figure 16B**). Curiously, this region of HSF1 lacks proline-rich sites that normally typify canonical SH3 binding proteins, suggesting that a non-canonical SH3-binding motif might mediate the interaction between HSF1 and ABL2. To test this possibility, we generated 10-amino acid truncation mutants of HSF1 from residues 166-206 to more precisely identify the residues responsible for binding the SH3 domain of ABL2. We found that the loss of residues spanning 187-195 of HSF1 completely ablated the interaction between these two molecules (**Figure 16C**). As recent work revealed that SH3 domains can bind to proline-independent hydrophobic motifs (154), we hypothesized that a hydrophobic six amino acid KLIQFL motif spanning residues 188-193 of HSF1 (**Figure 16A**) might be responsible for the SH3-dependent interaction with ABL2. Deletion of this domain in HSF1 del188-193 and HSF1 del187-195 mutants ablated the interaction between HSF1 and ABL2 in cells (**Figure 16D**). Furthermore, GST *in vitro*

pulldown assays with purified His-HSF1 WT, His-HSF1 del187-195 or His-HSF1 del188-193 mutants in the presence of purified GST-ABL2 SH3 protein revealed a complete loss in the interaction between the ABL2 SH3 domain and the HSF1 deletion mutants (**Figure 16E**). Together these findings uncover a novel intramolecular interaction between a non-canonical, proline-independent motif of HSF1 with the ABL2 SH3 domain.

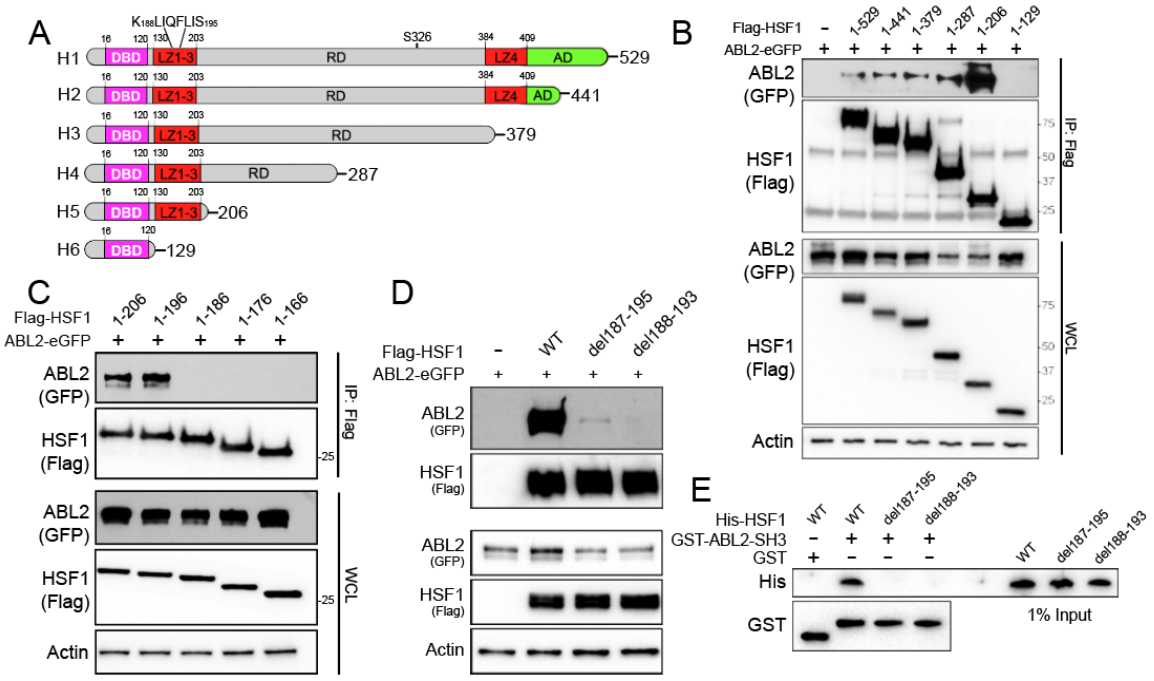

Figure 16: The ABL2 SH3 domain binds HSF1 on a non-canonical, proline-independent motif. A) Diagram depicting HSF1 truncation mutants used in co-immunoprecipitation pulldown assays. DBD = DNA binding domain, LZ = leucine zipper domains, RD = regulatory domain, AD = activation domain. B) Co-immunoprecipitation pulldown assay of HSF1 truncation mutants and immunoblots for corresponding proteins in 293T cells co-transfected with HSF1 truncation mutants and ABL2-GFP. C) Co-immunoprecipitation pulldown assay of HSF1 truncation mutants and immunoblots for corresponding proteins in 293T cells co-transfected with HSF1 1-166 through 1-206 truncation mutants and ABL2-GFP. HSF1 and GFP-tagged ABL2 WT, ABL2 R198K, ABL2 K317M or empty vector control. D) Co-immunoprecipitation pulldown assay of HSF1 (Flag) in 293T cells transiently transfected with Flag-tagged HSF1 WT or indicated deletion mutants with ABL2-eGFP. E) GST in vitro pulldown

assay of purified HSF1 (His) WT or deletion mutants incubated with purified ABL2 SH3 domain (GST). WCL = whole cell lysate.

2.2.5 Allosteric inhibition of the ABL kinases impairs HSF1-E2F expression.

We previously showed that the BBB-penetrable allosteric inhibitor ABL001 (Asciminib) is effective in mouse models of lung cancer brain metastasis (75). Thus, we examined if the loss of HSF1 protein observed in ABL2 knockdown cells was also induced by pharmacologic inhibition of the ABL2 kinase with ABL001. Treatment of HCC4006-BrM cells with ABL001 resulted in a dose-dependent decrease in the expression of HSF1, E2F1 and E2F8 proteins, while expression of HSP90 remained unchanged (**Figure 17A**). Notably, inhibition of the ABL kinases with ABL001 via oral gavage in mice harboring established lung cancer brain metastases resulted in near complete loss of HSF1 protein expression and inhibited phosphorylation of the ABL kinase substrate CRKL (**Figure 17B**). ABL2-dependent regulation of HSF1 protein expression occurs post-transcriptionally, as RT-qPCR analysis of PC9-BrM3 cells treated with ABL001 showed no measurable change in HSF1 mRNA expression (**Figure 17C**) and it is independent of the proteasome, as proteasomal inhibition with MG132 in cells treated with an ABL allosteric inhibitor did not rescue HSF1 protein expression (**Figure 17D**).

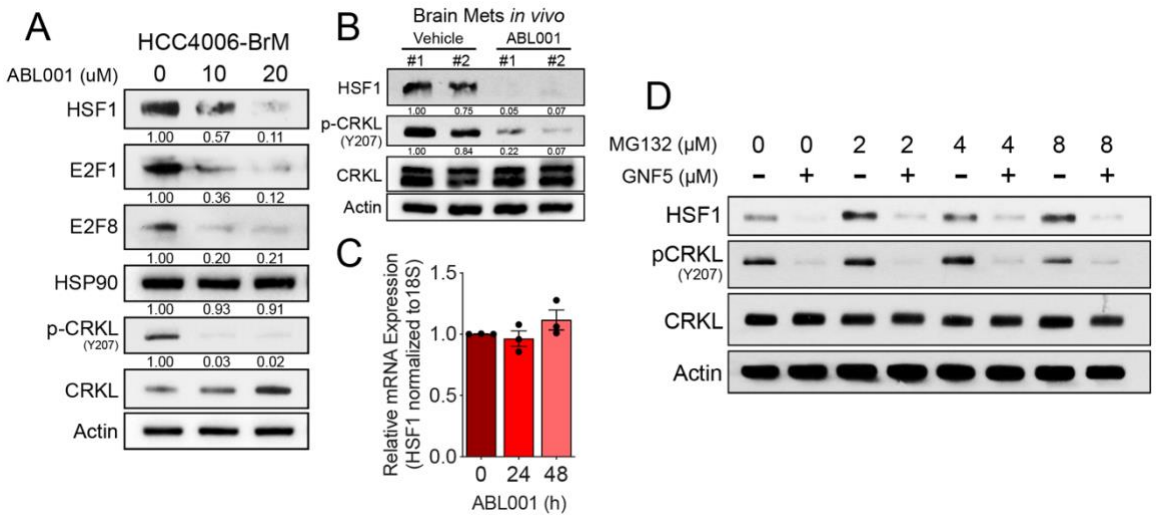

Figure 17: ABL allosteric inhibition regulates HSF1 expression in a transcription- and proteasomal-independent manner. A) Immunoblots of indicated proteins in HCC4006-BrM cells treated with indicated concentrations of ABL001 for 72 h. Quantification normalized to actin loading control and DMSO control (left lane). B) Immunoblots of indicated proteins in established in vivo brain metastases from mice injected with H1975 lung cancer cells and treated with vehicle (n=2) or 100 mg/kg ABL001 (n=2) via oral gavage. Mice were treated at 3, 12, and 24 h prior to harvesting brain metastases. Protein quantification data normalized to actin loading control and the leftmost lane (Vehicle #1). C) RT-qPCR analysis of HSF1 mRNA expression in PC9-BrM3 cells treated with 10 μM ABL001 for the indicated timepoints. HSF1 mRNA expression was normalized to mRNA expression of housekeeping gene 18S. n=3 biological replicates. Statistical analysis performed by two-way ANOVA followed by Tukey's multiple comparison post-hoc testing. ** p-value < 0.01, *** p-value < 0.005, **** p-value < 0.001, ns = not significant. D) Immunoblots of PC9-BrM3 cells treated with either DMSO or the ABL allosteric inhibitor GNF5 (24h) in addition to DMSO or MG132 at the indicated concentrations. *Acknowledgment: Experiment from Figure 17B was performed by Dr. Jacob Hoj.*

ABL kinase inhibitors can be classified into two broad categories: 1) selective allosteric inhibitors that target the unique myristate-binding pocket located within the ABL kinase (SH1) domain, and 2) ATP-competitive inhibitors that bind to the catalytic site within the kinase domain and target not only ABL but several other tyrosine kinases

(20). Notably, comparison of ABL allosteric inhibitors (GNF5, ABL001) with ATP-competitive inhibitors (Nilotinib, Imatinib and Dasatinib) revealed that cells treated with the ABL allosteric inhibitors exhibited a profound loss in HSF1, E2F1 and E2F8 proteins relative to ATP-competitive inhibitor treatment (**Figure 18A**). Expression of CDC6, an HSF1-E2F target gene, was preferentially decreased by the ABL allosteric inhibitors, whereas expression of HSP90 was not affected by any of the inhibitors tested (**Figure 18A**). Similar to HSF1 knockdown, treatment with the ABL allosteric inhibitor GNF5 resulted in loss of Cyclin B1 expression as well as a robust increase in cleaved PARP levels that were not observed by treatment with Nilotinib (**Figure 18B**). These findings are consistent with published data showing that in contrast to ABL allosteric inhibitors, the ATP-competitive inhibitors elicit ERK activation in lung cancer cells and other tumors (73). Notably, co-immunoprecipitation and immunoblot analysis of Flag-HSF1 co-transfected with ABL2-GFP in cells treated with either an allosteric or ATP-competitive inhibitor revealed a complete loss in the interaction between HSF1 and ABL2 only under allosteric inhibition (**Figure 18C**). Structural studies revealed striking differences in ABL kinase conformation and activity states under ATP-competitive- vs. allosteric-inhibited conditions (155). In line with these findings, our work suggests that, in contrast to ATP-competitive inhibition, allosteric inhibition of the ABL2 kinase results in an inactive state wherein the ABL2 SH3 domain is sterically inaccessible to binding with SH3-interacting proteins such as HSF1 (**Figure 18D**). Collectively, our results show

that in contrast to the ATP-competitive inhibitors, the ABL allosteric inhibitors phenocopy the effects of ABL2 knockdown and might be used to disrupt HSF1-E2F transcription in brain-metastatic lung cancer cells. In this regard, PC9-BrM3 and HCC4006-BrM cells treated with ABL001 exhibited profound decreases in mRNA expression of the HSF1-E2F target gene panel (**Figures 18 E-F**). Together these results demonstrate that HSF1-E2F-transcription networks can be pharmacologically targeted with ABL kinase allosteric inhibitors.

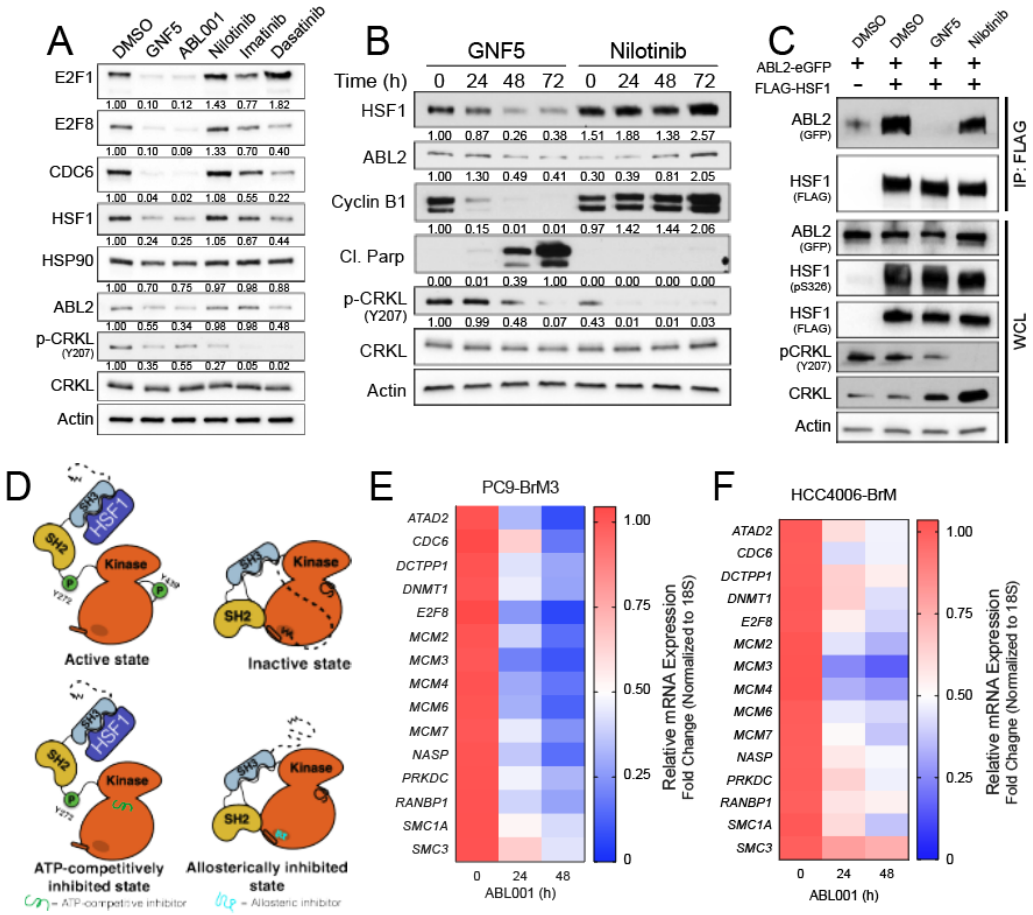

Figure 18: ABL allosteric, but not ATP-competitive inhibition decreases HSF1 protein expression and ABL2-HSF1 complex formation. A) Immunoblots of PC9-BrM3

cells treated with DMSO or the ABL allosteric inhibitors GNF5 (10 μM) or ABL001 (10 μM), and ATP-competitive Nilotinib (1 μM), Imatinib (2 μM), or Dasatinib (150 nM) for 48 h. Indicated equipotent doses for each drug were selected after determining corresponding IC50 values. Phospho-CRKL Y207 blot used as surrogate marker for ABL kinase inhibition. B) Immunoblots of PC9-BrM3 cells treated with 10 μM GNF5 or 1 μM Nilotinib for the indicated timepoints. Protein quantification data normalized to actin loading control and the leftmost lane (DMSO). For all immunoblots of phospho-CRKL, quantification data were normalized to total CRKL levels. C) Co-immunoprecipitation pulldown assay for Flag-HSF1 in 293T cells co-transfected with ABL2-GFP and treated with the indicated inhibitors for 24 h. D) Proposed diagram of the SH3-dependent interaction between ABL2 and HSF1 in the absence (upper) and presence (lower) of ABL allosteric versus ATP-competitive pharmacologic inhibitors. E-F) RT-qPCR analysis of E2F target gene mRNA expression in PC9-BrM3 (E) or HCC4006-BrM (F) cells treated with 10 μM ABL001 for indicated timepoints. *Acknowledgment: Experiments from Figure 18E and 18F were performed by Dr. Jacob Hoj.*

2.2.6 An HSF1-E2F transcriptional signature is upregulated in lung adenocarcinoma patients and is predictive of poor survival

To evaluate whether the HSF1-E2F target gene signature is clinically relevant, we analyzed patient datasets to determine if HSF1-E2F target gene expression is predictive of patient survival outcomes. Analysis of microarray-based mRNA expression correlated to overall patient survival data revealed that high expression of the HSF1-E2F-coregulated target genes *ATAD2, CDC6, PRKDC, RANBP1, MCM2, MCM3, MCM4,* and *MCM7* each individually were predictive of significantly poorer overall survival in lung adenocarcinoma patients (**Figures 19 A-H**). In addition, analysis of TCGA datasets for lung adenocarcinoma showed that high expression of the HSF1-E2F target gene signature co-occurred in the same patients, and mutual exclusivity analysis showed high co-occurrence for almost all gene pairs tested from the HSF1-E2F gene panel (**Figures 19 I-J**). Collectively, these data provide supporting evidence for an HSF1-E2F-coregulated

transcriptional gene signature that may be clinically relevant as a prognostic marker for patient survival in lung adenocarcinoma (**Figure 19K**).

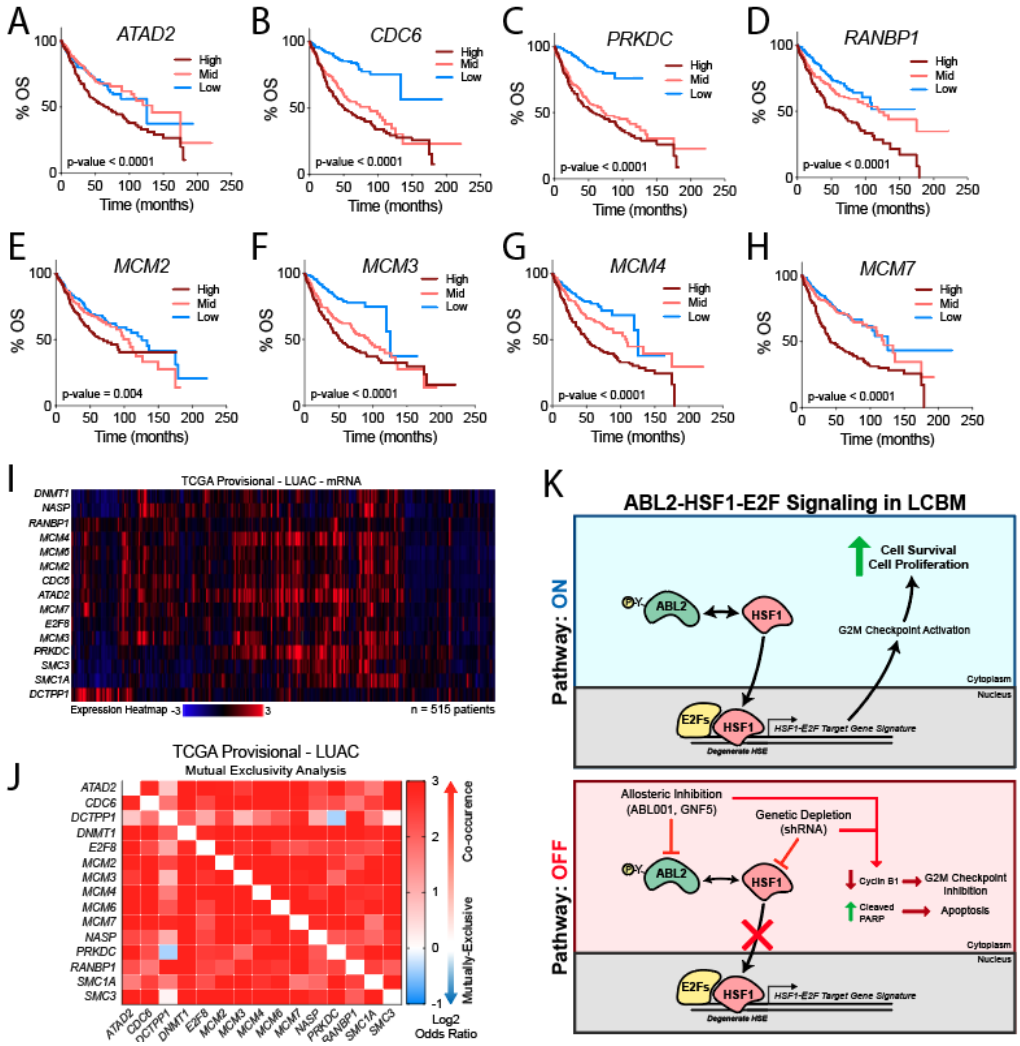

Figure 19: Expression of HSF1-E2F target genes is predictive of poor survival outcomes and co-occurs in lung adenocarcinoma patients. A-H) Overall survival (OS) curves derived from human lung adenocarcinoma patient microarray datasets with high versus low expression of HSF1-E2F target genes A) ATAD2, B) CDC6, C) PRKDC, D) RANBP1, E) MCM2, F) MCM3, G) MCM4, and H) MCM7. Curves were generated using KMPlot analysis tool and patient groups were stratified by tertile (n = 720 total patients). For all survival curves, statistical analysis performed by Log Rank Mantel Cox test. I) Clustered heatmap depicting mRNA expression for HSF1-E2F target gene panel in human lung adenocarcinoma provisional patient dataset available through TCGA. Data

were analyzed using the cBioPortal online analysis software. J) Mutual exclusivity analysis of HSF1-E2F target gene expression in the same TCGA lung adenocarcinoma dataset to demonstrate high co-occurrence of target gene expression. Heat map scaling based on Log2 Odds Ratio as calculated using cBioPortal analysis tool. K) Model diagram illustrating ABL2-HSF1-E2F signaling in lung adenocarcinoma brain metastasis. *Acknowledgment: Experiments from Figure 19 were performed by Dr. Jacob Hoj.*

2.3 Discussion

While HSF1 has been shown to support initiation and progression of distinct types of primary tumors, little is known regarding the role of HSF1 during metastasis (142, 144, 146). We now show that brain-colonizing lung cancer cells upregulate expression of HSF1 and that loss of HSF1 in these cells results in dramatic decreases in cell survival *in vitro* and metastatic burden *in vivo*. Additionally, our data show that the transcriptional response driven by HSF1 is strikingly divergent from its canonical role as the master regulator of the heat shock response. Unbiased transcriptomic profiling comparing brain-metastatic and parental cell lines reveals significant enrichment of E2F transcription family gene signatures in brain-metastatic cells whose expression is dependent on HSF1. Previous work in *C. elegans* revealed an HSF1-E2F transcriptional program is required during development, whereby HSF1 binds DNA at promoter regions of E2F target genes in a heat-shock-independent manner (150). Similarly, analysis of promoter regions for predicted HSF1-E2F-coregulated genes in human cells revealed the presence of "degenerate" HSEs downstream of E2F DNA binding motifs which were confirmed empirically to be occupied by HSF1, thus supporting the hypothesis that HSF1 is a cofactor required for expression of these E2F gene targets in

metastatic lung cancer cells. Importantly, analysis of human patient data revealed that high expression of an HSF1-E2F transcriptional signature co-occurs in patient populations with poor survival outcomes, suggesting that an HSF1-E2F target gene panel may hold prognostic value in patients with aggressive metastatic disease. Future studies comparing samples of paired patient primary tumors and corresponding brain metastases should be undertaken to evaluate whether HSF1 protein expression and an HSF1-E2F-coregulated transcription network may be relevant to progression in this disease setting. Furthermore, the importance of HSF1 activation and E2F-coregulated transcription in extracranial metastasis merits further investigation.

The ABL kinases, ABL1 and ABL2, function downstream of known HSF1 activators including EGFR, HER2, and RAS (73, 93, 95, 144, 156, 157). Additionally, the ABL kinases regulate expression and activity of multiple factors that function as HSF1 transcriptional co-regulators, including E2F1 (158-160). Recent work by our lab uncovered a critical role for the ABL2 kinase in the regulation of a TAZ-dependent transcriptional network required for the early colonization of lung cancer brain metastases (75). We now show that the SH3 domain of ABL2 forms a complex with a hydrophobic KLIQFL motif located within the LZ1-3 domains of HSF1, and knockdown of ABL2 results in impaired expression of HSF1, E2F1 and E2F8 proteins in brain-metastatic lung cancer cell lines. Notably, we found that pharmacologic inhibition of the ABL kinases using selective ABL allosteric inhibitors, but not ATP-competitive

inhibitors, ablates the physical interaction between ABL2 and HSF1, results in markedly decreased expression of HSF1, E2F1 and E2F8 proteins in brain-metastatic lung cancer cells, and results in depletion of HSF1-E2F transcriptional targets. These findings highlight potential differences affecting intra- and inter-molecular protein-protein interactions induced by allosteric versus ATP-competitive kinase inhibitors that might have important therapeutic implications. Importantly, the targetable nature of the ABL2-HSF1-E2F signaling network identifies ABL allosteric inhibitors as a potentially effective therapy for the treatment of metastatic lung cancers characterized by high expression of HSF1.

3. ABL kinases regulate the stabilization of HIF-1α and MYC through CPSF1

Material from this chapter is adapted from a manuscript currently under review at *PNAS*.

3.1 Introduction

Oxygen is essential for the survival of all aerobic organisms. As a result, pathways have evolved to allow cells to sense and respond to fluctuations in oxygen availability. In the presence of oxygen, hypoxia inducible factor-α (HIF-α) is prolyl-hydroxylated by a family of 2-oxoglutarate dependent dioxygenases (PHD1-3) and, subsequently, interacts with the von Hippel-Lindau ubiquitin ligase (pVHL) complex (161-167). This complex ubiquitinates HIF-α, promoting its degradation by the 26*S* proteosome. In hypoxic cellular environments VHL does not interact with HIF-α resulting in its accumulation in cells (164). Stabilized HIF-α dimerizes with constitutively expressed HIF-1β to form an active HIF transcriptional complex that controls the expression of target genes needed for adaptation to hypoxic environments (**Figure 20**) (161, 162, 164).

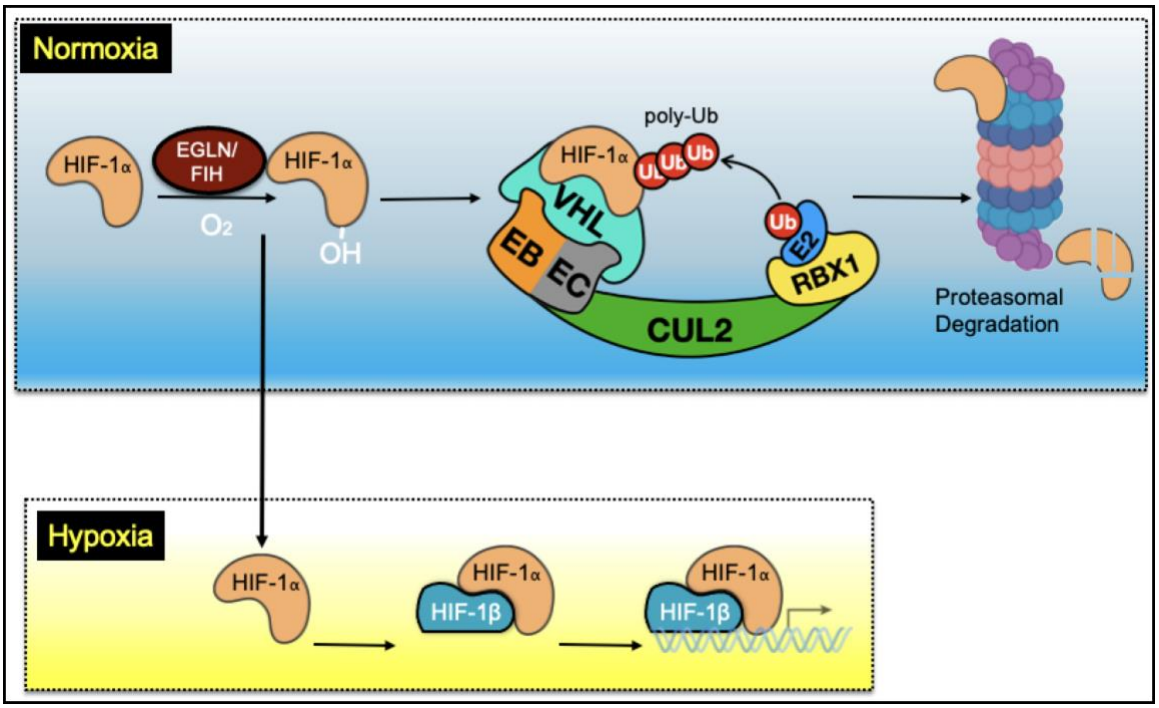

Figure 20: Schematic of normoxic degradation and hypoxic stabilization of HIF-1α.

While the mechanism(s) regulating the degradation of HIF-α during normoxia by the pVHL complex are well understood. However, the signaling pathways and factors that support the sustained expression and activation of HIF-α during hypoxia outside of PHD inhibition are not as clearly defined (168). We and others have shown that the ABL family of non-receptor tyrosine kinases, ABL1 and ABL2, enable cancer cells to respond to diverse stress stimuli by activating pathways necessary for survival (20, 75, 169, 170). The ABL kinases often potentiate these responses by inducing the stability and/or transactivation of transcriptional regulators (20, 73-75, 171, 172). Thus, we hypothesized that the ABL kinases may modulate the cellular response to hypoxia. We found that ABL kinase activity is necessary for the stabilization of HIF-1α protein

during hypoxia, and activation of the ABL kinases during normoxia was sufficient to elevate HIF-1α protein levels. Further, we show that the ABL kinases promote HIF-1α protein stability in hypoxia by protecting it from proteasomal degradation. Using a flow-cytometry-based CRISPR/Cas9 screen, we identified CPSF1 as the E3-ligase targeting HIF-1α for destruction after ABL kinase inhibition. Notably, we uncovered that a second oncoprotein transcription factor, MYC, is also regulated by the ABL-CPSF1 axis. These data reveal a critical role for the ABL kinases in supporting the stabilization of the oncogenic transcription factors HIF-1α and MYC by antagonizing the activity of the CPSF1 E3-ligase complex.

3.2 Results

3.2.1 ABL kinase inhibition decreases HIF-1α protein levels in hypoxia

Pharmacological inhibition of the ABL kinases using the allosteric inhibitors ABL001 or GNF5 decreased HIF transcriptional activity as assessed using a hypoxia response element reporter stably expressed in either EGFR-mutant PC9 lung cancer cells or in HEK293T cells under hypoxic conditions (**Figures 21 A-E**).

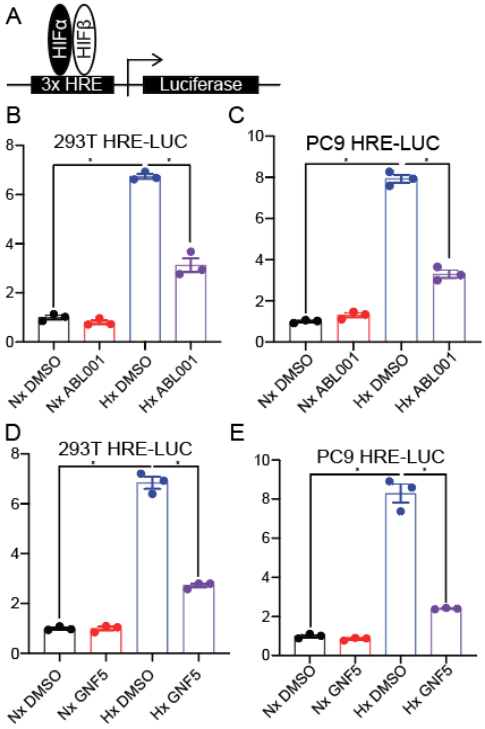

Figure 21: ABL kinase inhibition decreases HIF transcriptional activity. A) Scheme of hypoxia response element reporter. (B-E) Bioluminescence levels of PC9 and 293T cells transduced with a hypoxia response element reporter and treated with GNF5 or ABL001 (20 μM) as indicated during normoxia (Nx) or hypoxia (Hx) (1 % O2) for 24 h.

As the ABL kinases have previously been shown to regulate the expression of transcriptional regulators (20, 73-75, 171, 172), we investigated if the decrease in HIF activity observed in hypoxic conditions was due to changes in the abundance of the HIF family members , HIF-1α, -2α, and 1β. Treatment with allosteric ABL kinase inhibitors resulted in decreased HIF-1α protein levels in multiple EGFR- or KRAS-mutant lung cancer cells and in triple-negative breast cancer cells without a consistent change in HIF-2α nor HIF-1β levels (**Figure 22 A-B**). Treatment with an orthosteric, ATP-competitive ABL kinase inhibitor, nilotinib, elicited a similar decrease in HIF-1α levels without

impacting HIF-2α or HIF-1β levels (**Figure 22C**). The maintenance of HIF-1α protein levels during pseudohypoxia (chemically induced hypoxia) was also dependent on ABL kinase activity (**Figure 22D**).

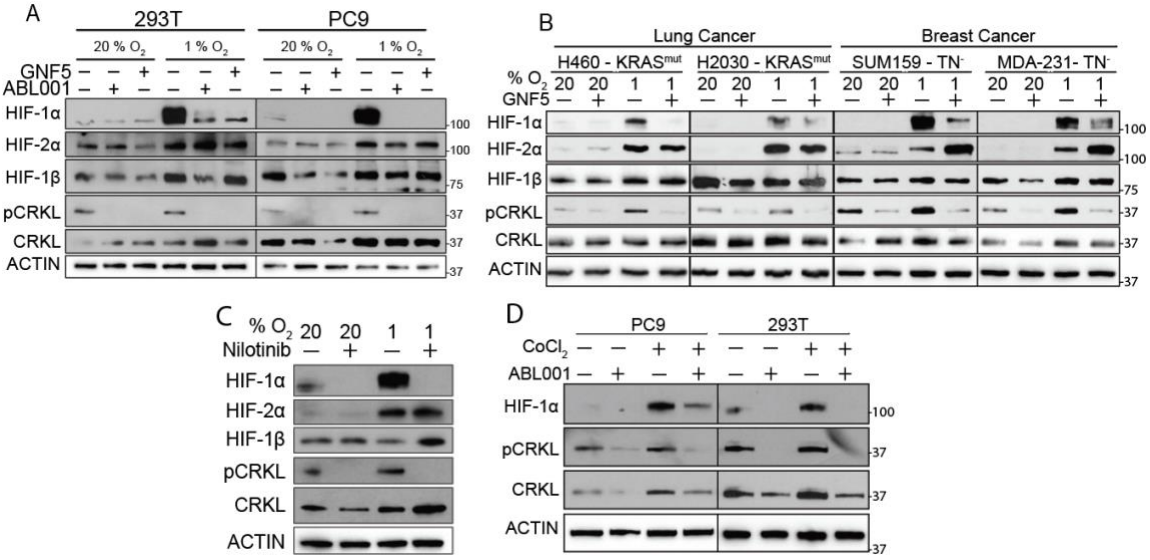

Figure 22: ABL kinase inhibition decreases HIF-1α protein levels. (A) Immunoblots (IB) analysis of whole cell lysates (WCL) derived from HEK293T and PC9 cells treated with ABL001 (20 μM) or GNF5 (20 μM) during normoxia or hypoxia (1 % O_2) for 24 h. (B) IB analysis of WCL derived from KRAS-mutant lung cancer cells (H460, H2030) and Triple Negative (TN-) breast cancer cells (SUM159, MDA-MB-231) treated with GNF5 during normoxia or hypoxia (1 % O2) for 24 h. (C) IB analysis of whole cell lysates (WCL) from PC9 lung cancer cells treated with nilotinib (5 μM) during normoxia or hypoxia for 24 h. (D) IB analysis of WCL from PC9 and HEK293T cells treated with pseudo-hypoxia inducer CoCl2 (PC9: 250 μM; 293T: 125 μM) and ABL001 as indicated for 24 h.

The ABL1 and ABL2 non-receptor tyrosine kinases have a highly homologous amino terminal kinase domain (90%) and a carboxy terminal domain (29%) that evolutionarily diverged after a gene duplication event (25). We and others have found overlapping and non-redundant functions for the ABL kinases (20). We observed that

knockdown of either ABL1 or ABL2 resulted in a profound decrease in the hypoxic induction of HIF-1α protein (**Figures 23 A-B**).

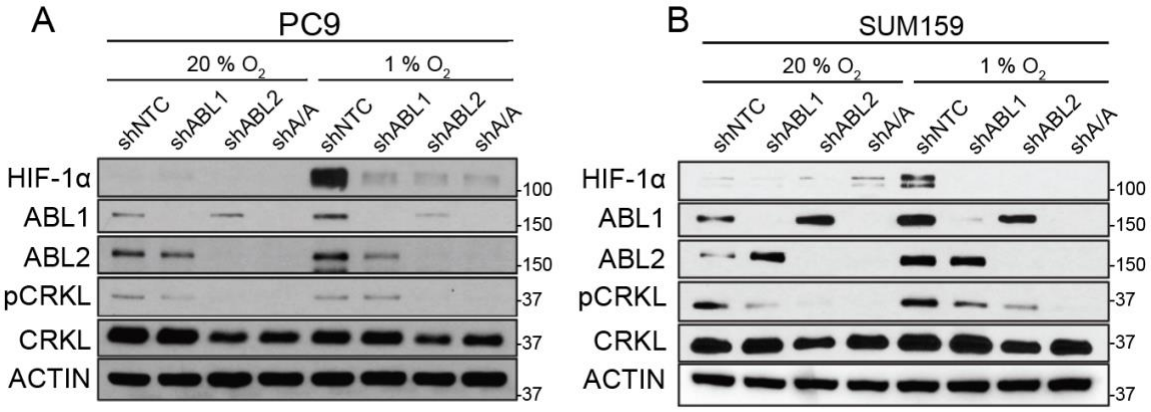

Figure 23: Knockdown of the ABL kinases decreases HIF-1α protein levels. (A-B) IB analysis of WCL derived from (A) PC9 or (B) SUM159 cells transduced with indicated short hairpin RNA (shRNA) lentiviruses and cultured under normoxia or hypoxia for 24 h

3.2.2 ABL activation increases HIF-1α protein levels

We next investigated if activation of the ABL kinases was sufficient to increase HIF-1α levels. The ABL kinases can be activated with point mutations or treatment with an allosteric activator (**Figure 24A**). Site-direct mutagenesis of two proline residues located in the ABL SH2-SH1 linker to glutamate residues leads to an opening of the ABL autoinhibited state and increased kinase activity (30). Mutation of one proline (P) residue to glutamic acid (E) led to a partial activation, while mutation of both proline residues produced a maximally activated ABL1 and ABL2 kinases (**Figures 24 B-C**). This dose-dependent increase in ABL kinase activity resulted in a dose-dependent increase in HIF-1α levels (**Figures 24 B-C**). Further, dose-dependent increase in ABL kinase

expression resulted in a dose-dependent increase in HIF-1α levels (**Figures 24 D-E**). Conversely, treatment with an allosteric activator (DPH) increased HIF-1α levels (**Figure 24F**).

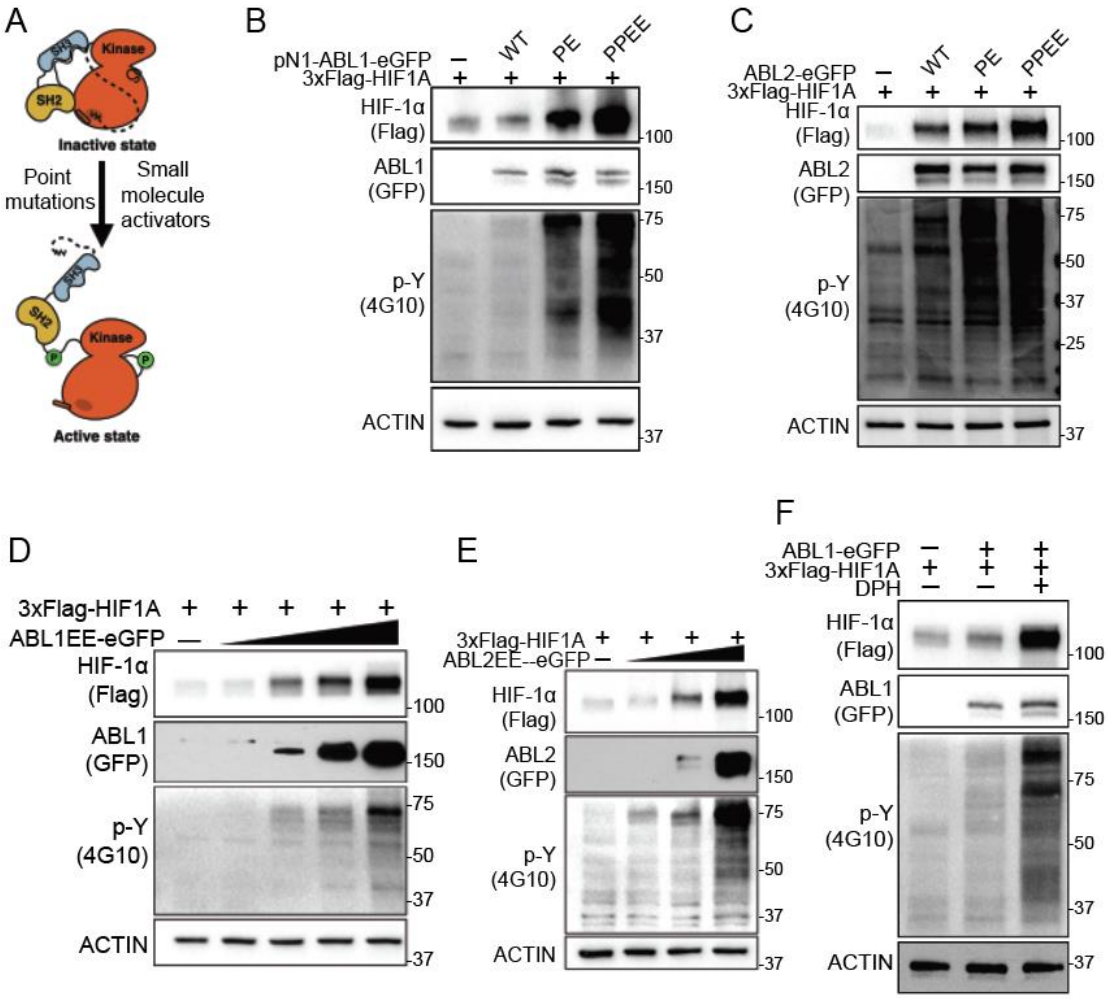

Figure 24: ABL kinase activation induces HIF-1α protein stabilization. (A) Model depicting mutational and pharmacological activation of the ABL kinases. (B-E) IB analysis of WCL derived from HEK293T cells transfected with 3xFlag-HIF1A and indicated ABL1-eGFP constructs for 48 h. ABL1 PE has a moderate increase in ABL kinase activity and ABL1 PPEE has a high increase in ABL kinase activity. (F) IB analysis of WCL derived from HEK293T cells transfected with 3xFlag-HIF1A and ABL1-eGFP

constructs for 24 h and then treated with the ABL kinase allosteric activator DPH (2.5 μM) as indicated for 24 h before harvesting.

The enhanced accumulation of HIF-1α protein levels observed upon co-expression of activated ABL1EEwas reversed by ABL allosteric inhibitors (**Figure 25A**). Further support for this conclusion, was the finding that wild-type and the activated SH3-domain mutated (P131L) ABL1 induced HIF-1α expression, while catalytically dead (K290M) ABL1 was without effect on HIF-1α levels (**Figure 25B**). Mutation of the SH2 domain of ABL1 (R171K), which disrupts the binding to tyrosine-phosphorylated substrates, resulted in a partial reduction in the levels of HIF-1α (**Figure 25B**). These data demonstrate that the ABL kinases are necessary to maintain HIF-1α protein under conditions of hypoxia and that activation of the ABL kinases is sufficient to increase HIF-1α protein levels.

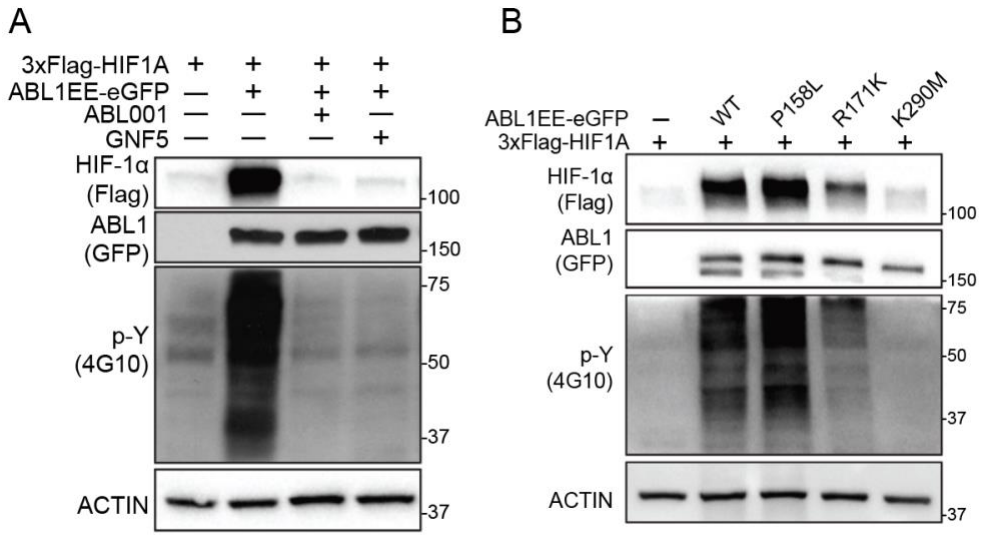

Figure 25: ABL tyrosine kinase activity is necessary for HIF-1α protein stabilization. (A) IB analysis of WCL derived from HEK293T cells transfected with

3xFlag-HIF1A and ABL1-eGFP constructs for 24 h and then treated with ABL001 and GNF5 as indicated for 24 h before harvesting. (B) IB analysis of WCL derived from HEK293T cells transfected with 3xFlag-HIF1A and indicated ABL1-eGFP constructs for 48 h.

3.2.3 ABL kinase regulation of HIF-1α does not occur transcriptionally

A complex network of signaling pathways enable the accumulation of HIF-1α in hypoxia through transcriptional, translational, and post-translational processes (161, 162, 166-168). To investigate the mechanism through which ABL kinase activity impacts HIF-1α levels, we first examined *HIF1A* mRNA levels. While *HIF1A* mRNA decreased during hypoxia as shown previously (173), neither pharmacologic inhibition nor shRNA-mediated knockdown of the ABL kinases resulted in significant alterations of *HIF1A* mRNA levels (**Figures 26 A-B**). Given this result, we investigated whether the hypoxic stabilization of HIF-1α produced from an ectopically expressed HIF-1α transgene under the control of a heterologous promoter, was impacted by ABL kinase inhibition. Indeed, similar to endogenous HIF-1α, ABL kinase inhibition resulted in the loss of a 3xFlag-HIF-1α protein during hypoxia (**Figure 26C**). These results suggest that the ABL kinase regulation of HIF-1α may occur post-translationally.

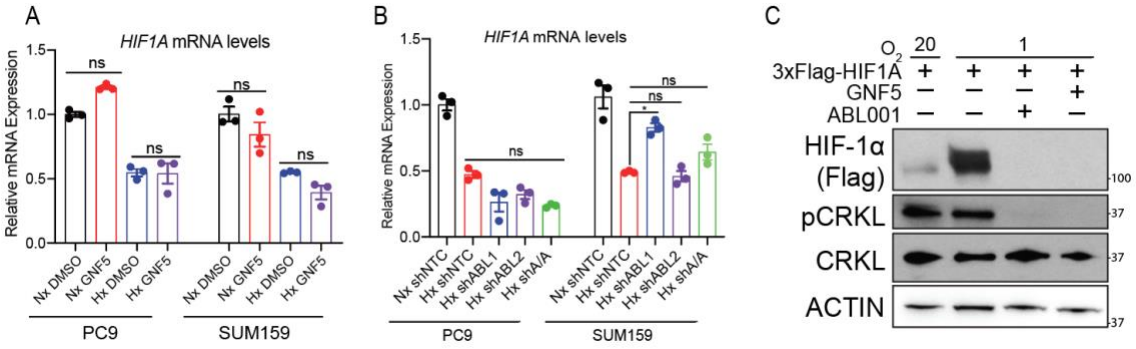

Figure 26: ABL kinase regulation of HIF-1α does not occur transcriptionally. (A-B) qRT-PCR analysis of WCL derived from PC9 and SUM159 cells cultured under normoxia or hypoxia for 24 h and either A) treated with GNF5 or B) transduced with indicated shRNA lentiviruses. (C) IB analysis of WCL derived 293T cells transfected with 3xFlag-HIF1A for 24 h and then treated with ABL001 or GNF5 during hypoxia for 24 h.

3.2.4 The ABL kinases regulate the proteasomal degradation of HIF-1α

HIF-1α protein levels are regulated in large part by the activity of the ubiquitin-dependent 26S proteasomal pathway (161, 162). We found that endogenous HIF-1α protein levels were stabilized upon inhibition of the proteasome using MG132 in PC9 lung cancer cells treated with the GNF5 allosteric inhibitor or upon knockdown of ABL1 and ABL2 in these cells (**Figures 27 A-B**) Proteasomal inhibition also reversed the decreased of exogenous HIF-1α protein levels after ABL kinase inhibition with allosteric inhibitors in HEK293T cells co-expressing kinase active ABL1EE-eGFP and 3xFlag-HIF-1α (**Figure 27C**).

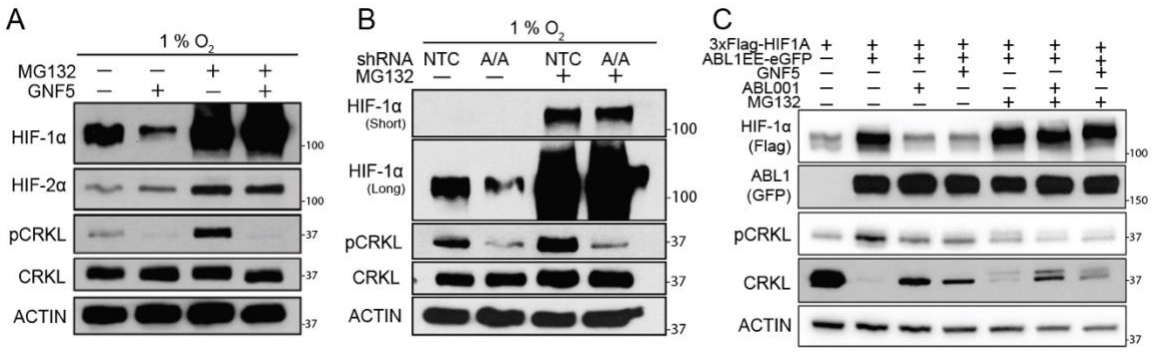

Figure 27: The ABL kinases regulate the proteasomal degradation of HIF-1α. (A) IB analysis of WCL derived from PC9 cells treated with ABL001 and MG132 (4 μM) as indicated during hypoxia for 24 h. (B) IB analysis of WCL derived from PC9 cells transduced with indicated shRNA lentiviruses and treated with MG132 cultured under hypoxia for 24 h. (C) IB analysis of WCL derived from HEK293T cells transfected with 3xFlag-HIF1A and ABL1-eGFP constructs for 24 h and then treated with ABL001, GNF5, and MG132 as indicated for 24 h before harvesting.

Further, we found that endogenous HIF-1α was highly ubiquitinated after loss of ABL kinase activity in both lung cancer and breast cancer cells (**Figures 28 A-B**). Moreover, activation of ABL1 and ABL2 decreased HIF-1α ubiquitination (**Figures 28 C-D**). These data support the hypothesis that ABL kinase activity impairs HIF-1α ubiquitination and proteasome-mediated protein degradation (**Figure 28E**).

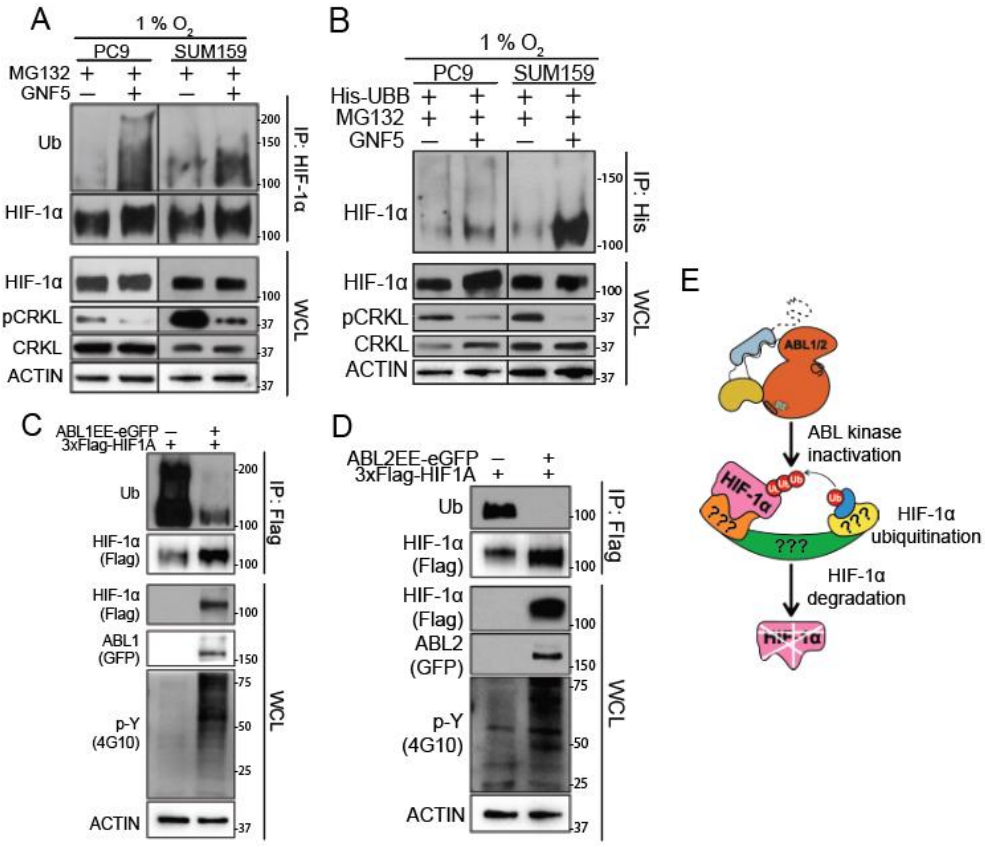

Figure 28: The ABL kinases regulate the ubiquitination of HIF-1α. (A) IB analysis of IP and WCL derived from PC9 and SUM159 cells treated with ABL001 and MG132 as indicated during hypoxia for 24 h. (B) IB analysis of IP and WCL derived PC9 and SUM159 cells transfected with a His-UBB construct and then treated with ABL001 (24 h) and MG132 (final 6 h) during hypoxia for 24 h before harvesting. (C) IB analysis of IP and WCL derived from HEK293T cells transfected with 3xFlag-HIF1A and ABL1-eGFP constructs for 24 h. (D) IB analysis of IP and WCL derived from HEK293T cells transfected with 3xFlag-HIF1A and ABL2-eGFP constructs for 24 h. (E) Proposed model depicting loss of ABL kinase activity leading to HIF-1α ubiquitination and proteasome-mediated protein degradation.

3.2.5 FACS-based CRISPR/Cas9 nominates CPSF1 as the ABL-dependent HIF-1α targeting E3-ligase.

The mechanism by which ABL kinases regulate the proteasomal degradation of HIF-1α was next explored. To identify the ABL-dependent E3-ligase(s) regulating HIF-

1α protein stability, we conducted a fluorescence-activated cell sorting (FACS)-based CRISPR/Cas9 screen using a custom sgRNA library targeting 593 known and predicted human E3-ligases in PC9 lung cancer cells. We transduced this library into PC9 cells followed by incubation in the presence of an ABL kinase inhibitor in hypoxic conditions for 24 hours (**Figure 29A**). Staining with a fluorophore-conjugated antibody against HIF-1α and subsequent FACS-based sorting of HIF-1α high- and low-expressing cell populations, revealed E3-ligase components that impacted HIF-1α protein levels after ABL inhibition (**Figures 29 A-F**). The top scoring genes whose loss rescued HIF-1α protein levels during ABL inhibition included RBX1 and CPSF1, while VHL did not score as a hit (**Figure 29A, Figures 29 G-I**). RBX1 is a component of the catalytic core in the majority of multi-subunit Cullin ring ligase (CRLs) complexes (~500 complexes) (174). Thus, we evaluated how CPSF1 protein might be involved in the regulation of HIF-1α stability.

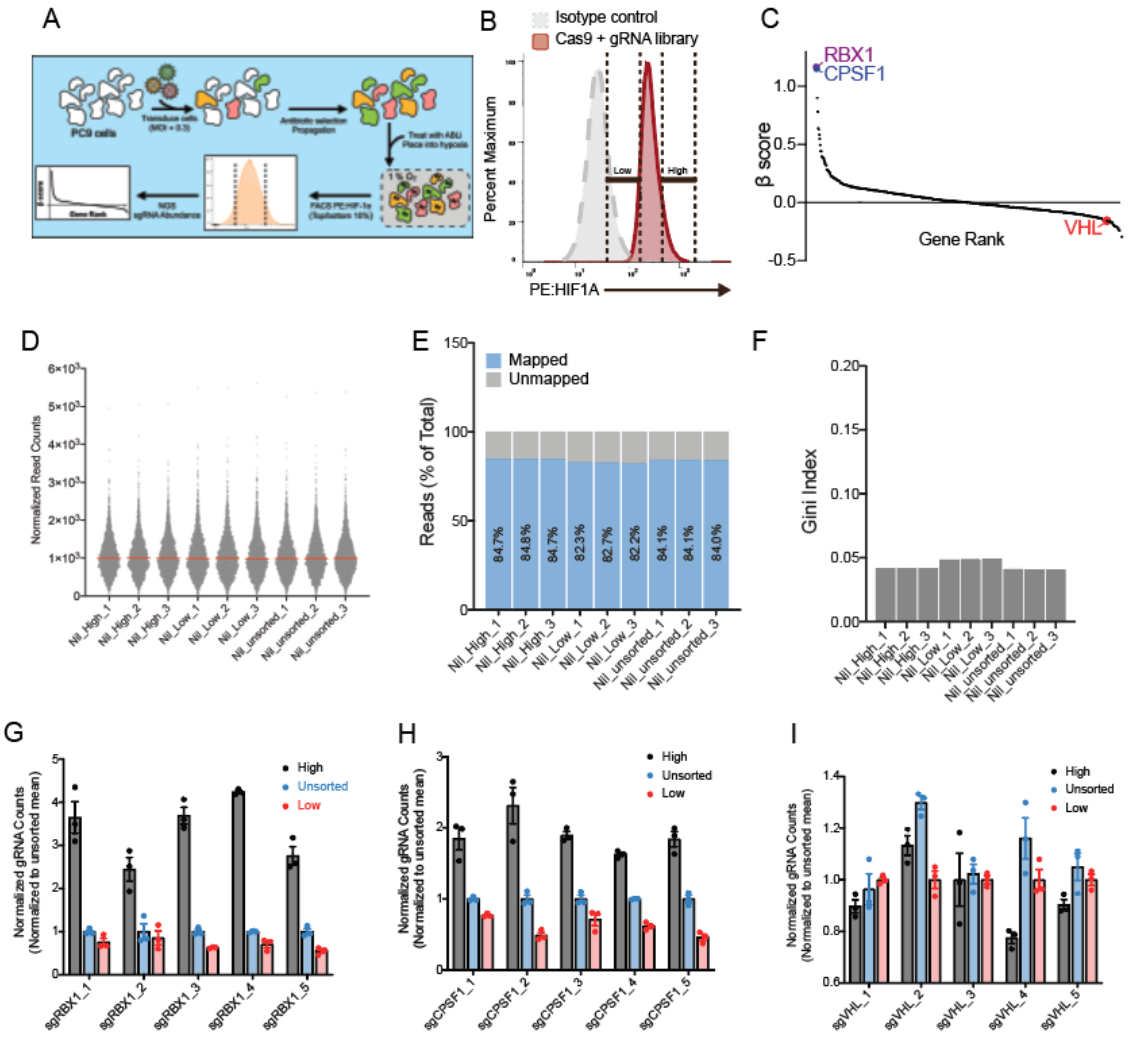

Figure 29: FACS-based CRISPR screen identifies E3 ligase targeting HIF-1α protein after ABL kinase inhibition. (A) Scheme of the FACS-based CRISPR E3 ligase screen performed. (B) Fluorescence-activated cell sorting of PC9 cells stained with a PE conjugated HIF-1α antibody with gating for top and bottom 10% expressing cells indicated. (C) Snake plot depicting the β scores across 593 E3-ligase related gene identified in PC9 lung cancer cells. (D) Normalized sequencing read counts for each sgRNA across samples included in the FACS-based E3 ligase screen. Individual dots represent sequencing read coverage for each sgRNA represented in the screen. Red lines represent median distribution of counts for each sample. (E) Quantification of the percentage of mapped and unmapped reads across samples in the FACS-based E3 ligase screen. (F) GINI index quantification, representing the evenness of sgRNA read count distribution across target genes for each sample. (G-I) Normalized sgRNA abundance of indicated sgRNAs across high, low, and unsorted cell populations. *Acknowledgment:*

Experiments from Figure 29 were performed by Dr. Jacob Hoj, Christian Cerda-Smith, and Haley Hutchinson.

3.2.6 CPSF1 is an E3 ligase targeting HIF-1α

CPSF1 is an essential gene whose primary known function is as a core scaffolding component of the cleavage and polyadenylation specificity factor (CPSF) complex (175). This complex is necessary for proper 3'-polyadenylation of eukaryotic pre-mRNAs, and loss of CPSF1 impairs the maturation of the bulk of eukaryotic mRNA transcripts (176). In addition to its role in mRNA maturation, CPSF1 shares significant structural similarity with the CRL adaptor DDB1 (177). However, an E3-ligase activity has not previously been ascribed to CPSF1 although it was shown by others that immunoprecipitated CPSF1 complexes from cultured cells have *in vitro* E3-ligase activity (177, 178). Here we show that that CPSF1 forms a complex with the E3-ligase scaffold proteins CUL4A and CUL4B suggesting that CPSF1 might function as a component of E3-ligase complexes (**Figure 30A**).

Mining the BioGRID database we identified CPSF1 as a potential HIF-1α interactor (179, 180). This interaction was confirmed in studies demonstrating that CPSF1 immunoprecipates with HIF-1α in the presence of the proteasome inhibitor, MG132 (**Figure 30B**). We show that expression of CPSF1 led to a profound loss of HIF-1α protein that was reversed by proteasomal inhibition (**Figures 30 C-D**). Importantly, we found that HIF-1α was highly ubiquitinated following CPSF1 expression, thereby

establishing a link between this E3 ligase, ubiquitination and the 26S proteasome (**Figures 30 E-F**).

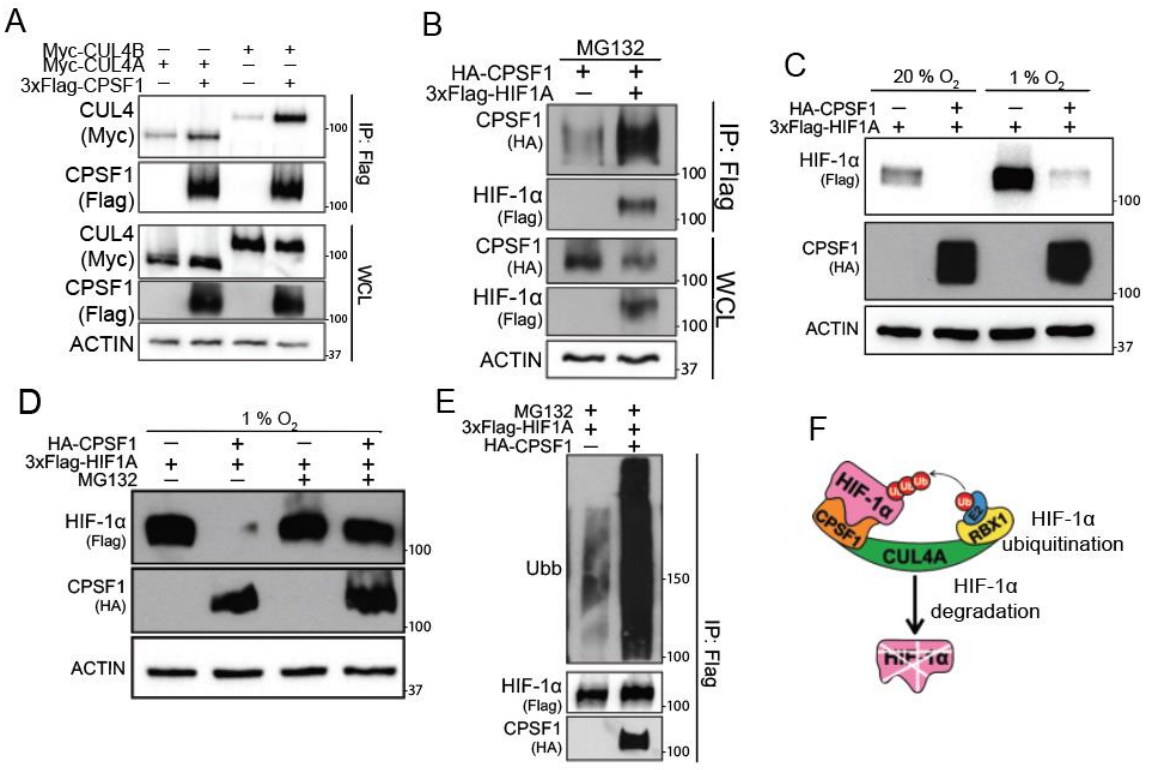

Figure 30: CPSF1 is a HIF-1*α* targeting E3-ligase. (A) IB analysis of IP and WCL derived from HEK293T cells transfected with 3xFlag-CPSF1 and Myc-CUL4/B constructs for 48 h. (B) IB analysis of IP and WCL derived HEK293T cells transfected with 3xFlag-HIF1A and HA-CPSF1 constructs for 24 h and then treated with MG132 during hypoxia for 24 h before harvesting. (C) IB analysis of WCL derived from HEK293T cells transfected with 3xFlag-HIF1A and HA-CPS1 constructs for 24 h and then exposed to normoxia or hypoxia for 24 h. (D) IB analysis of WCL derived from HEK293T cells transfected with 3xFlag-HIF1A and HA-CPSF1 constructs for 24 h and then treated with MG132 during hypoxia for 24 h before harvesting. (E) IB analysis of IP derived from HEK293T cells transfected with 3xFlag-HIF1A and HA-CSPF1 constructs for 24 h and then treated with MG132 for the final 24 h. (F) Proposed model depicting CPSF1-dependent HIF-1*α* ubiquitination and proteasome-mediated protein degradation.

3.2.7 CPSF1 is an E3 ligase targeting the HIF-1α DNA binding domain

We next mapped the sites/domains within HIF-1α that were required for CPSF1-dependent degradation. It was determined using deletion analysis that a mutant encompassing the basic-helix-loop-helix (bHLH) DNA binding domain (DBD) of HIF-1α (AA 1-71) remained responsive to CPSF1 (**Figure 31A**). Since the structures of full length CPSF1 and the DBD of HIF-1α are available, we performed *in silico* docking of the HIF-1α DBD onto CPSF1 using the HDOCK protein-protein docking server. CPSF1 was predicted to interact with the HIF-1α DBD using the equivalent pocket that DDB1 uses to interact with DDB2 (**Figure 31B**) (177). The CPSF1 paralog DDB1 has been shown to interact with DxR/DxxR/DxxxR motifs in binding partners, and mutation of the D and R residues are often sufficient to break complex formation (181). Thus, we evaluated whether the single DxxR motif in the HIF-1α DBD might be engaged at the HIF-1α-CPSF1 interface. Indeed, mutation of D24 and R27 to alanine residues (HIF-1α D24A/R27A) resulted in a HIF-1α protein that was not subject to degradation by CPSF1 (**Figure 31C, lanes 2 and 4**). Further, HIF-1α DRAA failed to co-immunoprecipitate with CPSF1 (**Figure 31D**). HIF-1α D24 is predicted to pair with CPSF1 R1049 using the HDOCK program (**Figure 31B**). Notably, a CPSF1 R1049A mutant did not induce HIF-1α turnover (**Figure 31B**). Together, these results support a role for CPSF1 as a component of an E3-ligase targeting HIF-1α.

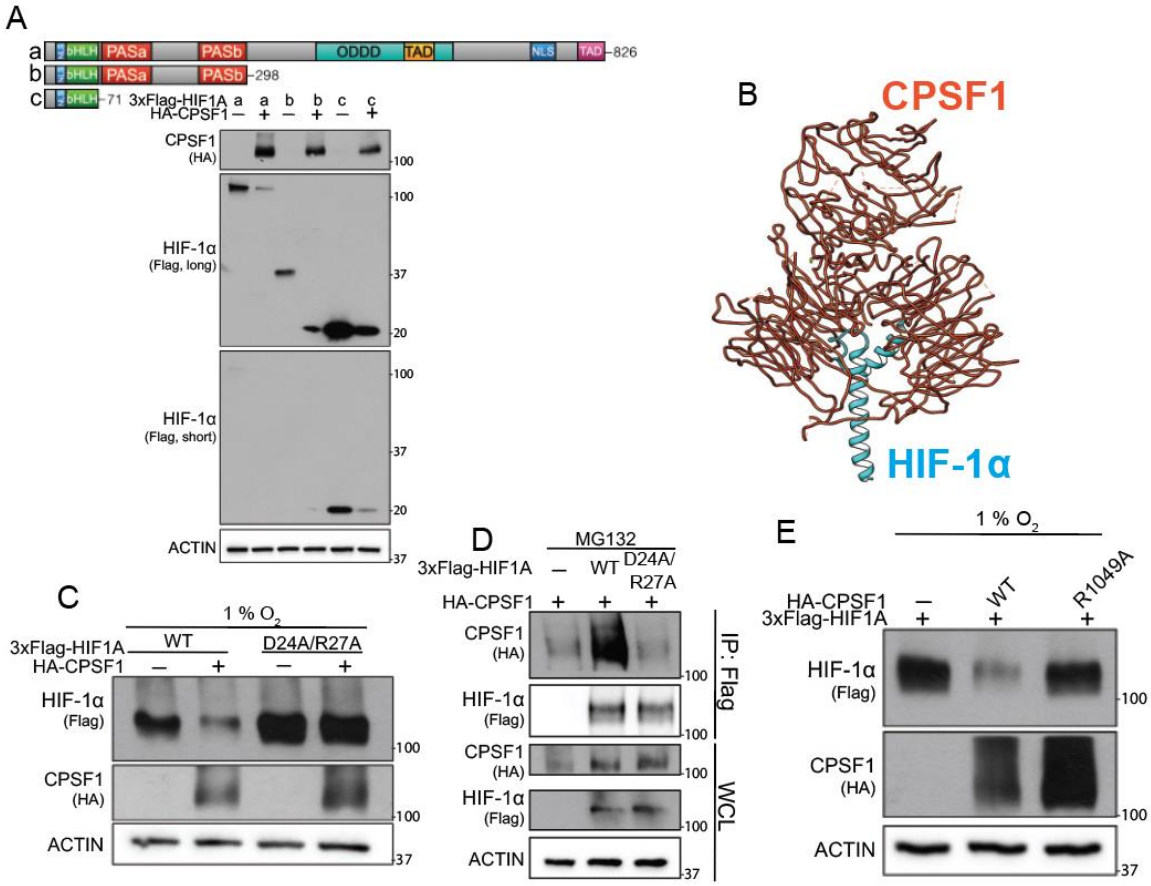

Figure 31: CPSF1 is an E3 ligase targeting the HIF-1α DNA binding domain. (A, top) Structural diagram of full length CPSF1 and truncation mutants. (A, bottom) IB analysis of WCL derived from HEK293T cells transfected with HA-CPSF1 and indicated 3xFlag-HIF1A truncation constructs for 24 h and exposed to hypoxia for 24 h. (B) HDOCK protein-protein docking server prediction of the interaction of full-length CPSF1 (PDB: 6F9N) with HIF-1α AA 1-71 (PDB:4ZPR). CPSF1 is shown in orange and HIF-1α is shown in blue. (C) IB analysis of WCL derived from HEK293T cells transfected with indicated 3xFlag-HIF1A and HA-CPSF1 constructs for 24 h and exposed to hypoxia for 24 h. (D) IB and IP analysis of WCL derived from HEK293T cells transfected with HA-CPSF1 and indicated 3xFlag-HIF1A constructs for 24 h and exposed to hypoxia for 24 h. (E) IB analysis of WCL derived from HEK293T cells transfected with 3xFlag-HIF1A and indicated HA-CPSF1 constructs for 24 h and exposed to hypoxia for 24 h.

3.2.8 ABL kinases protect HIF-1α from CPSF1 dependent degradation

To determine if CPSF1 is the E3-ligase responsible for ABL inhibitor dependent HIF-1α turnover we generated pools of cells (in the PC9 and HEK293T cell background) in which CPSF1 was knocked out using CRISPR/Cas9. In these CPSF1-depleted cells HIF-1α protein is stabilized and is rendered insensitive to ABL kinase inhibition. (**Figure 32A**). Further, expression of ABL1 reversed the CPSF1-dependent loss of HIF-1α (**Figure 32B**). These data are consistent with the hypothesis that ABL kinases support the stabilization of HIF-1α by inhibiting CPSF1 activity (**Figure 32C).**

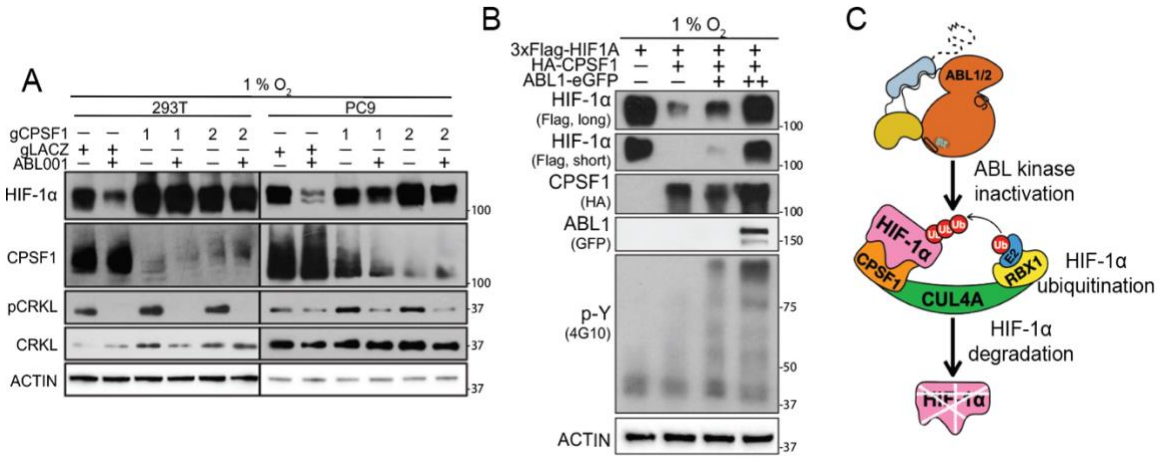

Figure 32 ABL kinases protect HIF-1α from CPSF1 dependent degradation. (A) IB analysis of WCL derived from 293T and PC9 cells transduced with indicated gRNA/CRISPR-Cas9 constructs lentiviruses and treated with ABL001 during hypoxia for 24 h. (B) IB analysis of WCL derived from HEK293T cells transfected with 3xFlag-HIF1A, ABL1-eGFP, and HA-CPSF1 constructs for 24 h and then exposed to hypoxia for 24 h. (C) Proposed model depicting loss of ABL kinase activity leading to CPSF1-dependent HIF-1α ubiquitination and proteasome-mediated protein degradation.

3.2.9 ABL kinases protect MYC from CPSF1 dependent degradation

We next mined the BioGRID database for additional CPSF1 interactors. Using a dataset generated in U2OS cells, we found that MYC might be a potential CPSF1 interactor (179, 182). MYC, like HIF-1α, is a bHLH transcription factor that functions as an oncoprotein by inducing expression of genes that drive cancer pathobiology (183). Indeed, we showed that CPSF1 immunoprecipitates with MYC in the presence of a proteasome inhibitor, and that increased expression of CPSF1 led to a dose-dependent loss of MYC protein levels that was reversed upon proteasomal inhibition (**Figures 33 A-C**).

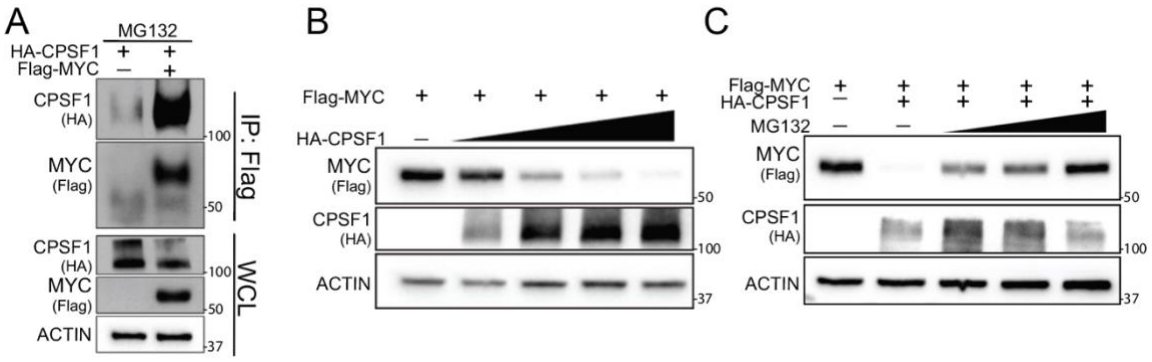

Figure 33: CPSF1 is a MYC targeting E3-ligase. (A) IB analysis of IP and WCL derived HEK293T cells transfected with Flag-MYC and HA-CPSF1 constructs for 48 h. (B) IB analysis of WCL derived from HEK293T cells transfected with Flag-MYC and HA-CPSF1 constructs for 48 h. (C) IB analysis of WCL derived from HEK293T cells transfected with Flag-MYC and HA-CPSF1 constructs for 24 h and then treated with MG132 for 24 h before harvesting during normoxia.

Importantly, activation of ABL1 led to an increase in MYC protein levels (**Figure 34A**). Moreover, treatment with ABL kinase inhibitors decreased endogenous and exogenous MYC protein levels in a proteasome dependent manner under normoxic

conditions (**Figures 34 B-D**). Further, expression of exogenous activated ABL1-EE reversed the CPSF1-dependent degradation of MYC (**Figure 34E**). These studies highlight a previously unknown mechanism by which MYC protein levels are regulated in cancer.

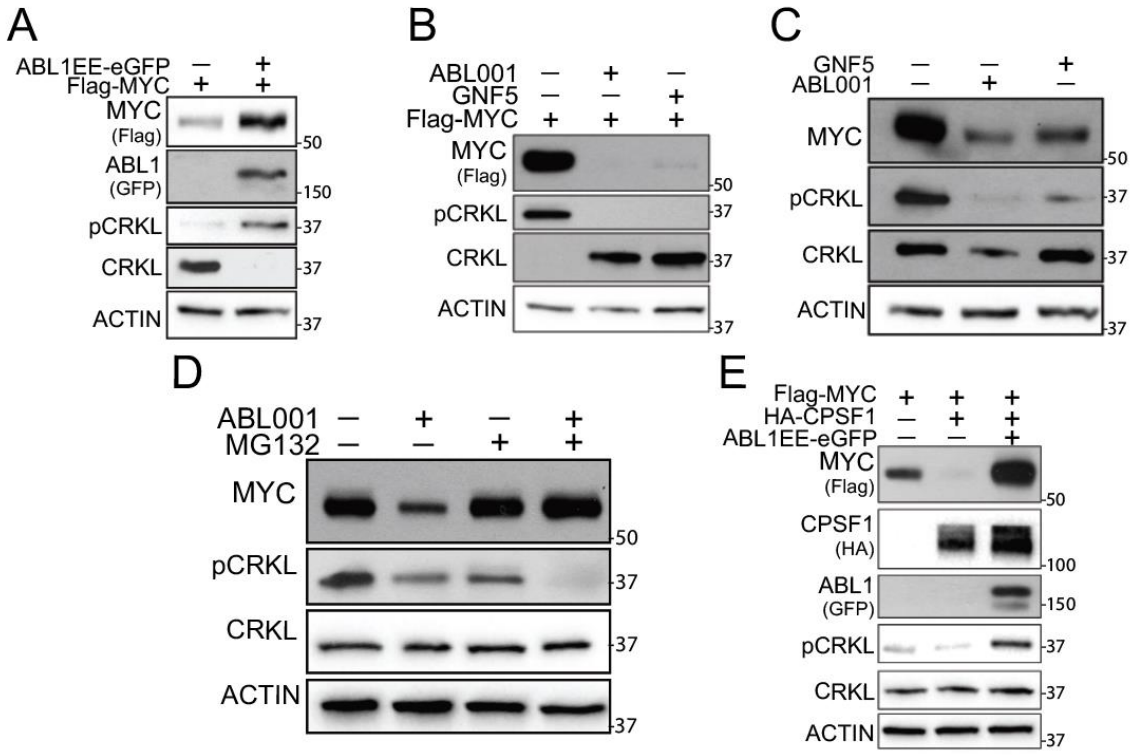

Figure 34: ABL kinases protect MYC from CPSF1 dependent degradation. (A) IB analysis of WCL derived from HEK293T cells transfected with Flag-MYC and ABL1-eGFP constructs for 48 h during normoxia. (B) IB analysis of WCL derived from HEK293T cells transfected Flag-MYC for 24 h and then treated with ABL001 and GNF5 as indicated for 24 h during normoxia. (C and D) IB analysis of WCL derived from PC9 cells treated with ABL001, GNF5, and MG132 as indicated for 24 h during normoxia. (E) IB analysis of WCL derived from HEK293T cells transfected with Flag-MYC, ABL1-eGFP, and HA-CPSF1 constructs for 48 h.

3.3 Discussion

The mechanism governing the normoxic turnover of HIF-1α by oxygen dependent prolyl-hydroxylation, ubiquitination by the VHL E3-ligase complex, and degradation by the 26S proteasome is well understood and validated (161-165). In contrast, much less is known regarding the regulators that maintain HIF-1α protein levels during hypoxia beyond inactivation of PHD1-3 (168). Our studies revealed that ABL kinase activity is necessary for the maintenance of HIF-1α during hypoxia. The ABL non-receptor tyrosine kinases are central signal transducers that are commonly exploited by cells to survive environmental and chemical stresses (20, 60). We report that ABL kinase activity is necessary for the hypoxic accumulation of HIF-1α. Treatment with allosteric and orthosteric ABL kinase inhibitors leads to a striking loss of HIF-1α protein levels in multiple cell and cancer types during hypoxia. Moreover, knockdown of the ABL kinases individually or together ablates hypoxic HIF-1α protein levels. Conversely, activation of the ABL kinases by point mutations or treatment with an allosteric activator is sufficient to decrease HIF-1α ubiquitination and increase total HIF-1α levels. These findings demonstrate that the ABL kinases are a druggable node that can be utilized to modulate HIF-1α protein levels.

We took an unbiased approach to identify the ABL-dependent E3-ligase(s) regulating HIF-1α protein stability. A FACS-based CRISPR/Cas9 screen using a custom E3-ligase targeted sgRNA library revealed CPSF1 as the ABL-dependent E3 ligase

regulator. CPSF1 is an understudied protein whose primary function is to serve as a core scaffolding component of the CPSF complex involved in 3′-polyadenylation of eukaryotic pre-mRNAs (175). Even though CPSF1 shares significant structural similarity with the known E3-ligase component DDB1 and immunoprecipitated CPSF1 complexes have been shown to possess *in vitro* E3-ligase activity (177, 178), to our knowledge no CPSF1 E3-ligase substrates have been previously identified.

In this study, we demonstrated that CPSF1 interacts with HIF-1α in cells in the presence of a proteasomal inhibitor. Ectopic expression of CPSF1 resulted in increased ubiquitination and proteasomal dependent degradation of HIF-1α. We mapped the interaction site of CPSF1 on HIF-1α to the HIF-1α DNA binding domain. Using *in silico* docking of the HIF-1α DBD onto CPSF1 and *in vitro* validation, we identified that amino acids D24 and R27 on HIF-1α and R1049 on CPSF1 are essential for the interaction. The site of interaction on HIF-1α (D24 and R27) is flanked by two mutation cluster regions found in patients tumors reported in the TCGA database (184). Even though genetic mutations in other genes have been shown to alter HIF-1α levels, few studies have investigated the impact of mutations in the *HIF1A* gene. Future studies evaluating the impact of these mutations on the CPSF1-dependent regulation of HIF-1α may be relevant in a disease setting. Further, we demonstrate that ABL kinases antagonize CPSF1-dependent degradation of HIF-1α as overexpression of ABL1 reversed the loss of HIF-1α after CPSF1 expression.

Tyrosine phosphorylation has been shown to regulate the proteasomal-degradation of substrates through multiple mechanisms including 1) phosphorylation of the substrate itself, 2) phosphorylation of the E3-ligase substrate receptor, and 3) phosphorylation of E3-ligase scaffolding proteins (185-187). Protein tyrosine kinases can promote activation of signaling cascades that target multiple steps of the ubiquitin-proteasomal degradation pathway (186-188). The ABL kinases and ABL-fusion proteins can regulate the stability of target proteins through direct tyrosine phosphorylation of substrates or activation of serine/threonine protein kinase signaling cascades (20, 25, 60, 189). Here we uncovered that ABL-meditated inactivation of the CPSF1 E3 ligase leads to degradation of HIF-1α in hypoxia conditions.

We found that the ABL1-CPSF1axis targets substrates other than HIF-1α. We mined the BioGRID database for CPSF1 interactors and identified an uncharacterized interaction between CPSF1 and the oncoprotein MYC (179, 182). MYC, like HIF-1α, belongs to the family of bHLH transcription factors and is commonly co-opted by cancer cells to drive expression of genes essential for tumor development and progression (183). We demonstrated that CPSF1 interacts with MYC. Further, expression of CPSF1 or loss of ABL kinase activity resulted in the proteasome mediated degradation of MYC. Conversely, activation of ABL1 was able to reverse the CPSF1 dependent loss of MYC. These findings suggest that the stability of both MYC and HIF-1α proteins are regulated

by an ABL-CPSF1 axis, and that these transcription factors might be effectively targeted by ABL kinase inhibitors (**Figure 35**).

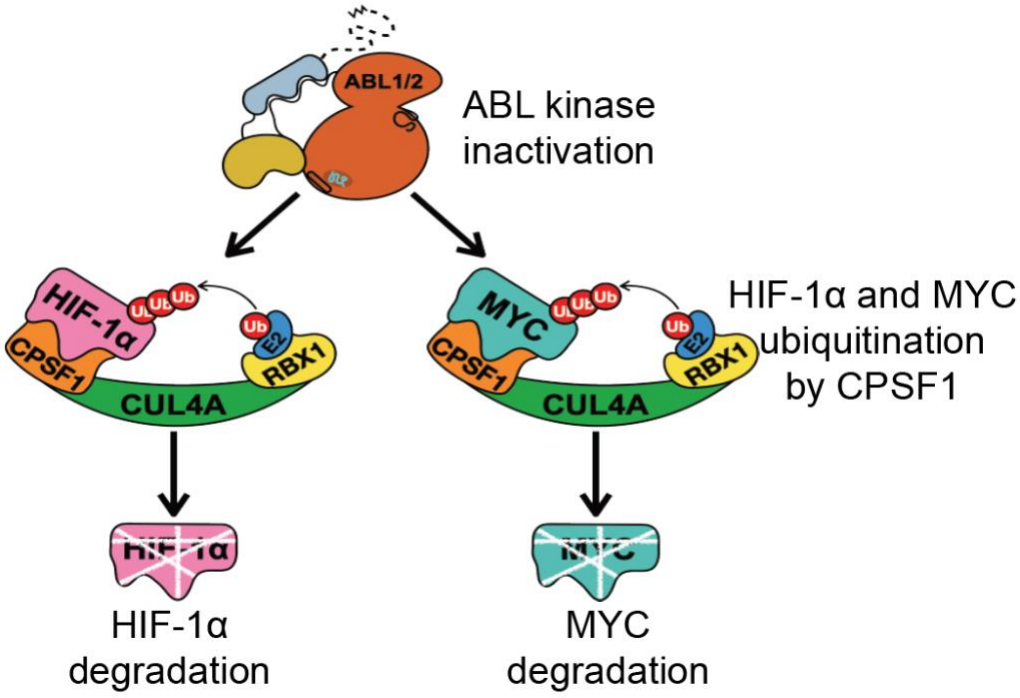

Figure 35: Model for the ABL kinases regulation of HIF-1*α* and MYC through CPSF1.

4. Conclusions and Discussion

The overarching aim of this body of work was to identify and interrogate transcription factor networks that are regulated by the ABL kinases. The majority of substrates that activated ABL kinases phosphorylate and regulate can be divided into two classes 1) cytoskeletal proteins and their regulators and 2) transcriptional regulators (25, 60). Previous work uncovered that the ABL2 kinase becomes activated in lung cancer brain metastatic cells, and this work demonstrates that ABL kinase activity becomes elevated in hypoxia. Supporting the role of active ABL kinases as regulators of transcription factors, we uncovered that the ABL2 kinase regulates HSF1 in lung cancer brain metastatic cells and HIF-1α in hypoxic cells.

We identified that brain metastatic lung cancer cell lines exhibit increased ABL tyrosine kinase activity and discovered a druggable, novel feed- forward signaling loop consisting of the nonreceptor tyrosine kinase ABL2, the receptor tyrosine kinase AXL, and the transcriptional co-activator TAZ(75). Subsequently, we uncovered that ABL2 mediates its brain metastatic cancer cell survival phenotype in part through the transcription factor HSF1. Two landmark papers revealed that 1) multiple cancer types become dependent on elevated HSF1 activity for survival, 2) the dependency on HSF1 increases as cells become more malignant, and 3) the transcriptional programs driven by HSF1 in cancer and heatshock are highly divergent (142, 144). We show that HSF1 protein levels are increased in brain metastatic lung cancer cells. Genetic inhibition of

HSF1 using shRNA knockdown resulted in a high level of cell death. Importantly, knockdown of HSF1 in a mouse model of lung cancer brain metastasis resulted in the ablation of the ability of brain metastatic lung cancer cells to colonize and outgrow in the brain parenchyma.

Our data demonstrated that HSF1 is required for survival of brain-metastatic cancer cells and suggest that targeting of HSF1 could be exploited as a potential therapeutic strategy. Despite the critical role of transcription factors (TFs) in many cancers, there has been limited success in the development of efficacious TF targeted inhibitors (190). Excitingly, we showed that the elevated HSF1 is indirectly targetable through ABL2 tyrosine kinase inhibition. Genetic knockdown of ABL2 led to a robust reduction of HSF1 protein levels and decreased expression of HSF1 target genes. Importantly, treatment (oral gavage) with the allosteric ABL inhibitor, ABL001, ablated HSF1 protein levels in established brain metastases, ascertaining that not only does the ABL2-HSF1 axis exist in vivo, but also ABL001 can reach tumors located in the brain in a mouse model of lung cancer brain metastasis. We observed HSF1 protein levels were only significantly lost upon treatment with STAMP ABL inhibitors with but not with Type II ABL inhibitors. We hypothesize this is due to the unique ability of the STAMP ABL inhibitors with but not with Type II ABL inhibitors to effectively disrupt the ABL2-HSF1 complex.

We and others have uncovered that the ABL kinases are central signal transducers utilized by cells undergoing diverse stress stimuli to activate pathways which are necessary for survival. The ABL kinases mediate this function, in part, by inducing the activation and/or stabilization of transcriptional regulators. Hypoxia is a form of cell stress that emerges due to low oxygen levels and the response to hypoxia is mediated by the transcription factor HIF-1α. Due to the ABL kinases often being activated by cell stress, we hypothesized that the ABL kinases may modulate the cellular response to hypoxia. Using mechanistic approaches, we uncovered that ABL kinase activity is necessary for the hypoxic stabilization of HIF-1α through a ubiquitin-proteasomal mechanism. Further, activation of the ABL kinases during normoxia was sufficient to elevate HIF-1α protein levels. To identify the ABL-dependent E3 ligase(s) regulating HIF-1α protein stability, we conducted a FACS-based CRISPR/Cas9 screen using a custom sgRNA library targeting 593 known and predicted human E3 ligases. The top scoring hit whose loss rescued HIF-1α protein levels during ABL inhibition was the understudied E3-ligase protein CPSF1. We showed that knockout of CPSF1 in cells ablated the ability of ABL kinase inhibition to decrease HIF-1α protein levels. Further, expression of ABL1 reversed the CPSF1-dependent loss of HIF-1α. We identified that the site of regulation on HIF-1α by CPSF1 was the bHLH DNA binding domain of HIF-1α. Using publicly available interactome datasets, we identified MYC as a second potential bHLH transcription factor interactor of CPSF1. We verified that CPSF1 expression

decreased MYC protein levels and the expression of ABL1 reversed the CPSF1-dependent loss of MYC.

4.1 Future Directions

This body of work identified and characterized the mechanisms through which the ABL family of tyrosine kinases modulate three critical cancer-related transcription factors, namely, TAZ, HSF1, and HIF-1α. Further, this work has laid the foundation for additional projects and testable hypotheses., some of which are below.

4.1.1 The impact of different classes of ABL kinase inhibitors on ABL interactome

We uncovered that ABL2 regulates an HSF1 transcriptional network in a model of lung cancer brain metastasis. A highlight of this study is that only allosteric ABL kinase inhibition, but not ATP- competitive inhibition 1) decreased HSF1 protein levels, 2) decreased HSF1 transcriptional targets, and 3) ablated the interaction between HSF1 and ABL2. Previous trainees in the Pendergast lab have uncovered various phenotypic divergences between the classes of ABL kinases inhibitors. Gu et al. uncovered that in NSCLC cell lines treatment with the Type II ABL inhibitor nilotinib led to a hyperactivation of the ERK pathway that was not observed with treatment with the STAMP inhibitor GNF5 (73). Wang et al. recapitulated this work in TNBC cell lines. This work demonstrated that treatment with the Type II ABL inhibitor imatinib led to a hyperactivation of the ERK pathway that was not observed with treatment with the

STAMP inhibitor GNF5 (74). Luttman et al. did extensive work discovering a cell death pathway that is differentially impacted by the different classes of ABL kinase inhibitors (191). This work demonstrated that the ABL STAMP inhibitors, ABL001 and GNF5, preferentially impair mitochondria function in lung cancer cells (191). However, neither Type II ABL inhibitors, nilotinib or imatinib, impacted mitochondria function (191). Further, this work demonstrated that HMGCR inactivation using statins sensitizes lung cancer cells to decreased colony formation and reduced cell viability in combination with STAMP inhibitors but not Type II ABL inhibitors (191).

One possible explanation of this phenotype is that the STAMP inhibitors and Type II ABL inhibitors differentially alter the interactome of the ABL kinases. This hypothesis is supported by our work showing that the HSF1 interaction is broken with ABL2 only upon treatment with a STAMP inhibitor. Further support is provided by Skora et al (155). This work revealed using NMR and cellular experiments that treatment with the Type II ABL inhibitor imatinib led to inactivation of ABL kinase activity and the adoption of the inactive active site structure (155). Surprisingly, the SH3 and SH2 remained undocked from the kinase domain. This can be partially explained by the αI helix remaining in the unbent position, which occludes the SH2 domain from docking onto the C-terminal kinase lobe. Divergently, treatment with the STAMP inhibitor GNF5 mirrors the insertion of the myristoyl moiety into the hydrophobic pocket unique to the ABL kinases (155). GNF5 treatment induced the bend of the αI helix, and the docking of

the SH2 and SH3 domains on the kinase domain (155). Future work identifying how Type I, Type II, and STAMP ABL inhibitors divergently and convergently impact the interactome of ABL1 and ABL2 may lead to 1) improved understanding of already observed phenotypes and 2) identification of additional signaling pathways divergently impacted by the different classes of ABL inhibitors. While Luttman et al. performed a sensitization CRISPR-Cas9 dependency screen using the STAMP inhibitor GNF5 (191). Future studies should extend this work with all three classes of ABL kinase inhibitors to determine universal and selective sensitizing agents.

4.1.2 The use of an HSF1 inhibitor in a model of lung cancer brain metastasis.

We uncovered that brain metastatic lung cancer cells are highly dependent on HSF1 in both *in vitro* and *in vivo* models. After the publication of our work, a direct HSF1 inhibitor (DTHIB) targeting the HSF1 DNA binding domain was reported (192). In immunocompetent and immunocompromised mouse models of pancreatic cancer treatment of DTHIB lead to cancer regression (192). Future studies examining the impact of DTHIB alone or in combination with an ABL STAMP inhibitor in a mouse model of brain metastatic lung cancer cells may provide enhanced therapeutic effects.

4.1.2 Determination of the CPSF1-mediated degradome.

We identified the first two substrates of the CPSF1 E3-ligase complex using a low-throughput, hypothesis driven approach. Future work interrogating the CPSF1-

mediate degradome using an unbiased proteomics approach would reveal additional substrates. The two substrates we identified, HIF-1α and MYC, are bHLH transcription factors. Importantly, we demonstrated that the site of regulation by CPSF1 is the bHLH DNA binding domain. The bHLH transcription factor in humans contains over 130 family members divided into five families (Family A- Family E) (193). HIF-1α and MYC are located on different branches of the E Family (193). It would be of interest to determine whether additional bHLH transcription factors are CPSF1 substrates, and, if so, whether the substrates cluster in the E Family or whether CPSF1-regulation uncovers a novel way of categorizing the the bHLH transcription factor superfamily. We identified that the CPSF1-dependent regulation of HIF-1α and MYC is antagonized by ABL kinase activity. If we identify additional CPSF1-substrates, it will be worthwhile to investigate if they are also ABL-dependent.

4.1.3 Interrogation of the ABL-CPSF1- HIF-1α/ MYC axes in in vivo models.

We identified a signaling pathway where elevated ABL kinase activity protects two transcription factors, HIF-1α and MYC, from CPSF1-dependent degradation. Both HIF-1α and MYC are oncogenic transcription factors that are utilized by multiple solid tumor types to support tumor initiation, progression, and metastasis (162, 183). Future work should thus determine if ABL kinase inhibitor treatment induces the loss of HIF-1α and MYC *in vivo* using orthotopic and metastatic murine models of TNBC and NSCLC, if so, does ABL-dependent loss of HIF-1α/MYC lead to decreased tumor

progression/metastasis. Due to technical difficulty of performing immunohistochemistry for HIF-1α the protocols described in Hoefflin et al. should be followed for detection of HIF-1α protein levels in *in vivo* samples (194). Additionally, the translocation of the *MYC* gene to the heavily transcribed *immunoglobulin* promoters is the oncogenic event that leads to the formation Burkitt lymphoma (195). As these tumors are dependent on MYC protein expression, it be worthwhile to determine if ABL inhibition decreases MYC protein and tumor progression in an CPSF1-dependent manner in murine models of Burkitt lymphoma.

CPSF1 has been previously characterized to play a key role in pre-mRNA 3'-end formation, while our work describes an additional role of CPSF1 as part of an E3-ligase complex (177). Future work should endeavor to disentangle the impact of CPSF1 in these two roles by generating CPSF1 mutants that function either 1) exclusively as a member of an E3-ligase complex or 2) as part of the CPSF complex and subsequently interrogating the ability of these mutants to rescue the *in vitro* and *in vivo* phenotypes seen after loss of CPSF1 and ABL kinase inhibition.

4.1.4 Interrogation of the mutations in CPSF1, HIF-1α, MYC found in patients with cancer.

Datasets of patient tumors and cancer cells present mutations in the *HIF1A* and *MYC* genes (196, 197). Further, we identified the bHLH DBD as site of regulation on HIF-1α by CPSF1 and Kim et al. uncovered two mutational clusters that flank the CPSF1 binding site in the HIF-1α bHLH DBD (184). Future studies should examine if the *HIF1A*

and *MYC* patient mutations impact their protein product's half-life and, if so, determine if these effects are due to impaired CPSF1-dependent degradation.

4.1.5 Interrogation of the mechanism driving ABL kinase activity in hypoxia

We demonstrated that ABL kinase activity becomes elevated in hypoxia (**Figure 22B** and **Figure 36**). The ABL kinases can become activated through increased phosphorylation of key tyrosine residues (e.g., Y89, Y245, Y412) (25). The tyrosine phosphorylation status of the ABL kinases is modulated by the activity of RTKs and protein tyrosine phosphatases (PTPs) (25). Cancer cells adapt to low oxygen levels through the rewiring and activation of phosphorylation dependent signaling pathways (198, 199). Current research on tyrosine phosphorylation in hypoxia has mainly concentrated on HIF-related transcriptional activation of RTKs (e.g., EGFR, MET, and AXL) and RTK ligands (e.g., EGF and GAS6) (198). Additionally, hypoxia has been shown to elevate the activity and/or protein levels of multiple PTPs, such SHP-2, PTP-PEST, and PTPRZ1 (200-202). Contrarily, hypoxia has also been shown to decrease the expression and/or activity of other PTPs, such as PTP-1B, PTP-SH1 and PTP-SH2 (203). Therefore, future work should identify if the elevated ABL kinase activity is mediated by hypoxia induced elevation of RTK activity, hypoxia induced diminishing of PTP activity, or a combination of both. Further, the individual RTKs and PTPs that mediate the elevated ABL kinase activity should be identified as well as the mechanism for their hypoxia induced (in)-activation.

Appendix A: List of Primers

Table 1: List of Primers. All primers were purchased through Sigma, and applications for each primer set are listed in parentheses.

Primer (Application)	Oligo Sequence
18S-F (RT-qPCR)	GAGGATGAGGTGGAACGTGT
18S-R (RT-qPCR)	AGAAGTGACGCAGCCCTCTA
AXL-F (RT-qPCR)	GTGGGCAACCCAGGGAATATC
AXL-R (RT-qPCR)	GTACTGTCCCGTGTCGGAAAG
ABL1-F (RT-qPCR)	AAGCCGCTCGTTGGAACTC
ABL1-R (RT-qPCR)	AGACCCGGAGCTTTTCACCT
ABL2-F (RT-qPCR)	GTTGAACCCCAGGCACTAAAT
ABL2-R (RT-qPCR)	CAACGAAGAGATTAGGGTCACTC
ATAD2-F (RT-qPCR)	AAGGAAGTTGAAACCTACCACCG
ATAD2-R (RT-qPCR)	GCAAGTTGCTCCGTTATTTCCA
CDC6-F (RT-qPCR)	CCAGGCACAGGCTACAATCAG
CDC6-R (RT-qPCR)	AACAGGTTACGGTTTGGACATT
DCTPP1-F (RT-qPCR)	CGCCTCCATGCTGAGTTTG
DCTPP1-R (RT-qPCR)	CCAGGTTCCCCATCGGTTTTC
DNMT1-F (RT-qPCR)	CCTAGCCCCAGGATTACAAGG
DNMT1-R (RT-qPCR)	ACTCATCCGATTTGGCTCTTTC
E2F1-F (RT-qPCR)	ACGTGACGTGTCAGGACCT
E2F1-R (RT-qPCR)	GATCGGGCCTTGTTTGCTCTT
E2F2-F (RT-qPCR)	CGTCCCTGAGTTCCCAACC
E2F2-R (RT-qPCR)	GCGAAGTGTCATACCGAGTCTT
E2F3-F (RT-qPCR)	AGAAAGCGGTCATCAGTACCT
E2F3-R (RT-qPCR)	TGGACTTCGTAGTGCAGCTCT
E2F4-F (RT-qPCR)	ATCGGGCTAATCGAGAAAAAGTC
E2F4-R (RT-qPCR)	TGCTGGTCTAGTTCTTGCTCC
E2F5-F (RT-qPCR)	TCATTCAGGACCTATCCATGTGC
E2F5-R (RT-qPCR)	GTCACTGGAGTCAAGGACTGG
E2F6-F (RT-qPCR)	TCCATGAACAGATCGTCATTGC
E2F6-R (RT-qPCR)	TCCGTTGGTGCTCCTTATGTG
E2F7-F (RT-qPCR)	AAAGGGACTATTCCGACCCAT
E2F7-R (RT-qPCR)	ACTTGGATAGCGAGCTAGAAACT
E2F8-F (RT-qPCR)	AAGTACGCCGAGCAGATTATG
E2F8-R (RT-qPCR)	ATGTCTGGGTGTCCATTTGGG
HIF1A-F (RT-qPCR)	GAACGTCGAAAAGAAAAGTCTCG
HIF1A-R (RT-qPCR)	CCTTATCAAGATGCGAACTCACA
MCM2-F (RT-qPCR)	ATGGCGGAATCATCGGAATCC
MCM2-R (RT-qPCR)	GGTGAGGGCATCAGTACGC
MCM3-F (RT-qPCR)	TCAGAGAGATTACCTGGACTTCC

MCM3-R (RT-qPCR)	TCAGCCGGTATTGGTTGTCAC
MCM4-F (RT-qPCR)	GACGTAGAGGCGAGGATTCC
MCM4-R (RT-qPCR)	GCTGGGAGTGCCGTATGTC
MCM6-F (RT-qPCR)	GAGGAACTGATTCGTCCTGAGA
MCM6-R (RT-qPCR)	CAAGGCCCGACACAGGTAAG
MCM7-F (RT-qPCR)	GCCTGTGGGAAATATCCCTCG
MCM7-R (RT-qPCR)	GTACCACCTGTCGGAACCC
NASP-F (RT-qPCR)	AGATTGGGAACCTAGAGCTTGC
NASP-R (RT-qPCR)	ACTTCTCCGAGTTTAAGATGTGC
PRKDC-F (RT-qPCR)	CCTGGCCGGTCATCAACTG
PRKDC-R (RT-qPCR)	AGTAAGGTGCGATCTTCTGGC
RANBP1-F (RT-qPCR)	AATACAGACGAGTCCAACCATGA
RANBP1-R (RT-qPCR)	GAACAGTTTTGCCCGCATTTTA
SMC1A-F (RT-qPCR)	AACCTGCGGGTAAAGACCCT
SMC1A-R (RT-qPCR)	GGCAAAGGTACGGTCCTCAG
SMC3-F (RT-qPCR)	ATGCGTGGAAGTCACTGCTGGA
SMC3-R (RT-qPCR)	GGCAGAAAAGTAACCTCTCCAGG
sgCPSF1 #1- F	AAGAAGCGAGTGGATGCGAG
sgCPSF1 #1- R	CTCGCATCCACTCGCTTCTT
sgCPSF1 #2- F	TACAGCGTGGACTTCATGGG
sgCPSF1 #2- R	CCCATGAAGTCCACGCTGTA
CPSF1 R1049E FWD	CTCGCCAGTCATGGCTGGGATGCGGGCA
CPSF1 R1049E REV	TGCCCGCATCCCAGCCATGACTGGCGAG
HIF1A D24A/R27A FWD (mutagenesis)	TCTTTACTTCGCCGAGATGCGGCTGCAGCTCGAGACTTTTCTTTTC
HIF1A D24A/R27A REV (mutagenesis)	GAAAAGAAAAGTCTCGAGCTGCAGCCGCATCTCGGCGAAGTAAAGA
HIF1A L72(STOP) FWD (mutagenesis)	ATCACCAGCATCCAGCTATTTCCTCACACGCAAATAGCTGATGGT
HIF1A L72(STOP) REV (mutagenesis)	ACCATCAGCTATTTGCGTGTGAGGAAATAGCTGGATGCTGGTGAT
HIF1A Q299(STOP) FWD (mutagenesis)	GTACTGTCCTGTGGTGACTTATCCTTTAGTAAACATATCATG
HIF1A Q299(STOP) REV (mutagenesis)	CATGATATGTTTACTAAAGGATAAGTCACCACAGGACAGTAC
ABL1 P249E FWD (mutagenesis)	TCTCCCACTTGTCGTAGTTCTCGGACACACCATAGACAGTG
ABL1 P249E REV (mutagenesis)	GCCCCAAAGCGCAACAAGGAGACTGTCTATGGTGTGTCC
ABL1 P242E FWD (mutagenesis)	GGACACACCATAGACAGTCTCCTTGTTGCGCTTTGGGGC
ABL1 P242E REV (mutagenesis)	GCCCCAAAGCGCAACAAGGAGACTGTCTATGGTGTGTCC

ABL1 P131L FWD (mutagenesis)	GGTGATGTAGTTGCTTAGGACCCATCCTTGGCC
ABL1 P131L REV (mutagenesis)	GGCCAAGGATGGGTCCTAAGCAACTACATCACC
ABL1 R171K FWD (mutagenesis)	CAGGACTGCTCTCACTCTCCTTCACCAAGAAGCTGCCATTG
ABL1 R171K REV (mutagenesis)	CAATGGCAGCTTCTTGGTGAAGGAGAGTGAGAGCAGTCCTG
ABL1 K290M FWD (mutagenesis)	CCTCCTTCAAGGTCATCACGGCCACCGTC
ABL1 K290M REV (mutagenesis)	GACGGTGGCCGTGATGACCTTGAAGGAGG
ABL2 P276E FWD (mutagenesis)	CATTTCCCACTTGTCATGGATCTCAGACACGCCATAGACGGTTGG
ABL2 P276E REV (mutagenesis)	CCAACCGTCTATGGCGTGTCTGAGATCCATGACAAGTGGGAAATG
ABL2 P269E FWD (mutagenesis)	AGACACGCCATAGACGGTCTCCTTGTTGCACTTCGGTGC
ABL2 P269E REV (mutagenesis)	GCACCGAAGTGCAACAAGGAGACCGTCTATGGCGTGTCT
ABL2 P158L FWD (mutagenesis)	AGTGATGTAGTTGCTTAGCACCCAACCCTGTCC
ABL2 P158L REV	GGACAGGGTTGGGTGCTAAGCAACTACATCACT
ABL2 R198K FWD (mutagenesis)	GCTGCTCTCACTCTCTTTGACCAGGAAGCTGCCG
ABL2 R198K REV (mutagenesis)	GCGGCAGCTTCCTGGTCAAAGAGAGTGAGAGCAGC
ABL2 K317M FWD (mutagenesis)	CTTCCTTCAGTGTCATCACAGCCACTGTAAGGCTGTACTT
ABL2 K317M REV (mutagenesis)	AAGTACAGCCTTACAGTGGCTGTGATGACACTGAAGGAAG
HSF1 1-129 FWD (mutagenesis)	CGCTGTCCTGGCGGATCTTCTAGTCTTCACTCTTCAGGGTG
HSF1 1-129 REV (mutagenesis)	CACCCTGAAGAGTGAAGACTAGAAGATCCGCCAGGACAGCG
HSF1 1-167 FWD (mutagenesis)	GGCCACCTCCCGCCACAGCTACTCATTCTCATGCTTCAT
HSF1 1-167 REV (mutagenesis)	ATGAAGCATGAGAATGAGTAGCTGTGGCGGGAGGTGGCC
HSF1 1-177 FWD (mutagenesis)	GGCCAGCCTTCGGTAGAAGCATGCCCA
HSF1 1-177 REV (mutagenesis)	GGCCAGCCTTCGGTAGAAGCATGCCCA
HSF1 1-187 FWD	TCAGGAACTGAATGAGCTTCTAGACGACTTTCTGTTGCTGG

(mutagenesis)	
HSF1 1-187 REV (mutagenesis)	CCAGCAACAGAAAGTCGTCTAGAAGCTCATTCAGTTCCTGA
HSF1 1-197 FWD (mutagenesis)	AGGATCCGGTTTGACTGCTACAGTGAGATCAGGAACTG
HSF1 1-197 REV (mutagenesis)	CAGTTCCTGATCTCACTGTAGCAGTCAAACCGGATCCT
HSF1 1-206 FWD (mutagenesis)	GGGGATCTTTCTCTACACCCCCAGGATCC
HSF1 1-206 REV (mutagenesis)	GGATCCTGGGGGTGTAGAGAAAGATCCCC
HSF1 1-287 FWD (mutagenesis)	GGGGGCTGCTGGATAGCTACCTCTCGTCTATGCTC
HSF1 1-287 REV (mutagenesis)	GAGCATAGACGAGAGGTAGCTATCCAGCAGCCCCC
HSF1 1-379 FWD (mutagenesis)	CACTGAGCTCATTCTTCTACAGGCAGGCTACGCTG
HSF1 1-379 REV (mutagenesis)	CAGCGTAGCCTGCCTGTAGAAGAATGAGCTCAGTG
HSF1 1-441 FWD (mutagenesis)	GCTCCTGGGGAGACAGCTACTCTTGGATACTGGCC
HSF1 1-441 REV (mutagenesis)	GCCAGTATCCAAGAGTAGCTGTCTCCCCAGGAGC
HSF1 187-195 del FWD (mutagenesis)	GGTTTGACTGCACCAGGACGACTTTCTGTTGC
HSF1 187-195 del REV (mutagenesis)	GCAACAGAAAGTCGTCCTGGTGCAGTCAAACC
HSF1 188-193 del FWD (mutagenesis)	TGACTGCACCAGTGAGATGTTGACGACTTTCTGTTG
HSF1 188-193 del REV (mutagenesis)	CAACAGAAAGTCGTCAACATCTCACTGGTGCAGTCA
sgRNA amplification FWD (CRISPR Screen)	AATGATACGGCGACCACCGAGATCTACACAATTTCTTGGGTAGTTTGCAGTT
sgRNA amplification REV (CRISPR Screen)	CAAGCAGAAGACGGCATACGAGAT
Read and index FWD (CRISPR Screen)	GATTTCTTGGCTTTATATATCTTGTGGAAAGGACGAAACACCG
Read and index REV (CRISPR Screen)	GCTAGTCCGTTATCAACTTGAAAAAGTGGCACCGAGTC

Appendix B: List of Antibodies

Table 2: List of Antibodies and Source Information.

ABL1 (8E9)	Millipore Sigma	MAB1130
ABL2 (6D5)	Abnova	H00000027-M03
Alexa Fluor 568 Phalloidin	Thermo Fisher	A12380
Anti-polyHistidine	Sigma	H1029
CDC6 (180.2)	Santa Cruz	sc-9964
CPSF1	Bethyl	A301-580A
CRKL (C-20)	Santa Cruz	sc-319
E2F1 (KH95)	Santa Cruz	sc-251
E2F8 (B-9)	Santa Cruz	sc-514064
FLAG (M2)	Millipore Sigma	F1804
GAPDH (6C5)	Santa Cruz	sc-32233
GFP	Cell Signaling	2956
Goat Anti-Rat IgG, HRP-linked	Cell Signaling	7077S
HA	Cell Signaling	2367
HIF-1α	BD Bioscience	610959
HIF-1β	Novus	NB100-124
HIF-2α	Novus	NB100-122
HSF1	Enzo Life Sciences	ADI-SPA-950-F
HSP90	Cell Signaling	4877S
Lamin B1 (D9V6H)	Cell Signaling	13435S
MYC	Cell Signaling	5605
Normal Mouse IgG	Santa Cruz	sc-2025
PE-conjugated HIF-1α	Biolegend	546-16

Peroxidase AffiniPure Goat Anti-Mouse IgG (H+L)	Jackson Immunoresearch	115-035-003
Peroxidase AffiniPure Goat Anti-Rabbit IgG (H+L)	Jackson Immunoresearch	115-035-144
Phospho-CrkL (Tyr207)	Cell Signaling	3181L
Phospho-HSF1 (Ser326)	Abcam	Ab76076
Phosphotyrosine (clone 4G10)	Millipore Sigma	05-321
Rabbit Anti-Mouse IgG (Light Chain Specific) (D3V2A)	Cell Signaling	58802S
TidyBlot	BioRad	STAR209
UBB	Santa Cruz	Sc-166553
β-Actin (8H10D10)	Cell Signaling	3700S

Appendix C: Materials and Methods

C.1: Cell lines and Cell Culture

Human HEK293T, MDA-MB-231, and SUM159, HCC4006, and H1975 cells were purchased from American Type Culture Collection (ATCC). PC9 parental, H2030 parental, and H2030-BrM3 cells were gifts from Joan Massagué (Memorial Sloan Kettering Cancer Center, New York). PC9-BrM3 and HCC4006-BrM cell lines were derived in the Pendergast laboratory by serial intracardiac injection(75). H460 cells were gifts from Fernando Lecanda (University of Navarra, Pamplona, Spain). Parental and derivative cell line pairs were subjected to short tandem repeat (STR) profiling through the Duke University DNA Analysis Facility Human cell line authentication (CLA) service to confirm their authenticity

The HEK293T cells and MDA-MB-231 cells were maintained in Dulbecco's Modified Eagle's Medium (DMEM) (Life Technologies) supplemented with 10% FBS. The SUM159 cells were maintained in Ham's F-12 Nutrient Mix (ThermoFisher) supplemented with 10% FBS, 10 mM Hepes, 5 μg/mL insulin, and 1 μg/mL hydrocortisone. The PC9, H2030, H460, HCC4006, and H1975 cells were maintained in RPMI 1640 (Life Technologies) supplemented with 10% FBS, 10 mM Hepes, 1 mM sodium pyruvate, and 0.2% glucose. All cells were grown at 37 °C in 5% CO2 with either 1 % or 20 % O2. Transient transfections were performed using Lipofectamine 2000 (Invitrogen) according to manufacturer instructions. Media was changed 24 h post

transfection and cells were harvested 24 h thereafter. Generation of lentivirus and transductions of target cell lines were performed as described previously (73, 75). For lentiviral expression of recombinant DNA, 2nd generation lentiviral packaging vectors (pMD2.G and PSPAX2) were used. Briefly, 293T cells were transfected with packaging DNAs and corresponding DNAs using FuGENE6 reagent (Promega). Culture supernatants containing virus were harvested and filtered 24 hours and 48 hours after transfection and were added to target cell cultures in the presence of 8 μg/mL polybrene (Sigma-Aldrich) a minimum of 6 h. Transduced cells were selected with 1 μg/mL puromycin.

For experiments assessing effects of pharmacologic agents in vitro, drugs were dissolved in DMSO unless indicated elsewise, with the final concentration of DMSO in culture media not exceeding 0.1% vol/vol. ABL001, GNF5, and Nilotinib were synthesized by the Duke University Small Molecule Synthesis Facility and were validated by 1H-NMR techniques and liquid chromatography–mass spectrometry. DPH (5-(1,3-diaryl-1H-pyrazol-4-yl)hydantoin, 5-[3-(4-fluorophenyl)-1-phenyl-1H-pyrazol-4-yl]-2,4-imidazolidinedione) (Sigma) was dissolved in DMSO. The proteasomal inhibitor MG132 (Selleckchem) was dissolved in DMSO. The hypoxia mimetic Cobalt Chloride ($CoCl_2$) (Sigma) was dissolved in water. All drugs were treated at concentrations indicated in figures and figure legends.

C.2: Plasmid construction

The following plasmids were obtained from Addgene. HA-HIF1alpha-pcDNA3 (#18949), pCMV4a-Flag-c-Myc (#102625), pcDNA3-myc3-CUL4A (#19951), pcDNA3-myc3-CUL4B (#19922), pCI-His-hUbi (#31815), 3xFLAG-FUS-WT (#44985), pcDNA3.1-HA (#128034). The pCMV-CPSF1-Flag-Myc (C203519) plasmid was purchased from Origene. The pcDNA-hHSF1 WT plasmid was a gift from Lea Sistonen (#71724) and the empty vector pcDNA3 Flag HA plasmid was a gift from William Sellers (#10792)

The shRNA constructs targeting the ABL kinases were described previously (75, 92). The pN1-ABL1 and ABL2 constructs were described previously(75, 92).

All constructs were confirmed by Sanger sequencing. The 3xFlag-HIF1A and CPSF1 constructs were generated by PCR amplification of HIF1A cDNA from HA-HIF1alpha-pcDNA3 and CPSF1 cDNA from pCMV-CPSF1-Flag-Myc prior to sub-cloning into the 3xFLAG-FUS-WT vector via restriction enzyme digestion. The HA-CPSF1 construct was generated by PCR amplification of CPSF1 cDNA from the pCMV-CPSF1-Flag-Myc plasmid and sub-cloned into the pcDNA3.1-HA construct after restriction enzyme digestion. The HA-Flag-HSF1 construct was generated by PCR amplification of HSF1 cDNA from pcDNA-hHSF1 WT plasmid and sub-cloned into the pcDNA3 HA-Flag construct after restriction enzyme digestion. Point mutation containing constructs were generated by using the QuickChange Lightning site-directed mutagenesis kit (Stratagene) according to the manufacturer's protocol.

The CPSF1 targeting gRNA-CRISPR/Cas9 lentiCRISPR2 constructs were generated using the Zhang lab protocol. The sgRNA sequences are listed below (5′-3′):

sgCPSF1 #1

1) FWD: AAGAAGCGAGTGGATGCGAG

2) REV: CTCGCATCCACTCGCTTCTT

sgCPSF1 #2

3) FWD: TACAGCGTGGACTTCATGGG

4) REV: CCCATGAAGTCCACGCTGTA

The tetracycline inducible shRNA constructs were generated using the following protocol. Sense and anti-sense oligos for respective shRNA sequences flanked by 5′ AgeI or 3′ EcoRI restriction site overhangs were mixed in 10X annealing buffer (1M NaCl, 100 mM Tris-HCl, pH=7.4) and annealed by placing in boiling water that was allowed to cool naturally to 30°C on a lab bench. The Tet-pLKO-puro vector backbone (Addgene #21915) was digested via restriction enzyme digest using AgeI and EcoRI (NEB), followed by gel-purification using the QIAquick Gel Extraction Kit (Qiagen). Gel-purified vector and annealed oligos were then ligated using T4 DNA ligase (NEB) followed by transformation into One Shot Stbl3 chemically competent cells (ThermoFisher). The following dox-inducible shRNA sequences were generated: HSF1 (Clone 7480: GCAGGTTGTTCATAGTCAGAA, cloneID: TRCN0000007480) (Clone 7481: GCACATTCCATGCCCAAGTAT, cloneID: TRCN0000007481), E2F1 (Clone 658:

CAGGATGGATATGAGATGGGA, cloneID: TRCN0000039658) (Clone 659: CGCTATGAGACCTCACTGAAT, cloneID: TRCN0000039659) and E2F8 (Clone 429: GCCCAGAAATCAGTCCAAATA, cloneID: TRCN0000017429) (Clone 800: GATGTTGGCTTAGTTTAATTT, cloneID: TRCN0000425800).

C.3: Immunoblot and Immunoprecipitation analyses

For Immunoblot analysis of whole cell lysates (WCL), cells were lysed in RIPA lysis buffer (RIPA buffer (50 mM Tris-HCl pH 7.4, 150 mM NaCl, 1 mM EDTA, 1% Triton X-100, 1% sodium deoxycholate and 0.1% SDS) containing protease-phosphatase inhibitor cocktail (Cell Signaling). Lysates were rotated for 10 min at 4 °C and cell debris were cleared by centrifugation at 15,000 RPM for 10 min at 4 °C. Protein concentration was determined using the DC Protein Assay (Bio-Rad). For WCL, 25 μg of total proteins were loaded per well.

For immunoprecipitation analysis, cells were lysed in RIPA lysis buffer (RIPA buffer (50 mM Tris-HCl pH 7.4, 150 mM NaCl, 1 mM EDTA, 1% Triton X-100, 1% sodium deoxycholate, and 0.1% SDS) containing protease-phosphatase inhibitor cocktail (Cell Signaling). Lysates were incubated on ice for 30 min and vortexed every ten minutes (30 min, 20 min, 10 min, and 0 min). Cell debris were cleared by centrifugation at 15,000 RPM for 10 min at 4 °C and protein concentration was determined using the DC Protein Assay (Bio-Rad). 1 mg of total protein were diluted to 800 μL and 200 μg of total protein were saved for later WCL immunoblotting. A total of 20 μL of anti-FLAG

M2 affinity gel was added to each sample and rotated overnight (~16 h) at 4 °C. Beads were washed three times with RIPA lysis buffer. Immunoprecipated proteins were eluted by boiling in 150 μL of 4x SDS Laemmli Sample Buffer (Biorad).

The immunocomplexes and WCL samples were separated by SDS-PAGE and transferred onto nitrocellulose membranes using the Transblot Turbo Transfer system (Bio-Rad). The nitrocellulose membranes were blocked in 5 % milk in TBST (20 mM Tris pH 7.6, 150 mM NaCl, and 0.1% w/v Tween 20 detergent) for 30 min at room-temperature and then incubated in primary antibodies overnight. All antibodies were diluted in 5 % milk in TBST, except for HIF-1α, HIF-2α, HIF-1β, pCRKL, and 4G10, which were diluted in 5 % BSA in TBST. Nitrocellulose membranes were washed 3 times with TBST and incubated in secondary antibodies diluted in 5 % milk in TBST for 1 h. After washing 3 times in TBST, the blots were developed using either film or a ChemiDoc XRS+ imager (Bio-Rad).

The following primary antibodies were used for immunoblot analyses: ABL1 (Sigma MAB1130 1:1000), ABL2 (Abnova, H00000027-M03, 1:500), ACTIN (Cell Signaling 3700 1:10000), CDC6 (Santa Cruz 180.2 sc-9964 1:1000), CPSF1 (Bethyl A301-580A 1:1000), CRKL (Santa Cruz sc-319 1:1000), CRKL p-Y207 (Cell Signaling 3181 1:500), Cyclin B1 (Santa Cruz H-20 sc-594 1:1000), Flag (Sigma M2 1:5000), E2F1 (Santa Cruz KH95 sc-251 1:1000), E2F2 (Santa Cruz TFE25sc-9967 1:1000), E2F3 (Santa Cruz PG30 sc-56665 1:1000), E2F4 (Santa Cruz RK-13 sc-511 1:1000), E2F6 (Santa Cruz TFE61 sc- 53273

1:1000), E2F8 (Santa Cruz B-9 sc-514064 1:1000), GFP (Cell Signaling 2956 1:1000), HA (Cell Signaling 2367 1:1000), HIF-1α (BD Bioscience 610959 1:1000), HIF-2α (Novus NB100-122 1:1000), HIF-1β (Novus NB100-124 1:1000), MYC (Cell Signaling 5605 1:5000), HSF1 (Enzo Life Sciences ADI-SPA-950-F); Phospho-HSF1 p-Ser326 (Abcam Ab76076 1:10000); HSP90 (Cell Signaling 4877S 1:2000), PARP (Cell Signaling 9542S 1:1000), PolyHistidine (Millipore Sigma H1029 1:2000), Ubb (Santa Cruz sc-166553 1:1000). and p-Y 4G10 (Sigma 05-321). The following secondary antibodies were used for immunoblot analyses: Peroxidase AffiniPure Goat Anti-Mouse IgG (H+L) (Jackson Immunoresearch 115-035-003 1:2000), AffiniPure Goat Anti-Mouse IgG (H+L) (Jackson Immunoresearch 115-035-1441:2000), TidyBlot (BioRad STAR209 1:500), Rabbit Anti-Mouse IgG (Light Chain Specific) (D3V2A) (58802S), Goat anti- Rat IgG, HRP-linked (7077S).

C.4: Real-time quantitative PCR

RNA was extracted and purified from cells using the RNeasy RNA Isolation Kit (QIAGEN). cDNA synthesis was generated by performing reverse transcription on 1 μg of total RNA using oligo(dT) primers and M-MLV reverse transcriptase (Invitrogen). Quantitative PCR was performed using Taq Universal SYBR Green Supermix (Bio-Rad). ad). All primers were purchased from Sigma Aldrich, and analysis of real-time data was collected using a Bio-Rad CFX384 machine and CFX Maestro software. Expression levels of target genes were normalized to 18S control housekeeping. Analysis was performed using the 2-ΔΔCt method.

C.5: Luciferase assay

Luciferase assay was performed using the Pierce Firefly Luciferase Glow Assay (Promega) according to the manufacturer-provided protocol. Cells were seeded into 96-well plates in triplicate and plates were read using a Tecan Infinite M1000 Microplate-Reader.

C.6: FACS screen

Lucifer A custom CRISPR sgRNA library targeting 593 known or predicted human E3 ligases (5 sgRNAs per gene, 2,965 total) and non-targeting controls (50 total) was designed and subsequently synthesized by Custom Array. The oligo pool was prepared and cloned into the lentiCRISPRv2 backbone (Addgene #52961) using Gibson assembly as described by Shalem et al., with minor modifications (204, 205). Lentivirus was produced by transfecting HEK293FT cells with the lentiCRISPRv2 sgRNA library plasmid pool and psPAX2 (Addgene #12260) and pMD2.G (Addgene #12259) packaging plasmids using lipofectamine 2000 and PLUS Reagent (Thermo). After 6 hours, the transfection mixture was replaced by harvest media (DMEM, 30% FBS). After 48 hours the virus-containing media was harvested, passed through a 0.45 um low-binding filter, and aliquoted and stored at -80oC. PC9 cells were seeded into non-tissue culture-treated 6-well plates at a density of 2x106 cells/well with 8 ug/mL polybrene and transduced at a low multiplicity of infection ~0.3 via spinfection to achieve greater than 3,000x coverage of the sgRNA library. Immediately following spinfection, cells were transferred from 6-

well plates to 15 cm tissue culture dishes at a seeding density of 4x106 cells per plate and were allowed to recover. After 24 hours, media was replaced with fresh media containing 2 ug/mL puromycin and cells selected for 48 hours. Cells were passaged and maintained above 3,000x coverage for 7 days post-spinfection to allow for stable integration and Cas9-directed knockout of target genes. Cells were then split into triplicate conditions (7.5x106 cells per replicate) and treated with 5 μM Nilotinib immediately prior to incubation in 1% O2 for 24 hours. After hypoxic incubation, cells were fixed and permeabilized using the eBioscience Foxp3 Transcription Factor Staining Buffer Set (Thermo) according to manufacturer recommendations, with minor modifications. Fixed and permeabilized cells were incubated overnight at 4 °C, rotating with a PE-conjugated HIF-1α antibody (Biolegend) at 5 μL per 1,000,000 cells. For each replicate, stained cells were then sorted by FACS, collecting the top and bottom 10% of HIF-1◎ expressing cells on the basis of PE signal; cell were collected in FBS-coated tubes, maintaining approximately 300x coverage per high and low population. An ungated control sample was also collected for each replicate. Immediately thereafter, collected samples were individually subjected to reverse-crosslinking and genomic DNA extraction using the Arcturus PicoPure DNA Extraction Kit (Thermo), according to manufacturer recommendations. sgRNA libraries were PCR-amplified from gDNA using NEBNext Ultra II Q5 Master Mix (New England BioLabs) according to manufacturer instructions, using the following primers:

FWD 5′-

AATGATACGGCGACCACCGAGATCTACACAATTTCTTGGGTAGTTTGCAGTT

ReV 5′- CAAGCAGAAGACGGCATACGAGAT (6 bp index sequence)

GACTCGGTGCCACTTTTTCAA

Amplified libraries were purified using SPRIselect beads (Beckman Coulter) using right-sided selection of 0.75x then to 1.2x the original volume. Each sample was quantified using the Quant-iT dsDNA Broad Range Assay Kit (Thermo). Samples were pooled and sequenced on a NextSeq 500 (Illumina) with 20bp single-end sequencing using the following custom read and index primers:

Custom Read 5′-

GATTTCTTGGCTTTATATATCTTGTGGAAAGGACGAAACACCG

Custom Index 5′- GCTAGTCCGTTATCAACTTGAAAAAGTGGCACCGAGTC

Raw sequencing read counts were trimmed and processed, and analysis of enrichment and depletion metrics comparing the top and bottom 10% sorted populations were performed using the MAGeCK software analysis pipeline under default settings.

C.7: Molecular docking

The HIF-1α DNA binding domain (AA 1-71) (PDB:4ZPR) was docked onto full-length CPSF1 (PDB: 6F9N) using the HDOCK protein-protein docking server

(http://hdock.phys.hust.edu.cn/). The predicted complexes with the highest scores were visualized using Chimera (UCSF).

C.8: RNA-sequencing analysis

For differential expression analysis of RNA-seq data comparing PC9 parental to PC9- BrM3 cells, total RNA was collected from equally sub-confluent cell cultures using the RNeasy (Qiagen) and 1 μg total RNA input was used for each sample. For differentional expression analysis comparing PC9-BrM3 Tet-shNTC vs Tet-shHSF1 (clone 7480) knockdown cells, PC9-BrM3 cells were plated overnight and were then treated with 500 ng/mL doxycycline for 48 hrs to induce shRNA knockdown prior to RNA isolation. Libraries were sequenced on an Illumina HiSeq 2000 sequencing system using 50-bp single-end reads by the Duke University Genome Sequencing facility. RNA-seq fastq data files were processed using the TrimGalore toolkit followed by read quality assessment with the Fast-QC analysis tool. Reads were mapped to the GRCh37 version of the human genome and transcriptome using the HISAT2 RNA-seq alignment tool (206). Reads were used for subsequent analysis if they mapped to a single genomic location, and gene counts were compiled using FeatureCounts (207). Normalization and differential expression were carried out using the DESeq2 Bioconductor package (208) in the R statistical programming environment. Datasets containing differential expression analysis corresponding to each RNA-seq experiment are provided as Supplementary

File 1 and Supplementary File 2. RNA sequencing raw data have been deposited in the NCBI Gene Expression Omnibus (GEO) under accession number GSE149246.

C.9: Gene set enrichment analysis

Following analysis of RNA-seq differential expression data comparing PC9 parental to PC9-BrM3 cells, data were sorted by statistical rank and imported into the GSEA software tool from the Broad Institute (152). The pre-ranked gene list was processed under default settings and size filters for analysis across all signatures contained within the following mSigDB databases: Hallmark (v6.2, 50 gene sets), Positional (v6.2, 259 gene sets), Curated (v6.2, 3,648 gene sets), Motif (v6.2, 776 gene sets), Computational (v6.2, 782 gene sets), Gene Ontology (v6.2, 4,364 gene sets), Oncogenic Signatures (v6.2, 187 gene sets), and Immunologic Signatures (v6.2, 4,872 gene sets).

C.10: Generation of HSF1-regulated E2F target gene panel

Following differential expression analysis of RNA-seq data from PC9-BrM3 Tet-shNTC vs Tet-shHSF1 RNA, a list of E2F-related target gene signatures depleted by HSF1 knockdown were assembled and compared for shared gene targets to create what we termed a "conserved" E2F target gene panel. Depleted E2F-related signatures available through the mSigDB that were included in the analysis were the HALLMARK_E2F_TARGETS, KONG_E2F3_TARGETS, E2F_03, E2F_Q3, E2F1_Q6, and E2F_Q4_01 signatures. We included E2F target genes from each of these signatures if

they were common to at least five of the six signatures, which generated a final list of 15 E2F targets. The genes included in this final list were: E2F8, MCM7, DNMT1, RANBP1, DCTPP1, MCM2, PRKDC, MCM4, MCM6, ATAD2, SMC1A, SMC3, NASP, MCM3, and CDC6.

To generate the HSF1 heat shock-induced gene panel, we analyzed HSF1 ChIP-sequencing data from Mendillo et al, 2012 (142). We created a rank order list of genes sorted by peak height values for HSF1 binding in low-malignant BPE cells, high-malignant BPLER derivative cells, or low-malignant BPE cells exposed to 42 °C heat shock (BPE+HS) as described in the original study. Gene lists were filtered to include gene targets bound by HSF1 under BPE+HS conditions to generate a list of 1569 heat shock-induced gene targets; genes that also scored in BPE control or BPLER samples in addition to BPE+HS were excluded. This filtered list of heat shock-induced genes was then cross-referenced to the present PC9-BrM3 Tet-shHSF1 knockdown RNA-seq dataset to identify log2foldchange values for each gene in the setting of brain metastasis. As a final filtering step, the top 20 genes from the BPE+HS gene list with reads present in the PC9-BrM3 RNA-sequencing data were included to form a representative HSF1 heat shock target gene panel.

C.11: Chromatin immunoprecipitation and quantitative PCR (ChIP-qPCR)

ChIP-qPCR analysis was performed as previously described (75). Briefly, cells were cross- linked with formaldehyde (1% final concentration) on ice for 5 min with

gentle shaking. Formaldehyde was quenched by adding 125 M glycine in PBS for 5 min on ice with gentle shaking. Cells were then lysed in cell lysis buffer (25 mM Tris, pH 7.5, 150 mM NaCl, 1 mM EDTA, 1% Triton X-100, 0.1% SDS) containing protease and phosphatase inhibitors and transferred to a 15 mL conical tube for 15 min on ice. 1 mL of IP buffer (50 mM Tris, pH 7.5, 150 mM NaCl, 1 mM EDTA, 1% Triton X-100) was added, and lysates were then sonicated ten times for 30 s each on ice using a microprobe on setting 5. Lysates were cleared by spinning down cellular debris at 13,000 RPM at 4°C for 30 min. Samples containing antibody against HSF1 (Enzo) or IgG control were rotated overnight at 4°C, after which Dynabeads Protein G were added to all samples and rotated at 4°C for 43h. Beads were washed twice with IP buffer, twice with IP buffer + 0.5 M NaCl, and twice with TE Buffer (10 mM Tris, pH 7.5, 1 mM EDTA). Proteins were then eluted by adding TE buffer + 1% SDS and incubating at 65°C for 10 min, and beads were spun down at 14,000 rpm for 10 min. Samples were then incubated overnight at 65°C to reverse cross- links, followed by treatment with proteinase K for 1.5 h at 37 °C and purification with a PCR cleanup kit (Qiagen) prior to analysis via qPCR.

C.12: Nuclear/Cytosolic Subcellular Fractionation Immunoprecipitation

ChIP-qPCR Cells plated onto 15 cm dishes were harvested by trypsinization and pelleted by spinning at 1,000 RPM for 4 min. The cell pellet was washed with 5 mL PBS, pelleted by centrifugation, and then resuspended in 1 mL PBS, transferred to a 1.5 mL tube, and re- pelleted. The cell pellet was resuspended in 500 μL cytosolic lysis buffer

(20 mM Tris- HCl, pH 7.5, 10 mM NaCl, 3 mM MgCl2) and incubated for 15 min on ice. 25 μL of 10 % NP-40 was added to the cell homogenate and the sample was vortexed for 10 s followed by centrifugation at 3,000 RPM for 10 min at 4°C. The supernatant was then removed and designated as the cytosolic fraction. The remaining nuclear pellet was resuspended in nuclear lysis buffer (50 mM Tris-HCl, pH 7.5, 150 mM NaCl, 1% NP-40) and incubated on ice for 30 min with vortexing at 10 min intervals. The sample was spun down at 14,000 RPM at 4°C for 30 min. The supernatant was transferred to a new 1.5 mL tube and designated the nuclear fraction. 1000 μg of each fraction were used for subsequent immunoprecipitation following the method described above.

C.13: FACS analysis

Subconfluent monolayers of PC9-BrM3 cells transduced with inducible shRNAs against non-target control (shNTC) or HSF1 (shHSF1 clone 7481) were treated with 500 ng/mL doxycycline for 48 h prior to harvest by trypsinization, fixation by EtOH, and staining with propidium iodide using the Propidium Iodide Flow Cytometry Kit (Abcam #ab139418) following the manufacturer-supplied protocol. Fixed and stained cells were analyzed by FACS on a BD FACSCanto IIs analyzer. Post-FACS cell cycle analysis was performed using FlowJo 10 software.

C.14: Kaplan-Meier Analysis and Mutual Exclusivity Analysis

Lung adenocarcinoma patient microarray data were analyzed using the KMplot analysis tool (kmplot.com) (209). Patient groups were stratified by tertile (n=720 total

patients across all cohorts). Affimetrix identifiers for each gene were as follows: 228361_at (E2F1), 219990_at (E2F8), 218782_s_at (ATAD2), (CDC6), 210543_s_at (PRKDC), 202482_x_at (RANBP1), 202107_s_at (MCM2), 201555_at (MCM3), 212142_at (MCM4), 210983_s_at (MCM7). Survival data were plotted in GraphPad Prism 8 software. Mutual exclusivity analysis of HSF1-E2F target genes was performed with CBioPortal using the TCGA. Provisional lung adenocarcinoma dataset (n=515 patients) (89, 196). A user-defined list of the 15 gene HSF1-E2F target panel was used, and patients with mRNA expression data (RNAseq, z-score threshold ± 2.0) were included. Heatmaps of patient cohorts were generated using default clustering settings on CBioPortal, and mutual exclusivity analysis heatmaps were plotted using GraphPad Prism 8 software.

C.15: Immunofluorescence and confocal microscopy

For immunofluorescence staining and imaging of HSF1 protein, 100,000 PC9-BrM3 lung cancer cells transduced with pLKO-Tet-ON-shNTC or pLKO-Tet-ON-shHSF1 (clone 7480) constructs were plated in triplicate wells on 18 mm glass coverslips in 12-well dishes for 24 h to allow for cell adhesion. The following day, 500 ng/mL dox was added to each well for an additional 48 h. At endpoint, cells were fixed in 4% ice-cold PFA and blocked in 3% BSA in PBS (w/v) prior to staining with anti-HSF1 antibody (1:100, Enzo) overnight at 4°C. The following day, cells were incubated with goat anti-rat Alexa Fluor 568 secondary antibody (1:100, ThermoFisher) for 1 h and nuclei were

stained with Hoechst 33342 diluted 1:10,000 in PBS for 15 minutes. Slides were mounted onto coverslips with Dako Fluorescence mounting medium, cells were imaged using a Leica Inverted SP5 confocal microscope, and analysis was performed using ImageJ software (210).

C.16: Preparation of GST-tagged Proteins

Plasmids expressing GST, GST-ABL2 SH2, or GST-ABL2 SH3-SH2 were transformed in BL21 DE3 Escherichia coli. Protein expression was induced with 1 mM isopropyl-β-d-thiogalactoside for 6 h at 37°C. Cells were lysed by sonication in the following buffer: 125 mM Tris-HCl, pH 7.4, 150 mM NaCl, 1 mM EDTA, 1 mM DTT, 1 % v/v Triton X-100, and protease inhibitors. GST-fusion proteins were captured on glutathione- Sepharose beads, and bound proteins were washed twice with wash buffer (125 mM Tris- HCl, pH 7.4, 150 mM NaCl, 1 mM EDTA, 1 mM DTT) and eluted with elution buffer (125 mM Tris-HCl, pH 7.4, 150 mM NaCl, 50 mM reduced glutathione, 1 mM DTT, 1 % v/v Triton X-100). The proteins were buffer exchanged into storage buffer (20 mM Tris- HCl, pH 7.4, 150 mM NaCl, 10 % glycerol and 1 mM DTT), and the purified protein was aliquoted, flash frozen in liquid nitrogen, and stored at -80 °C.

C.17: Preparation of His-tagged Proteins

Human HSF1 was cloned into the pET-32A vector and transformed in BL21 Gold DE3 Escherichia coli cells. Protein expression was induced with 1 mM thiogalactoside for 6 h at 37°C. Cells were lysed by sonication in the following buffer: 20 mM Tris-HCl,

pH 7.5, 400 mM NaCl, 10 mM imidazole, 1 mM DTT, 0.1 % v/v Triton X-100, and protease inhibitors. His fusion proteins were captured on Ni-NTA beads, and bound proteins were washed twice with wash buffer (20 mM Tris-HCl, pH 7.5, 400 mM NaCl, 40 mM imidazole, 1 mM DTT) and eluted with elution buffer (20 mM Tris-HCl, pH 7.5, 200 mM NaCl, 250 mM imidazole, 0.1 % v/v Triton X-100, and 1 mM DTT). The proteins were buffer exchanged into storage buffer (20 mM Tris-HCl, pH 7.5, 200 mM NaCl, 0.1 % v/v Triton X-100, 10 % glycerol and 1 mM DTT), and the purified protein was aliquoted, flash frozen in liquid nitrogen, and stored at -80 °C.

C.18: In vitro GST-pulldown assay

Human GST-ABL2 fragments were added dissolved at a final concentration of 1 μM in binding buffer (25 mM Tris HCl, pH 7.5, 100 mM NaCl, 0.1%, 1 mM DTT, and 5% glycerol). A 30 μL aliquot of glutathione-Sepharose beads were added to each sample and incubated overnight at 4°C. An equal molar concentration of recombinant His-HSF1 was added to each sample and rotated at 4°C for 4 h. Reactions were subsequently washed three times with binding buffer and resuspended in Laemmli sample buffer. Interactions were visualized by immunoblotting as described above. The GST-ABL2-SH3 construct was generated from the GST-ABL2-SH3-SH2 construct through site directed mutagenesis by inserting a stop codon at L168. The primers used to generate this construct were FWD 5′-

GTACCAGGAATGTTTCTCCTAGCTATTAACTGGAGTGATGT-3′; REV 5′-ACATCACTCCAGTTAATAGCTAGGAGAAACATTCCTGGTACC-3′.

C.19: Cell viability assay

Cells transduced with inducible lentiviral shRNAs as described in figure legends were seeded in 96-well plates in at least triplicate and measured each day using CellTiter-Glo reagent (Promega). Plates were read on a Tecan Infinite M1000 Microplate Reader and results were analyzed in GraphPad Prism 8 software. For inducible constructs, cells were seeded (500 cells/well for PC9, 200 cells/well H2030) at the beginning of the study and 500 ng/mL doxycycline was added every 24 h to corresponding wells to examine the impact of knockdown on cell growth.

C.20: Promoter analysis of predicted degenerate HSF1 binding sites at E2F target genes

To identify predicted degenerate HSEs located near promoter regions of canonical E2F targets identified in the 15-gene HSF1-regulated E2F target gene panel, we utilized Ensembl to download reference sequences for each gene containing a minimum of 5kb base pairs upstream of the predicted transcriptional start site (TSS) for each gene. We used the coding sequence (CDS) regions as deposited on GenBank (NCBI) to determine the TSS for each gene. We validated each gene for the presence of the canonical E2F DNA binding motif sequence, *TTTnnCGC*, where "*n*" represents either a *C* or a *G* nucleotide. For the canonical HSE nucleotide sequence, we used the following

established sequence containing triple tandem inverted repeats: *nGAAnnTTCnnGAAn*, where "*n*" represents any nucleotide *A*, *T*, *C*, or *G*. We then created sequence search strings for partial variations of the canonical HSE, which we termed a "degenerate" HSE, that contained slight variations in nucleotide sequences near the 5′ or 3′ end of the canonical HSE. This approach was based off of the findings published by Li et al, 2016 (150), where a degenerate HSE was identified in C. elegans. The following search strings were used for the degenerate HSEs: *GAAnnTTC*, *AAnnTTCnnGA*, and *TTCnnGAA*. Degenerate HSE sequences were then used to search the promoter regions of genes from the E2F target panel.

C.21: Intracardiac injection

All animal studies were performed in accordance with protocols approved by the Duke University Division of Laboratory Animal Resources Institutional Animal Care and Use Committee (IACUC). PC9-BrM3 cells transduced with a stable pFU-luciferase-Tomato (pFuLT) lentiviral vector in addition to shRNA constructs as described in figure legends were injected intracardially and mice were subsequently monitored *in vivo* using an IVIS XR bioluminescent imager to confirm both proper anatomical injection as well as to monitor for metastatic disease progression. 8-12-week old age-matched female athymic nu/nu mice were used for all studies (Jackson Laboratory). Mice were anesthetized with 5% isoflurane prior to injections. For all studies, $4x10^5$ lung cancer cells suspended in 100 μL PBS were injected into the left cardiac ventricle with a 30-gauge needle and animals were monitored until full recovery from anesthesia.

ABL001 (Asciminib) was used to pharmacologically inhibit the ABL kinases in tumor-bearing mice *in vivo* and was prepared as a suspension in sterile 0.5% methylcellulose/0.5% Tween-80 as described previously(124). To evaluate the pharmacologic effects of ABL001 on ABL kinase activity and downstream signaling in brain metastases *in vivo*, mice were injected with H1975 pFulT lung cancer cells and metastatic burden was allowed to progress over the span of one month. Mice with established brain metastases were administered either vehicle or 100 mg/kg ABL001 via oral gavage at 3, 12, and 24 h prior to euthanasia and tissue harvest. Immediately following euthanasia, mouse brains were freshly dissected and tissue sections with visible brain metastases were excised and lysed in RIPA buffer containing protease-phosphatase inhibitor cocktail (Cell Signaling). Harvested samples were digested for 15 minutes on a rotator at 4ºC followed by centrifugation for 15 minutes at 4ºC to clear the lysate of myelin and cell debris. Protein lysates were temporarily stored at -20ºC prior to immunoblotting.

Appendix D: Statistical Analysis

Statistical analyses were performed using JMP software for *in vitro* experiments and GraphPad Prism 8 for *in vivo* experiments software. Statistical differences between groups were determined using a repeated measure ANOVA followed by post hoc testing (Tukey's) only when statistical significance was achieved from the ANOVA. A p-value of 0.05 was selected as the significance cutoff. All data shown indicated averages with SEM unless otherwise noted.

Mouse numbers per group were determined through statistical power calculations (α=0.05) where 10 mice per group allows for 90% power to detect inter-group differences of 50% and assuming intra-group variability of 25%. For Kaplan-Meier survival analysis, *p* values were calculated using log-rank (Mantel-Cox) testing. Statistical comparisons of 2 groups were conducted using Student's *t* tests (unpaired, two-tailed). For comparisons between groups of unequal size, the mean value was used to allow for statistical analysis by ANOVA.

Appendix E: ABL kinase activity during hypoxia

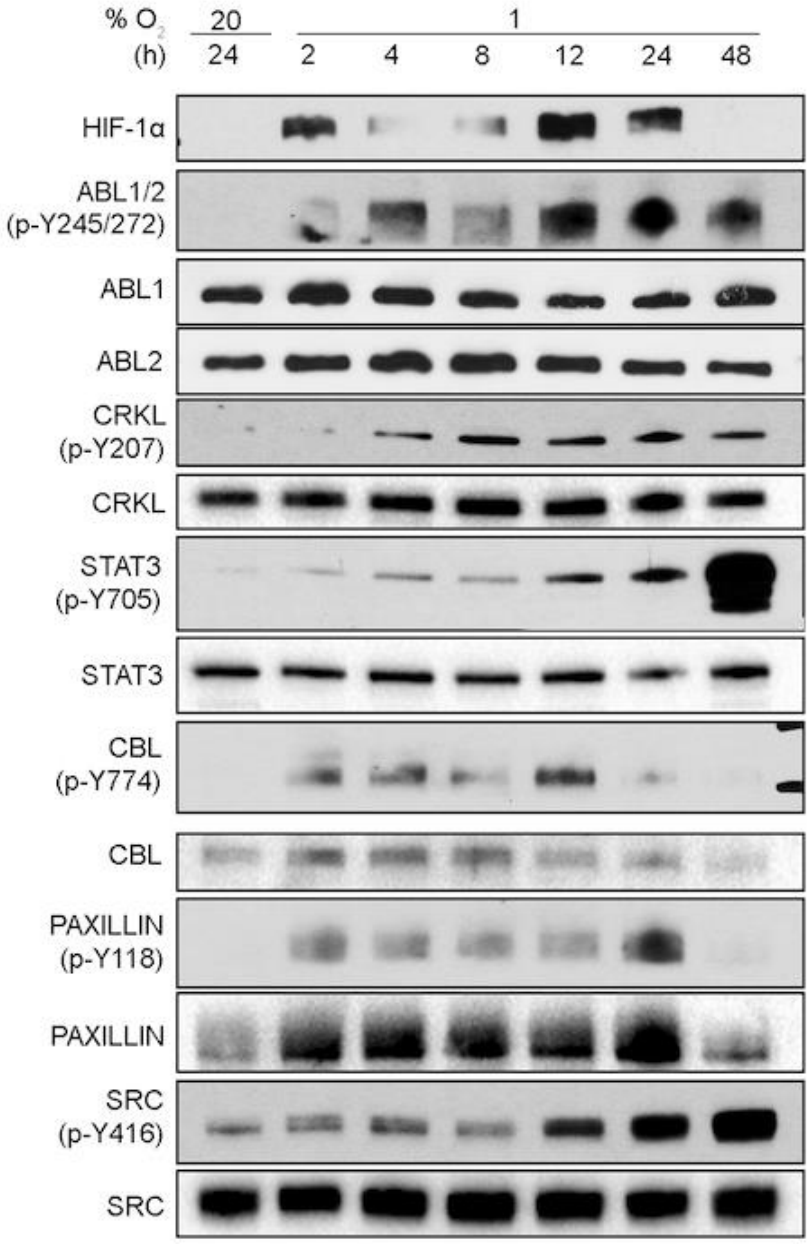

Figure 36: ABL kinase activity increases during hypoxia. Immunoblots (IB) analysis of whole cell lysates (WCL) derived from PC9 cells during normoxia or hypoxia (1 % O_2) for indicated time.

References

1. Manning G, Whyte DB, Martinez R, Hunter T, Sudarsanam S. The protein kinase complement of the human genome. Science. 2002;298(5600):1912-34. Epub 2002/12/10. doi: 10.1126/science.1075762. PubMed PMID: 12471243.

2. Hunter T. The genesis of tyrosine phosphorylation. Cold Spring Harb Perspect Biol. 2014;6(5):a020644. Epub 2014/05/03. doi: 10.1101/cshperspect.a020644. PubMed PMID: 24789824; PMCID: PMC3996475.

3. Lemmon MA, Schlessinger J. Cell signaling by receptor tyrosine kinases. Cell. 2010;141(7):1117-34. Epub 2010/07/07. doi: 10.1016/j.cell.2010.06.011. PubMed PMID: 20602996; PMCID: PMC2914105.

4. Ullrich A, Schlessinger J. Signal transduction by receptors with tyrosine kinase activity. Cell. 1990;61(2):203-12. Epub 1990/04/20. doi: 10.1016/0092-8674(90)90801-k. PubMed PMID: 2158859.

5. Schlessinger J. Signal transduction by allosteric receptor oligomerization. Trends Biochem Sci. 1988;13(11):443-7. Epub 1988/11/01. doi: 10.1016/0968-0004(88)90219-8. PubMed PMID: 3075366.

6. Collett MS, Erikson RL. Protein kinase activity associated with the avian sarcoma virus src gene product. Proc Natl Acad Sci U S A. 1978;75(4):2021-4. Epub 1978/04/01. doi: 10.1073/pnas.75.4.2021. PubMed PMID: 205879; PMCID: PMC392475.

7. Hunter T, Sefton BM. Transforming gene product of Rous sarcoma virus phosphorylates tyrosine. Proc Natl Acad Sci U S A. 1980;77(3):1311-5. Epub 1980/03/01. doi: 10.1073/pnas.77.3.1311. PubMed PMID: 6246487; PMCID: PMC348484.

8. Musacchio A, Saraste M, Wilmanns M. High-resolution crystal structures of tyrosine kinase SH3 domains complexed with proline-rich peptides. Nat Struct Biol. 1994;1(8):546-51. Epub 1994/08/01. doi: 10.1038/nsb0894-546. PubMed PMID: 7664083.

9. Mayer BJ, Hamaguchi M, Hanafusa H. Characterization of p47gag-crk, a novel oncogene product with sequence similarity to a putative modulatory domain of protein-tyrosine kinases and phospholipase C. Cold Spring Harb Symp Quant Biol. 1988;53 Pt 2:907-14. Epub 1988/01/01. doi: 10.1101/sqb.1988.053.01.104. PubMed PMID: 2855503.

10. Kurochkina N, Guha U. SH3 domains: modules of protein-protein interactions. Biophys Rev. 2013;5(1):29-39. Epub 2013/03/01. doi: 10.1007/s12551-012-0081-z. PubMed PMID: 28510178; PMCID: PMC5418429.

11. Overduin M, Rios CB, Mayer BJ, Baltimore D, Cowburn D. Three-dimensional solution structure of the src homology 2 domain of c-abl. Cell. 1992;70(4):697-704. Epub 1992/08/21. doi: 10.1016/0092-8674(92)90437-h. PubMed PMID: 1505033.

12. Sadowski I, Stone JC, Pawson T. A noncatalytic domain conserved among cytoplasmic protein-tyrosine kinases modifies the kinase function and transforming activity of Fujinami sarcoma virus P130gag-fps. Mol Cell Biol. 1986;6(12):4396-408. Epub 1986/12/01. doi: 10.1128/mcb.6.12.4396-4408.1986. PubMed PMID: 3025655; PMCID: PMC367222.

13. Panjarian S, Iacob RE, Chen S, Engen JR, Smithgall TE. Structure and dynamic regulation of Abl kinases. J Biol Chem. 2013;288(8):5443-50. Epub 2013/01/15. doi: 10.1074/jbc.R112.438382. PubMed PMID: 23316053; PMCID: PMC3581414.

14. Shah NH, Amacher JF, Nocka LM, Kuriyan J. The Src module: an ancient scaffold in the evolution of cytoplasmic tyrosine kinases. Crit Rev Biochem Mol Biol. 2018;53(5):535-63. Epub 2018/09/06. doi: 10.1080/10409238.2018.1495173. PubMed PMID: 30183386; PMCID: PMC6328253.

15. Siveen KS, Prabhu KS, Achkar IW, Kuttikrishnan S, Shyam S, Khan AQ, Merhi M, Dermime S, Uddin S. Role of Non Receptor Tyrosine Kinases in Hematological Malignances and its Targeting by Natural Products. Mol Cancer. 2018;17(1):31. Epub 2018/02/20. doi: 10.1186/s12943-018-0788-y. PubMed PMID: 29455667; PMCID: PMC5817858.

16. Scott JD, Pawson T. Cell communication: the inside story. Sci Am. 2000;282(6):72-9. Epub 2000/06/22. doi: 10.1038/scientificamerican0600-72. PubMed PMID: 10862426.

17. Songyang Z, Shoelson SE, Chaudhuri M, Gish G, Pawson T, Haser WG, King F, Roberts T, Ratnofsky S, Lechleider RJ, et al. SH2 domains recognize specific phosphopeptide sequences. Cell. 1993;72(5):767-78. Epub 1993/03/12. doi: 10.1016/0092-8674(93)90404-e. PubMed PMID: 7680959.

18. Songyang Z, Shoelson SE, McGlade J, Olivier P, Pawson T, Bustelo XR, Barbacid M, Sabe H, Hanafusa H, Yi T, et al. Specific motifs recognized by the SH2 domains of Csk, 3BP2, fps/fes, GRB-2, HCP, SHC, Syk, and Vav. Mol Cell Biol. 1994;14(4):2777-85.

Epub 1994/04/01. doi: 10.1128/mcb.14.4.2777-2785.1994. PubMed PMID: 7511210; PMCID: PMC358643.

19. Sparks AB, Rider JE, Hoffman NG, Fowlkes DM, Quillam LA, Kay BK. Distinct ligand preferences of Src homology 3 domains from Src, Yes, Abl, Cortactin, p53bp2, PLCgamma, Crk, and Grb2. Proc Natl Acad Sci U S A. 1996;93(4):1540-4. Epub 1996/02/20. doi: 10.1073/pnas.93.4.1540. PubMed PMID: 8643668; PMCID: PMC39976.

20. Greuber EK, Smith-Pearson P, Wang J, Pendergast AM. Role of ABL family kinases in cancer: from leukaemia to solid tumours. Nat Rev Cancer. 2013;13(8):559-71. Epub 2013/07/12. doi: 10.1038/nrc3563. PubMed PMID: 23842646; PMCID: PMC3935732.

21. Khatri A, Wang J, Pendergast AM. Multifunctional Abl kinases in health and disease. J Cell Sci. 2016;129(1):9-16. Epub 2016/01/06. doi: 10.1242/jcs.175521. PubMed PMID: 26729027; PMCID: PMC4732293.

22. Abelson HT, Rabstein LS. Lymphosarcoma: virus-induced thymic-independent disease in mice. Cancer Res. 1970;30(8):2213-22. Epub 1970/08/01. PubMed PMID: 4318922.

23. Ben-Neriah Y, Daley GQ, Mes-Masson AM, Witte ON, Baltimore D. The chronic myelogenous leukemia-specific P210 protein is the product of the bcr/abl hybrid gene. Science. 1986;233(4760):212-4. Epub 1986/07/11. doi: 10.1126/science.3460176. PubMed PMID: 3460176.

24. Kruh GD, Perego R, Miki T, Aaronson SA. The complete coding sequence of arg defines the Abelson subfamily of cytoplasmic tyrosine kinases. Proc Natl Acad Sci U S A. 1990;87(15):5802-6. Epub 1990/08/01. doi: 10.1073/pnas.87.15.5802. PubMed PMID: 2198571; PMCID: PMC54416.

25. Colicelli J. ABL tyrosine kinases: evolution of function, regulation, and specificity. Sci Signal. 2010;3(139):re6. Epub 2010/09/16. doi: 10.1126/scisignal.3139re6. PubMed PMID: 20841568; PMCID: PMC2954126.

26. Nagar B, Hantschel O, Young MA, Scheffzek K, Veach D, Bornmann W, Clarkson B, Superti-Furga G, Kuriyan J. Structural basis for the autoinhibition of c-Abl tyrosine kinase. Cell. 2003;112(6):859-71. Epub 2003/03/26. doi: 10.1016/s0092-8674(03)00194-6. PubMed PMID: 12654251.

27. Hantschel O, Nagar B, Guettler S, Kretzschmar J, Dorey K, Kuriyan J, Superti-Furga G. A myristoyl/phosphotyrosine switch regulates c-Abl. Cell. 2003;112(6):845-57. Epub 2003/03/26. doi: 10.1016/s0092-8674(03)00191-0. PubMed PMID: 12654250.

28. Xu W, Harrison SC, Eck MJ. Three-dimensional structure of the tyrosine kinase c-Src. Nature. 1997;385(6617):595-602. Epub 1997/02/13. doi: 10.1038/385595a0. PubMed PMID: 9024657.

29. Jackson P, Baltimore D. N-terminal mutations activate the leukemogenic potential of the myristoylated form of c-abl. EMBO J. 1989;8(2):449-56. Epub 1989/02/01. doi: 10.1002/j.1460-2075.1989.tb03397.x. PubMed PMID: 2542016; PMCID: PMC400826.

30. Barila D, Superti-Furga G. An intramolecular SH3-domain interaction regulates c-Abl activity. Nat Genet. 1998;18(3):280-2. Epub 1998/03/21. doi: 10.1038/ng0398-280. PubMed PMID: 9500553.

31. Brasher BB, Van Etten RA. c-Abl has high intrinsic tyrosine kinase activity that is stimulated by mutation of the Src homology 3 domain and by autophosphorylation at two distinct regulatory tyrosines. J Biol Chem. 2000;275(45):35631-7. Epub 2000/08/31. doi: 10.1074/jbc.M005401200. PubMed PMID: 10964922.

32. Hirai H, Varmus HE. SH2 mutants of c-src that are host dependent for transformation are trans-dominant inhibitors of mouse cell transformation by activated c-src. Genes Dev. 1990;4(12B):2342-52. Epub 1990/12/01. doi: 10.1101/gad.4.12b.2342. PubMed PMID: 1703982.

33. Grebien F, Hantschel O, Wojcik J, Kaupe I, Kovacic B, Wyrzucki AM, Gish GD, Cerny-Reiterer S, Koide A, Beug H, Pawson T, Valent P, Koide S, Superti-Furga G. Targeting the SH2-kinase interface in Bcr-Abl inhibits leukemogenesis. Cell. 2011;147(2):306-19. Epub 2011/10/18. doi: 10.1016/j.cell.2011.08.046. PubMed PMID: 22000011; PMCID: PMC3202669.

34. Nagar B, Hantschel O, Seeliger M, Davies JM, Weis WI, Superti-Furga G, Kuriyan J. Organization of the SH3-SH2 unit in active and inactive forms of the c-Abl tyrosine kinase. Mol Cell. 2006;21(6):787-98. Epub 2006/03/18. doi: 10.1016/j.molcel.2006.01.035. PubMed PMID: 16543148.

35. Filippakopoulos P, Kofler M, Hantschel O, Gish GD, Grebien F, Salah E, Neudecker P, Kay LE, Turk BE, Superti-Furga G, Pawson T, Knapp S. Structural coupling of SH2-kinase domains links Fes and Abl substrate recognition and kinase

activation. Cell. 2008;134(5):793-803. Epub 2008/09/09. doi: 10.1016/j.cell.2008.07.047. PubMed PMID: 18775312; PMCID: PMC2572732.

36. Mayer BJ, Hirai H, Sakai R. Evidence that SH2 domains promote processive phosphorylation by protein-tyrosine kinases. Curr Biol. 1995;5(3):296-305. Epub 1995/03/01. doi: 10.1016/s0960-9822(95)00060-1. PubMed PMID: 7780740.

37. Wojcik J, Hantschel O, Grebien F, Kaupe I, Bennett KL, Barkinge J, Jones RB, Koide A, Superti-Furga G, Koide S. A potent and highly specific FN3 monobody inhibitor of the Abl SH2 domain. Nat Struct Mol Biol. 2010;17(4):519-27. Epub 2010/04/02. doi: 10.1038/nsmb.1793. PubMed PMID: 20357770; PMCID: PMC2926940.

38. Duyster J, Baskaran R, Wang JY. Src homology 2 domain as a specificity determinant in the c-Abl-mediated tyrosine phosphorylation of the RNA polymerase II carboxyl-terminal repeated domain. Proc Natl Acad Sci U S A. 1995;92(5):1555-9. Epub 1995/02/28. doi: 10.1073/pnas.92.5.1555. PubMed PMID: 7533294; PMCID: PMC42558.

39. Popova M, Shimizu H, Yamamoto K, Lebechec M, Takahashi M, Fleury F. Detection of c-Abl kinase-promoted phosphorylation of Rad51 by specific antibodies reveals that Y54 phosphorylation is dependent on that of Y315. FEBS Lett. 2009;583(12):1867-72. Epub 2009/05/12. doi: 10.1016/j.febslet.2009.04.044. PubMed PMID: 19427856.

40. Songyang Z, Carraway KL, 3rd, Eck MJ, Harrison SC, Feldman RA, Mohammadi M, Schlessinger J, Hubbard SR, Smith DP, Eng C, et al. Catalytic specificity of protein-tyrosine kinases is critical for selective signalling. Nature. 1995;373(6514):536-9. Epub 1995/02/09. doi: 10.1038/373536a0. PubMed PMID: 7845468.

41. Cujec TP, Medeiros PF, Hammond P, Rise C, Kreider BL. Selection of v-abl tyrosine kinase substrate sequences from randomized peptide and cellular proteomic libraries using mRNA display. Chem Biol. 2002;9(2):253-64. Epub 2002/03/07. doi: 10.1016/s1074-5521(02)00098-4. PubMed PMID: 11880040.

42. Macias MJ, Wiesner S, Sudol M. WW and SH3 domains, two different scaffolds to recognize proline-rich ligands. FEBS Lett. 2002;513(1):30-7. Epub 2002/03/26. doi: 10.1016/s0014-5793(01)03290-2. PubMed PMID: 11911877.

43. Hernandez SE, Krishnaswami M, Miller AL, Koleske AJ. How do Abl family kinases regulate cell shape and movement? Trends Cell Biol. 2004;14(1):36-44. Epub 2004/01/20. doi: 10.1016/j.tcb.2003.11.003. PubMed PMID: 14729179.

44. Wen ST, Jackson PK, Van Etten RA. The cytostatic function of c-Abl is controlled by multiple nuclear localization signals and requires the p53 and Rb tumor suppressor gene products. EMBO J. 1996;15(7):1583-95. Epub 1996/04/01. PubMed PMID: 8612582; PMCID: PMC450068.

45. Henderson BR, Eleftheriou A. A comparison of the activity, sequence specificity, and CRM1-dependence of different nuclear export signals. Exp Cell Res. 2000;256(1):213-24. Epub 2000/03/31. doi: 10.1006/excr.2000.4825. PubMed PMID: 10739668.

46. Plattner R, Koleske AJ, Kazlauskas A, Pendergast AM. Bidirectional signaling links the Abelson kinases to the platelet-derived growth factor receptor. Mol Cell Biol. 2004;24(6):2573-83. Epub 2004/03/03. doi: 10.1128/MCB.24.6.2573-2583.2004. PubMed PMID: 14993293; PMCID: PMC355852.

47. Tanis KQ, Veach D, Duewel HS, Bornmann WG, Koleske AJ. Two distinct phosphorylation pathways have additive effects on Abl family kinase activation. Mol Cell Biol. 2003;23(11):3884-96. Epub 2003/05/16. doi: 10.1128/MCB.23.11.3884-3896.2003. PubMed PMID: 12748290; PMCID: PMC155218.

48. Furstoss O, Dorey K, Simon V, Barila D, Superti-Furga G, Roche S. c-Abl is an effector of Src for growth factor-induced c-myc expression and DNA synthesis. EMBO J. 2002;21(4):514-24. Epub 2002/02/16. doi: 10.1093/emboj/21.4.514. PubMed PMID: 11847100; PMCID: PMC125864.

49. Dorey K, Engen JR, Kretzschmar J, Wilm M, Neubauer G, Schindler T, Superti-Furga G. Phosphorylation and structure-based functional studies reveal a positive and a negative role for the activation loop of the c-Abl tyrosine kinase. Oncogene. 2001;20(56):8075-84. Epub 2002/01/10. doi: 10.1038/sj.onc.1205017. PubMed PMID: 11781820.

50. Schindler T, Sicheri F, Pico A, Gazit A, Levitzki A, Kuriyan J. Crystal structure of Hck in complex with a Src family-selective tyrosine kinase inhibitor. Mol Cell. 1999;3(5):639-48. Epub 1999/06/09. doi: 10.1016/s1097-2765(00)80357-3. PubMed PMID: 10360180.

51. Yamaguchi H, Hendrickson WA. Structural basis for activation of human lymphocyte kinase Lck upon tyrosine phosphorylation. Nature. 1996;384(6608):484-9. Epub 1996/12/05. doi: 10.1038/384484a0. PubMed PMID: 8945479.

52. Yoshida K, Yamaguchi T, Natsume T, Kufe D, Miki Y. JNK phosphorylation of 14-3-3 proteins regulates nuclear targeting of c-Abl in the apoptotic response to DNA damage. Nat Cell Biol. 2005;7(3):278-85. Epub 2005/02/08. doi: 10.1038/ncb1228. PubMed PMID: 15696159.

53. Yaffe MB, Rittinger K, Volinia S, Caron PR, Aitken A, Leffers H, Gamblin SJ, Smerdon SJ, Cantley LC. The structural basis for 14-3-3:phosphopeptide binding specificity. Cell. 1997;91(7):961-71. Epub 1998/01/15. doi: 10.1016/s0092-8674(00)80487-0. PubMed PMID: 9428519.

54. Nihira K, Taira N, Miki Y, Yoshida K. TTK/Mps1 controls nuclear targeting of c-Abl by 14-3-3-coupled phosphorylation in response to oxidative stress. Oncogene. 2008;27(58):7285-95. Epub 2008/09/17. doi: 10.1038/onc.2008.334. PubMed PMID: 18794806.

55. Jung JH, Pendergast AM, Zipfel PA, Traugh JA. Phosphorylation of c-Abl by protein kinase Pak2 regulates differential binding of ABI2 and CRK. Biochemistry. 2008;47(3):1094-104. Epub 2007/12/29. doi: 10.1021/bi701533j. PubMed PMID: 18161990.

56. di Bari MG, Ciuffini L, Mingardi M, Testi R, Soddu S, Barila D. c-Abl acetylation by histone acetyltransferases regulates its nuclear-cytoplasmic localization. EMBO Rep. 2006;7(7):727-33. Epub 2006/05/02. doi: 10.1038/sj.embor.7400700. PubMed PMID: 16648821; PMCID: PMC1500821.

57. Cao C, Li Y, Leng Y, Li P, Ma Q, Kufe D. Ubiquitination and degradation of the Arg tyrosine kinase is regulated by oxidative stress. Oncogene. 2005;24(15):2433-40. Epub 2005/03/01. doi: 10.1038/sj.onc.1208454. PubMed PMID: 15735735.

58. Soubeyran P, Barac A, Szymkiewicz I, Dikic I. Cbl-ArgBP2 complex mediates ubiquitination and degradation of c-Abl. Biochem J. 2003;370(Pt 1):29-34. Epub 2002/12/12. doi: 10.1042/BJ20021539. PubMed PMID: 12475393; PMCID: PMC1223168.

59. Echarri A, Pendergast AM. Activated c-Abl is degraded by the ubiquitin-dependent proteasome pathway. Curr Biol. 2001;11(22):1759-65. Epub 2001/11/24. doi: 10.1016/s0960-9822(01)00538-3. PubMed PMID: 11719217.

60. Wang JY. The capable ABL: what is its biological function? Mol Cell Biol. 2014;34(7):1188-97. Epub 2014/01/15. doi: 10.1128/MCB.01454-13. PubMed PMID: 24421390; PMCID: PMC3993570.

61. Luttman JH, Colemon A, Mayro B, Pendergast AM. Role of the ABL tyrosine kinases in the epithelial-mesenchymal transition and the metastatic cascade. Cell Commun Signal. 2021;19(1):59. Epub 2021/05/24. doi: 10.1186/s12964-021-00739-6. PubMed PMID: 34022881; PMCID: PMC8140471.

62. Baskaran R, Dahmus ME, Wang JY. Tyrosine phosphorylation of mammalian RNA polymerase II carboxyl-terminal domain. Proc Natl Acad Sci U S A. 1993;90(23):11167-71. Epub 1993/12/01. doi: 10.1073/pnas.90.23.11167. PubMed PMID: 7504297; PMCID: PMC47943.

63. Buratowski S. The CTD code. Nat Struct Biol. 2003;10(9):679-80. Epub 2003/08/28. doi: 10.1038/nsb0903-679. PubMed PMID: 12942140.

64. Mayer A, Heidemann M, Lidschreiber M, Schreieck A, Sun M, Hintermair C, Kremmer E, Eick D, Cramer P. CTD tyrosine phosphorylation impairs termination factor recruitment to RNA polymerase II. Science. 2012;336(6089):1723-5. Epub 2012/06/30. doi: 10.1126/science.1219651. PubMed PMID: 22745433.

65. Nie Y, Li HH, Bula CM, Liu X. Stimulation of p53 DNA binding by c-Abl requires the p53 C terminus and tetramerization. Mol Cell Biol. 2000;20(3):741-8. Epub 2000/01/11. doi: 10.1128/MCB.20.3.741-748.2000. PubMed PMID: 10629029; PMCID: PMC85189.

66. Goldberg Z, Vogt Sionov R, Berger M, Zwang Y, Perets R, Van Etten RA, Oren M, Taya Y, Haupt Y. Tyrosine phosphorylation of Mdm2 by c-Abl: implications for p53 regulation. EMBO J. 2002;21(14):3715-27. Epub 2002/07/12. doi: 10.1093/emboj/cdf384. PubMed PMID: 12110584; PMCID: PMC125401.

67. Haupt Y, Maya R, Kazaz A, Oren M. Mdm2 promotes the rapid degradation of p53. Nature. 1997;387(6630):296-9. Epub 1997/05/15. doi: 10.1038/387296a0. PubMed PMID: 9153395.

68. Yuan ZM, Shioya H, Ishiko T, Sun X, Gu J, Huang YY, Lu H, Kharbanda S, Weichselbaum R, Kufe D. p73 is regulated by tyrosine kinase c-Abl in the apoptotic response to DNA damage. Nature. 1999;399(6738):814-7. Epub 1999/07/03. doi: 10.1038/21704. PubMed PMID: 10391251.

69. Chen C, Shang X, Cui L, Xu T, Luo J, Ba X, Zeng X. L-selectin ligation-induced CSF-1 gene transcription is regulated by AP-1 in a c-Abl kinase-dependent manner.

Hum Immunol. 2008;69(8):501-9. Epub 2008/07/16. doi: 10.1016/j.humimm.2008.06.005. PubMed PMID: 18619508.

70. Gao B, Lee SM, Fang D. The tyrosine kinase c-Abl protects c-Jun from ubiquitination-mediated degradation in T cells. J Biol Chem. 2006;281(40):29711-8. Epub 2006/08/12. doi: 10.1074/jbc.M604596200. PubMed PMID: 16901904.

71. Levy D, Adamovich Y, Reuven N, Shaul Y. Yap1 phosphorylation by c-Abl is a critical step in selective activation of proapoptotic genes in response to DNA damage. Mol Cell. 2008;29(3):350-61. Epub 2008/02/19. doi: 10.1016/j.molcel.2007.12.022. PubMed PMID: 18280240.

72. Li B, He J, Lv H, Liu Y, Lv X, Zhang C, Zhu Y, Ai D. c-Abl regulates YAPY357 phosphorylation to activate endothelial atherogenic responses to disturbed flow. J Clin Invest. 2019;129(3):1167-79. Epub 2019/01/11. doi: 10.1172/JCI122440. PubMed PMID: 30629551; PMCID: PMC6391101.

73. Gu JJ, Rouse C, Xu X, Wang J, Onaitis MW, Pendergast AM. Inactivation of ABL kinases suppresses non-small cell lung cancer metastasis. JCI Insight. 2016;1(21):e89647. Epub 2016/12/27. doi: 10.1172/jci.insight.89647. PubMed PMID: 28018973; PMCID: PMC5161211.

74. Wang J, Rouse C, Jasper JS, Pendergast AM. ABL kinases promote breast cancer osteolytic metastasis by modulating tumor-bone interactions through TAZ and STAT5 signaling. Sci Signal. 2016;9(413):ra12. Epub 2016/02/04. doi: 10.1126/scisignal.aad3210. PubMed PMID: 26838548; PMCID: PMC4991033.

75. Hoj JP, Mayro B, Pendergast AM. A TAZ-AXL-ABL2 Feed-Forward Signaling Axis Promotes Lung Adenocarcinoma Brain Metastasis. Cell Rep. 2019;29(11):3421-34 e8. Epub 2019/12/12. doi: 10.1016/j.celrep.2019.11.018. PubMed PMID: 31825826; PMCID: PMC7254883.

76. Wong S, Witte ON. The BCR-ABL story: bench to bedside and back. Annu Rev Immunol. 2004;22:247-306. Epub 2004/03/23. doi: 10.1146/annurev.immunol.22.012703.104753. PubMed PMID: 15032571.

77. Nowell PC. The minute chromosome (Phl) in chronic granulocytic leukemia. Blut. 1962;8:65-6. Epub 1962/04/01. doi: 10.1007/BF01630378. PubMed PMID: 14480647.

78. Rowley JD. Letter: A new consistent chromosomal abnormality in chronic myelogenous leukaemia identified by quinacrine fluorescence and Giemsa staining. Nature. 1973;243(5405):290-3. Epub 1973/06/01. doi: 10.1038/243290a0. PubMed PMID: 4126434.

79. Shepherd P, Suffolk R, Halsey J, Allan N. Analysis of molecular breakpoint and m-RNA transcripts in a prospective randomized trial of interferon in chronic myeloid leukaemia: no correlation with clinical features, cytogenetic response, duration of chronic phase, or survival. Br J Haematol. 1995;89(3):546-54. Epub 1995/03/01. doi: 10.1111/j.1365-2141.1995.tb08362.x. PubMed PMID: 7734353.

80. Cario G, Leoni V, Conter V, Baruchel A, Schrappe M, Biondi A. BCR-ABL1-like acute lymphoblastic leukemia in childhood and targeted therapy. Haematologica. 2020;105(9):2200-4. Epub 2020/10/16. doi: 10.3324/haematol.2018.207019. PubMed PMID: 33054045; PMCID: PMC7556506.

81. Neuendorff NR, Burmeister T, Dorken B, Westermann J. BCR-ABL-positive acute myeloid leukemia: a new entity? Analysis of clinical and molecular features. Ann Hematol. 2016;95(8):1211-21. Epub 2016/06/15. doi: 10.1007/s00277-016-2721-z. PubMed PMID: 27297971.

82. Martiat P, Mecucci C, Nizet Y, Stul M, Philippe M, Cassiman JJ, Michaux JL, Van den Berghe H, Sokal G. P190 BCR/ABL transcript in a case of Philadelphia-positive multiple myeloma. Leukemia. 1990;4(11):751-4. Epub 1990/11/01. PubMed PMID: 2232886.

83. De Keersmaecker K, Rocnik JL, Bernad R, Lee BH, Leeman D, Gielen O, Verachtert H, Folens C, Munck S, Marynen P, Fornerod M, Gilliland DG, Cools J. Kinase activation and transformation by NUP214-ABL1 is dependent on the context of the nuclear pore. Mol Cell. 2008;31(1):134-42. Epub 2008/07/11. doi: 10.1016/j.molcel.2008.05.005. PubMed PMID: 18614052.

84. Papadopoulos P, Ridge SA, Boucher CA, Stocking C, Wiedemann LM. The novel activation of ABL by fusion to an ets-related gene, TEL. Cancer Res. 1995;55(1):34-8. Epub 1995/01/01. PubMed PMID: 7805037.

85. Golub TR, Goga A, Barker GF, Afar DE, McLaughlin J, Bohlander SK, Rowley JD, Witte ON, Gilliland DG. Oligomerization of the ABL tyrosine kinase by the Ets protein TEL in human leukemia. Mol Cell Biol. 1996;16(8):4107-16. Epub 1996/08/01. doi: 10.1128/MCB.16.8.4107. PubMed PMID: 8754809; PMCID: PMC231407.

86. Iijima Y, Ito T, Oikawa T, Eguchi M, Eguchi-Ishimae M, Kamada N, Kishi K, Asano S, Sakaki Y, Sato Y. A new ETV6/TEL partner gene, ARG (ABL-related gene or ABL2), identified in an AML-M3 cell line with a t(1;12)(q25;p13) translocation. Blood. 2000;95(6):2126-31. Epub 2000/03/09. PubMed PMID: 10706884.

87. De Braekeleer E, Douet-Guilbert N, Rowe D, Bown N, Morel F, Berthou C, Ferec C, De Braekeleer M. ABL1 fusion genes in hematological malignancies: a review. Eur J Haematol. 2011;86(5):361-71. Epub 2011/03/26. doi: 10.1111/j.1600-0609.2011.01586.x. PubMed PMID: 21435002.

88. Testoni E, Stephenson NL, Torres-Ayuso P, Marusiak AA, Trotter EW, Hudson A, Hodgkinson CL, Morrow CJ, Dive C, Brognard J. Somatically mutated ABL1 is an actionable and essential NSCLC survival gene. EMBO Mol Med. 2016;8(2):105-16. Epub 2016/01/14. doi: 10.15252/emmm.201505456. PubMed PMID: 26758680; PMCID: PMC4734836.

89. Cerami E, Gao J, Dogrusoz U, Gross BE, Sumer SO, Aksoy BA, Jacobsen A, Byrne CJ, Heuer ML, Larsson E, Antipin Y, Reva B, Goldberg AP, Sander C, Schultz N. The cBio cancer genomics portal: an open platform for exploring multidimensional cancer genomics data. Cancer Discov. 2012;2(5):401-4. Epub 2012/05/17. doi: 10.1158/2159-8290.CD-12-0095. PubMed PMID: 22588877; PMCID: PMC3956037.

90. Behbahani TE, Thierse C, Baumann C, Holl D, Bastian PJ, von Ruecker A, Muller SC, Ellinger J, Hauser S. Tyrosine kinase expression profile in clear cell renal cell carcinoma. World J Urol. 2012;30(4):559-65. Epub 2011/10/05. doi: 10.1007/s00345-011-0767-z. PubMed PMID: 21969129.

91. Wu CW, Li AF, Chi CW, Huang CJ, Huang CL, Lui WY, Lin WC. Arg tyrosine kinase expression in human gastric adenocarcinoma is associated with vessel invasion. Anticancer Res. 2003;23(1A):205-10. Epub 2003/04/12. PubMed PMID: 12680214.

92. McKernan CM, Khatri A, Hannigan M, Child J, Chen Q, Mayro B, Snyder D, Nicchitta CV, Pendergast AM. ABL kinases regulate translation in HER2+ cells through Y-box-binding protein 1 to facilitate colonization of the brain. Cell Rep. 2022;40(9):111268. Epub 2022/09/01. doi: 10.1016/j.celrep.2022.111268. PubMed PMID: 36044842; PMCID: PMC9472557.

93. Srinivasan D, Plattner R. Activation of Abl tyrosine kinases promotes invasion of aggressive breast cancer cells. Cancer Res. 2006;66(11):5648-55. Epub 2006/06/03. doi: 10.1158/0008-5472.CAN-06-0734. PubMed PMID: 16740702.

94. Srinivasan D, Sims JT, Plattner R. Aggressive breast cancer cells are dependent on activated Abl kinases for proliferation, anchorage-independent growth and survival. Oncogene. 2008;27(8):1095-105. Epub 2007/08/19. doi: 10.1038/sj.onc.1210714. PubMed PMID: 17700528.

95. Mader CC, Oser M, Magalhaes MA, Bravo-Cordero JJ, Condeelis J, Koleske AJ, Gil-Henn H. An EGFR-Src-Arg-cortactin pathway mediates functional maturation of invadopodia and breast cancer cell invasion. Cancer Res. 2011;71(5):1730-41. Epub 2011/01/25. doi: 10.1158/0008-5472.CAN-10-1432. PubMed PMID: 21257711; PMCID: PMC3057139.

96. Plattner R, Kadlec L, DeMali KA, Kazlauskas A, Pendergast AM. c-Abl is activated by growth factors and Src family kinases and has a role in the cellular response to PDGF. Genes Dev. 1999;13(18):2400-11. Epub 1999/09/29. doi: 10.1101/gad.13.18.2400. PubMed PMID: 10500097; PMCID: PMC317022.

97. Rossari F, Minutolo F, Orciuolo E. Past, present, and future of Bcr-Abl inhibitors: from chemical development to clinical efficacy. J Hematol Oncol. 2018;11(1):84. Epub 2018/06/22. doi: 10.1186/s13045-018-0624-2. PubMed PMID: 29925402; PMCID: PMC6011351.

98. Cohen MH, Williams G, Johnson JR, Duan J, Gobburu J, Rahman A, Benson K, Leighton J, Kim SK, Wood R, Rothmann M, Chen G, U KM, Staten AM, Pazdur R. Approval summary for imatinib mesylate capsules in the treatment of chronic myelogenous leukemia. Clin Cancer Res. 2002;8(5):935-42. Epub 2002/05/15. PubMed PMID: 12006504.

99. Capdeville R, Buchdunger E, Zimmermann J, Matter A. Glivec (STI571, imatinib), a rationally developed, targeted anticancer drug. Nat Rev Drug Discov. 2002;1(7):493-502. Epub 2002/07/18. doi: 10.1038/nrd839. PubMed PMID: 12120256.

100. Buchdunger E, O'Reilly T, Wood J. Pharmacology of imatinib (STI571). Eur J Cancer. 2002;38 Suppl 5:S28-36. Epub 2003/01/17. doi: 10.1016/s0959-8049(02)80600-1. PubMed PMID: 12528770.

101. Hantschel O, Rix U, Superti-Furga G. Target spectrum of the BCR-ABL inhibitors imatinib, nilotinib and dasatinib. Leuk Lymphoma. 2008;49(4):615-9. Epub 2008/04/10. doi: 10.1080/10428190801896103. PubMed PMID: 18398720.

102. Vijayan RS, He P, Modi V, Duong-Ly KC, Ma H, Peterson JR, Dunbrack RL, Jr., Levy RM. Conformational analysis of the DFG-out kinase motif and biochemical profiling of structurally validated type II inhibitors. J Med Chem. 2015;58(1):466-79. Epub 2014/12/06. doi: 10.1021/jm501603h. PubMed PMID: 25478866; PMCID: PMC4326797.

103. Garuti L, Roberti M, Bottegoni G. Non-ATP competitive protein kinase inhibitors. Curr Med Chem. 2010;17(25):2804-21. Epub 2010/07/01. doi: 10.2174/092986710791859333. PubMed PMID: 20586715.

104. Zhao Z, Wu H, Wang L, Liu Y, Knapp S, Liu Q, Gray NS. Exploration of type II binding mode: A privileged approach for kinase inhibitor focused drug discovery? ACS Chem Biol. 2014;9(6):1230-41. Epub 2014/04/16. doi: 10.1021/cb500129t. PubMed PMID: 24730530; PMCID: PMC4068218.

105. Ohren JF, Chen H, Pavlovsky A, Whitehead C, Zhang E, Kuffa P, Yan C, McConnell P, Spessard C, Banotai C, Mueller WT, Delaney A, Omer C, Sebolt-Leopold J, Dudley DT, Leung IK, Flamme C, Warmus J, Kaufman M, Barrett S, Tecle H, Hasemann CA. Structures of human MAP kinase kinase 1 (MEK1) and MEK2 describe novel noncompetitive kinase inhibition. Nat Struct Mol Biol. 2004;11(12):1192-7. Epub 2004/11/16. doi: 10.1038/nsmb859. PubMed PMID: 15543157.

106. Hasford J, Baccarani M, Hoffmann V, Guilhot J, Saussele S, Rosti G, Guilhot F, Porkka K, Ossenkoppele G, Lindoerfer D, Simonsson B, Pfirrmann M, Hehlmann R. Predicting complete cytogenetic response and subsequent progression-free survival in 2060 patients with CML on imatinib treatment: the EUTOS score. Blood. 2011;118(3):686-92. Epub 2011/05/04. doi: 10.1182/blood-2010-12-319038. PubMed PMID: 21536864.

107. Hochhaus A, Kreil S, Corbin AS, La Rosee P, Muller MC, Lahaye T, Hanfstein B, Schoch C, Cross NC, Berger U, Gschaidmeier H, Druker BJ, Hehlmann R. Molecular and chromosomal mechanisms of resistance to imatinib (STI571) therapy. Leukemia. 2002;16(11):2190-6. Epub 2002/10/26. doi: 10.1038/sj.leu.2402741. PubMed PMID: 12399961.

108. Nicolini FE, Mauro MJ, Martinelli G, Kim DW, Soverini S, Muller MC, Hochhaus A, Cortes J, Chuah C, Dufva IH, Apperley JF, Yagasaki F, Pearson JD, Peter S, Sanz Rodriguez C, Preudhomme C, Giles F, Goldman JM, Zhou W. Epidemiologic study on survival of chronic myeloid leukemia and Ph(+) acute lymphoblastic leukemia patients with BCR-ABL T315I mutation. Blood. 2009;114(26):5271-8. Epub 2009/10/22. doi: 10.1182/blood-2009-04-219410. PubMed PMID: 19843886; PMCID: PMC4916939.

109. Azam M, Seeliger MA, Gray NS, Kuriyan J, Daley GQ. Activation of tyrosine kinases by mutation of the gatekeeper threonine. Nat Struct Mol Biol. 2008;15(10):1109-18. Epub 2008/09/17. doi: 10.1038/nsmb.1486. PubMed PMID: 18794843; PMCID: PMC2575426.

110. Gorre ME, Mohammed M, Ellwood K, Hsu N, Paquette R, Rao PN, Sawyers CL. Clinical resistance to STI-571 cancer therapy caused by BCR-ABL gene mutation or amplification. Science. 2001;293(5531):876-80. Epub 2001/06/26. doi: 10.1126/science.1062538. PubMed PMID: 11423618.

111. Zhou T, Parillon L, Li F, Wang Y, Keats J, Lamore S, Xu Q, Shakespeare W, Dalgarno D, Zhu X. Crystal structure of the T315I mutant of AbI kinase. Chem Biol Drug Des. 2007;70(3):171-81. Epub 2007/08/28. doi: 10.1111/j.1747-0285.2007.00556.x. PubMed PMID: 17718712.

112. Hazarika M, Jiang X, Liu Q, Lee SL, Ramchandani R, Garnett C, Orr MS, Sridhara R, Booth B, Leighton JK, Timmer W, Harapanhalli R, Dagher R, Justice R, Pazdur R. Tasigna for chronic and accelerated phase Philadelphia chromosome--positive chronic myelogenous leukemia resistant to or intolerant of imatinib. Clin Cancer Res. 2008;14(17):5325-31. Epub 2008/09/04. doi: 10.1158/1078-0432.CCR-08-0308. PubMed PMID: 18765523.

113. Davies A, Jordanides NE, Giannoudis A, Lucas CM, Hatziieremia S, Harris RJ, Jorgensen HG, Holyoake TL, Pirmohamed M, Clark RE, Mountford JC. Nilotinib concentration in cell lines and primary CD34(+) chronic myeloid leukemia cells is not mediated by active uptake or efflux by major drug transporters. Leukemia. 2009;23(11):1999-2006. Epub 2009/08/28. doi: 10.1038/leu.2009.166. PubMed PMID: 19710702.

114. Brave M, Goodman V, Kaminskas E, Farrell A, Timmer W, Pope S, Harapanhalli R, Saber H, Morse D, Bullock J, Men A, Noory C, Ramchandani R, Kenna L, Booth B, Gobburu J, Jiang X, Sridhara R, Justice R, Pazdur R. Sprycel for chronic myeloid leukemia and Philadelphia chromosome-positive acute lymphoblastic leukemia resistant to or intolerant of imatinib mesylate. Clin Cancer Res. 2008;14(2):352-9. Epub 2008/01/29. doi: 10.1158/1078-0432.CCR-07-4175. PubMed PMID: 18223208.

115. Kantarjian HM, Shah NP, Cortes JE, Baccarani M, Agarwal MB, Undurraga MS, Wang J, Ipina JJ, Kim DW, Ogura M, Pavlovsky C, Junghanss C, Milone JH, Nicolini FE, Robak T, Van Droogenbroeck J, Vellenga E, Bradley-Garelik MB, Zhu C, Hochhaus A. Dasatinib or imatinib in newly diagnosed chronic-phase chronic myeloid leukemia: 2-

year follow-up from a randomized phase 3 trial (DASISION). Blood. 2012;119(5):1123-9. Epub 2011/12/14. doi: 10.1182/blood-2011-08-376087. PubMed PMID: 22160483; PMCID: PMC4916556.

116. Zhou T, Commodore L, Huang WS, Wang Y, Thomas M, Keats J, Xu Q, Rivera VM, Shakespeare WC, Clackson T, Dalgarno DC, Zhu X. Structural mechanism of the Pan-BCR-ABL inhibitor ponatinib (AP24534): lessons for overcoming kinase inhibitor resistance. Chem Biol Drug Des. 2011;77(1):1-11. Epub 2010/12/02. doi: 10.1111/j.1747-0285.2010.01054.x. PubMed PMID: 21118377.

117. Cortes JE, Kantarjian H, Shah NP, Bixby D, Mauro MJ, Flinn I, O'Hare T, Hu S, Narasimhan NI, Rivera VM, Clackson T, Turner CD, Haluska FG, Druker BJ, Deininger MW, Talpaz M. Ponatinib in refractory Philadelphia chromosome-positive leukemias. N Engl J Med. 2012;367(22):2075-88. Epub 2012/11/30. doi: 10.1056/NEJMoa1205127. PubMed PMID: 23190221; PMCID: PMC3777383.

118. Adrian FJ, Ding Q, Sim T, Velentza A, Sloan C, Liu Y, Zhang G, Hur W, Ding S, Manley P, Mestan J, Fabbro D, Gray NS. Allosteric inhibitors of Bcr-abl-dependent cell proliferation. Nat Chem Biol. 2006;2(2):95-102. Epub 2006/01/18. doi: 10.1038/nchembio760. PubMed PMID: 16415863.

119. Zhang J, Adrian FJ, Jahnke W, Cowan-Jacob SW, Li AG, Iacob RE, Sim T, Powers J, Dierks C, Sun F, Guo GR, Ding Q, Okram B, Choi Y, Wojciechowski A, Deng X, Liu G, Fendrich G, Strauss A, Vajpai N, Grzesiek S, Tuntland T, Liu Y, Bursulaya B, Azam M, Manley PW, Engen JR, Daley GQ, Warmuth M, Gray NS. Targeting Bcr-Abl by combining allosteric with ATP-binding-site inhibitors. Nature. 2010;463(7280):501-6. Epub 2010/01/15. doi: 10.1038/nature08675. PubMed PMID: 20072125; PMCID: PMC2901986.

120. Deng X, Okram B, Ding Q, Zhang J, Choi Y, Adrian FJ, Wojciechowski A, Zhang G, Che J, Bursulaya B, Cowan-Jacob SW, Rummel G, Sim T, Gray NS. Expanding the diversity of allosteric bcr-abl inhibitors. J Med Chem. 2010;53(19):6934-46. Epub 2010/09/11. doi: 10.1021/jm100555f. PubMed PMID: 20828158; PMCID: PMC2951064.

121. Schoepfer J, Jahnke W, Berellini G, Buonamici S, Cotesta S, Cowan-Jacob SW, Dodd S, Drueckes P, Fabbro D, Gabriel T, Groell JM, Grotzfeld RM, Hassan AQ, Henry C, Iyer V, Jones D, Lombardo F, Loo A, Manley PW, Pelle X, Rummel G, Salem B, Warmuth M, Wylie AA, Zoller T, Marzinzik AL, Furet P. Discovery of Asciminib (ABL001), an Allosteric Inhibitor of the Tyrosine Kinase Activity of BCR-ABL1. J Med

Chem. 2018;61(18):8120-35. Epub 2018/08/24. doi: 10.1021/acs.jmedchem.8b01040. PubMed PMID: 30137981.

122. Eide CA, Zabriskie MS, Savage Stevens SL, Antelope O, Vellore NA, Than H, Schultz AR, Clair P, Bowler AD, Pomicter AD, Yan D, Senina AV, Qiang W, Kelley TW, Szankasi P, Heinrich MC, Tyner JW, Rea D, Cayuela JM, Kim DW, Tognon CE, O'Hare T, Druker BJ, Deininger MW. Combining the Allosteric Inhibitor Asciminib with Ponatinib Suppresses Emergence of and Restores Efficacy against Highly Resistant BCR-ABL1 Mutants. Cancer Cell. 2019;36(4):431-43 e5. Epub 2019/09/24. doi: 10.1016/j.ccell.2019.08.004. PubMed PMID: 31543464; PMCID: PMC6893878.

123. Rea D, Mauro MJ, Boquimpani C, Minami Y, Lomaia E, Voloshin S, Turkina A, Kim DW, Apperley JF, Abdo A, Fogliatto LM, Kim DDH, le Coutre P, Saussele S, Annunziata M, Hughes TP, Chaudhri N, Sasaki K, Chee L, Garcia-Gutierrez V, Cortes JE, Aimone P, Allepuz A, Quenet S, Bedoucha V, Hochhaus A. A phase 3, open-label, randomized study of asciminib, a STAMP inhibitor, vs bosutinib in CML after 2 or more prior TKIs. Blood. 2021;138(21):2031-41. Epub 2021/08/19. doi: 10.1182/blood.2020009984. PubMed PMID: 34407542.

124. Wylie AA, Schoepfer J, Jahnke W, Cowan-Jacob SW, Loo A, Furet P, Marzinzik AL, Pelle X, Donovan J, Zhu W, Buonamici S, Hassan AQ, Lombardo F, Iyer V, Palmer M, Berellini G, Dodd S, Thohan S, Bitter H, Branford S, Ross DM, Hughes TP, Petruzzelli L, Vanasse KG, Warmuth M, Hofmann F, Keen NJ, Sellers WR. The allosteric inhibitor ABL001 enables dual targeting of BCR-ABL1. Nature. 2017;543(7647):733-7. Epub 2017/03/23. doi: 10.1038/nature21702. PubMed PMID: 28329763.

125. Schuette W. Treatment of brain metastases from lung cancer: chemotherapy. Lung Cancer. 2004;45 Suppl 2:S253-7. Epub 2004/11/24. doi: 10.1016/j.lungcan.2004.07.967. PubMed PMID: 15552807.

126. Stelzer KJ. Epidemiology and prognosis of brain metastases. Surg Neurol Int. 2013;4(Suppl 4):S192-202. Epub 2013/05/30. doi: 10.4103/2152-7806.111296. PubMed PMID: 23717790; PMCID: PMC3656565.

127. Fox BD, Cheung VJ, Patel AJ, Suki D, Rao G. Epidemiology of metastatic brain tumors. Neurosurg Clin N Am. 2011;22(1):1-6, v. Epub 2010/11/27. doi: 10.1016/j.nec.2010.08.007. PubMed PMID: 21109143.

128. Zeng Q, Michael IP, Zhang P, Saghafinia S, Knott G, Jiao W, McCabe BD, Galvan JA, Robinson HPC, Zlobec I, Ciriello G, Hanahan D. Synaptic proximity enables

NMDAR signalling to promote brain metastasis. Nature. 2019;573(7775):526-31. Epub 2019/09/20. doi: 10.1038/s41586-019-1576-6. PubMed PMID: 31534217; PMCID: PMC6837873.

129. Valiente M, Obenauf AC, Jin X, Chen Q, Zhang XH, Lee DJ, Chaft JE, Kris MG, Huse JT, Brogi E, Massague J. Serpins promote cancer cell survival and vascular co-option in brain metastasis. Cell. 2014;156(5):1002-16. Epub 2014/03/04. doi: 10.1016/j.cell.2014.01.040. PubMed PMID: 24581498; PMCID: PMC3988473.

130. Chen Q, Boire A, Jin X, Valiente M, Er EE, Lopez-Soto A, Jacob L, Patwa R, Shah H, Xu K, Cross JR, Massague J. Carcinoma-astrocyte gap junctions promote brain metastasis by cGAMP transfer. Nature. 2016;533(7604):493-8. Epub 2016/05/27. doi: 10.1038/nature18268. PubMed PMID: 27225120; PMCID: PMC5021195.

131. Er EE, Valiente M, Ganesh K, Zou Y, Agrawal S, Hu J, Griscom B, Rosenblum M, Boire A, Brogi E, Giancotti FG, Schachner M, Malladi S, Massague J. Pericyte-like spreading by disseminated cancer cells activates YAP and MRTF for metastatic colonization. Nat Cell Biol. 2018;20(8):966-78. Epub 2018/07/25. doi: 10.1038/s41556-018-0138-8. PubMed PMID: 30038252; PMCID: PMC6467203.

132. Shih DJH, Nayyar N, Bihun I, Dagogo-Jack I, Gill CM, Aquilanti E, Bertalan M, Kaplan A, D'Andrea MR, Chukwueke U, Ippen FM, Alvarez-Breckenridge C, Camarda ND, Lastrapes M, McCabe D, Kuter B, Kaufman B, Strickland MR, Martinez-Gutierrez JC, Nagabhushan D, De Sauvage M, White MD, Castro BA, Hoang K, Kaneb A, Batchelor ED, Paek SH, Park SH, Martinez-Lage M, Berghoff AS, Merrill P, Gerstner ER, Batchelor TT, Frosch MP, Frazier RP, Borger DR, Iafrate AJ, Johnson BE, Santagata S, Preusser M, Cahill DP, Carter SL, Brastianos PK. Genomic characterization of human brain metastases identifies drivers of metastatic lung adenocarcinoma. Nat Genet. 2020;52(4):371-7. Epub 2020/03/24. doi: 10.1038/s41588-020-0592-7. PubMed PMID: 32203465; PMCID: PMC7136154.

133. Fecci PE, Champion CD, Hoj J, McKernan CM, Goodwin CR, Kirkpatrick JP, Anders CK, Pendergast AM, Sampson JH. The Evolving Modern Management of Brain Metastasis. Clin Cancer Res. 2019;25(22):6570-80. Epub 2019/06/20. doi: 10.1158/1078-0432.CCR-18-1624. PubMed PMID: 31213459.

134. Anckar J, Sistonen L. Regulation of HSF1 function in the heat stress response: implications in aging and disease. Annu Rev Biochem. 2011;80:1089-115. Epub 2011/03/23. doi: 10.1146/annurev-biochem-060809-095203. PubMed PMID: 21417720.

135. Gomez-Pastor R, Burchfiel ET, Thiele DJ. Regulation of heat shock transcription factors and their roles in physiology and disease. Nat Rev Mol Cell Biol. 2018;19(1):4-19. Epub 2017/08/31. doi: 10.1038/nrm.2017.73. PubMed PMID: 28852220; PMCID: PMC5794010.

136. Neef DW, Jaeger AM, Gomez-Pastor R, Willmund F, Frydman J, Thiele DJ. A direct regulatory interaction between chaperonin TRiC and stress-responsive transcription factor HSF1. Cell Rep. 2014;9(3):955-66. Epub 2014/12/02. doi: 10.1016/j.celrep.2014.09.056. PubMed PMID: 25437552; PMCID: PMC4488849.

137. Shi Y, Mosser DD, Morimoto RI. Molecular chaperones as HSF1-specific transcriptional repressors. Genes Dev. 1998;12(5):654-66. Epub 1998/04/16. doi: 10.1101/gad.12.5.654. PubMed PMID: 9499401; PMCID: PMC316571.

138. Zou J, Guo Y, Guettouche T, Smith DF, Voellmy R. Repression of heat shock transcription factor HSF1 activation by HSP90 (HSP90 complex) that forms a stress-sensitive complex with HSF1. Cell. 1998;94(4):471-80. Epub 1998/09/04. doi: 10.1016/s0092-8674(00)81588-3. PubMed PMID: 9727490.

139. Akerfelt M, Morimoto RI, Sistonen L. Heat shock factors: integrators of cell stress, development and lifespan. Nat Rev Mol Cell Biol. 2010;11(8):545-55. Epub 2010/07/16. doi: 10.1038/nrm2938. PubMed PMID: 20628411; PMCID: PMC3402356.

140. Neudegger T, Verghese J, Hayer-Hartl M, Hartl FU, Bracher A. Structure of human heat-shock transcription factor 1 in complex with DNA. Nat Struct Mol Biol. 2016;23(2):140-6. Epub 2016/01/05. doi: 10.1038/nsmb.3149. PubMed PMID: 26727489.

141. Mercier PA, Winegarden NA, Westwood JT. Human heat shock factor 1 is predominantly a nuclear protein before and after heat stress. J Cell Sci. 1999;112 (Pt 16):2765-74. Epub 1999/07/22. PubMed PMID: 10413683.

142. Mendillo ML, Santagata S, Koeva M, Bell GW, Hu R, Tamimi RM, Fraenkel E, Ince TA, Whitesell L, Lindquist S. HSF1 drives a transcriptional program distinct from heat shock to support highly malignant human cancers. Cell. 2012;150(3):549-62. Epub 2012/08/07. doi: 10.1016/j.cell.2012.06.031. PubMed PMID: 22863008; PMCID: PMC3438889.

143. Kourtis N, Lazaris C, Hockemeyer K, Balandran JC, Jimenez AR, Mullenders J, Gong Y, Trimarchi T, Bhatt K, Hu H, Shrestha L, Ambesi-Impiombato A, Kelliher M, Paietta E, Chiosis G, Guzman ML, Ferrando AA, Tsirigos A, Aifantis I. Oncogenic

hijacking of the stress response machinery in T cell acute lymphoblastic leukemia. Nat Med. 2018;24(8):1157-66. Epub 2018/07/25. doi: 10.1038/s41591-018-0105-8. PubMed PMID: 30038221; PMCID: PMC6082694.

144. Dai C, Whitesell L, Rogers AB, Lindquist S. Heat shock factor 1 is a powerful multifaceted modifier of carcinogenesis. Cell. 2007;130(6):1005-18. Epub 2007/09/25. doi: 10.1016/j.cell.2007.07.020. PubMed PMID: 17889646; PMCID: PMC2586609.

145. Kourtis N, Moubarak RS, Aranda-Orgilles B, Lui K, Aydin IT, Trimarchi T, Darvishian F, Salvaggio C, Zhong J, Bhatt K, Chen EI, Celebi JT, Lazaris C, Tsirigos A, Osman I, Hernando E, Aifantis I. FBXW7 modulates cellular stress response and metastatic potential through HSF1 post-translational modification. Nat Cell Biol. 2015;17(3):322-32. Epub 2015/02/28. doi: 10.1038/ncb3121. PubMed PMID: 25720964; PMCID: PMC4401662.

146. Dai C, Santagata S, Tang Z, Shi J, Cao J, Kwon H, Bronson RT, Whitesell L, Lindquist S. Loss of tumor suppressor NF1 activates HSF1 to promote carcinogenesis. J Clin Invest. 2012;122(10):3742-54. Epub 2012/09/05. doi: 10.1172/JCI62727. PubMed PMID: 22945628; PMCID: PMC3461912.

147. Xi C, Hu Y, Buckhaults P, Moskophidis D, Mivechi NF. Heat shock factor Hsf1 cooperates with ErbB2 (Her2/Neu) protein to promote mammary tumorigenesis and metastasis. J Biol Chem. 2012;287(42):35646-57. Epub 2012/08/01. doi: 10.1074/jbc.M112.377481. PubMed PMID: 22847003; PMCID: PMC3471706.

148. Jin X, Moskophidis D, Mivechi NF. Heat shock transcription factor 1 is a key determinant of HCC development by regulating hepatic steatosis and metabolic syndrome. Cell Metab. 2011;14(1):91-103. Epub 2011/07/05. doi: 10.1016/j.cmet.2011.03.025. PubMed PMID: 21723507; PMCID: PMC3214631.

149. Su KH, Dai S, Tang Z, Xu M, Dai C. Heat Shock Factor 1 Is a Direct Antagonist of AMP-Activated Protein Kinase. Mol Cell. 2019;76(4):546-61 e8. Epub 2019/09/29. doi: 10.1016/j.molcel.2019.08.021. PubMed PMID: 31561952.

150. Li J, Chauve L, Phelps G, Brielmann RM, Morimoto RI. E2F coregulates an essential HSF developmental program that is distinct from the heat-shock response. Genes Dev. 2016;30(18):2062-75. Epub 2016/11/01. doi: 10.1101/gad.283317.116. PubMed PMID: 27688402; PMCID: PMC5066613.

151. Kienast Y, von Baumgarten L, Fuhrmann M, Klinkert WE, Goldbrunner R, Herms J, Winkler F. Real-time imaging reveals the single steps of brain metastasis formation. Nat Med. 2010;16(1):116-22. Epub 2009/12/22. doi: 10.1038/nm.2072. PubMed PMID: 20023634.

152. Subramanian A, Tamayo P, Mootha VK, Mukherjee S, Ebert BL, Gillette MA, Paulovich A, Pomeroy SL, Golub TR, Lander ES, Mesirov JP. Gene set enrichment analysis: a knowledge-based approach for interpreting genome-wide expression profiles. Proc Natl Acad Sci U S A. 2005;102(43):15545-50. Epub 2005/10/04. doi: 10.1073/pnas.0506580102. PubMed PMID: 16199517; PMCID: PMC1239896.

153. Morgunova E, Yin Y, Jolma A, Dave K, Schmierer B, Popov A, Eremina N, Nilsson L, Taipale J. Structural insights into the DNA-binding specificity of E2F family transcription factors. Nat Commun. 2015;6:10050. Epub 2015/12/04. doi: 10.1038/ncomms10050. PubMed PMID: 26632596; PMCID: PMC4686757.

154. Gkourtsa A, van den Burg J, Avula T, Hochstenbach F, Distel B. Binding of a proline-independent hydrophobic motif by the Candida albicans Rvs167-3 SH3 domain. Microbiol Res. 2016;190:27-36. Epub 2016/07/10. doi: 10.1016/j.micres.2016.04.018. PubMed PMID: 27393996.

155. Skora L, Mestan J, Fabbro D, Jahnke W, Grzesiek S. NMR reveals the allosteric opening and closing of Abelson tyrosine kinase by ATP-site and myristoyl pocket inhibitors. Proc Natl Acad Sci U S A. 2013;110(47):E4437-45. Epub 2013/11/06. doi: 10.1073/pnas.1314712110. PubMed PMID: 24191057; PMCID: PMC3839726.

156. Li D, Yallowitz A, Ozog L, Marchenko N. A gain-of-function mutant p53-HSF1 feed forward circuit governs adaptation of cancer cells to proteotoxic stress. Cell Death Dis. 2014;5:e1194. Epub 2014/04/26. doi: 10.1038/cddis.2014.158. PubMed PMID: 24763051; PMCID: PMC4001312.

157. Meng L, Gabai VL, Sherman MY. Heat-shock transcription factor HSF1 has a critical role in human epidermal growth factor receptor-2-induced cellular transformation and tumorigenesis. Oncogene. 2010;29(37):5204-13. Epub 2010/07/14. doi: 10.1038/onc.2010.277. PubMed PMID: 20622894; PMCID: PMC2940982.

158. Birchenall-Roberts MC, Yoo YD, Bertolette DC, 3rd, Lee KH, Turley JM, Bang OS, Ruscetti FW, Kim SJ. The p120-v-Abl protein interacts with E2F-1 and regulates E2F-1 transcriptional activity. J Biol Chem. 1997;272(14):8905-11. Epub 1997/04/04. doi: 10.1074/jbc.272.14.8905. PubMed PMID: 9083010.

159. Wong KK, Zou X, Merrell KT, Patel AJ, Marcu KB, Chellappan S, Calame K. v-Abl activates c-myc transcription through the E2F site. Mol Cell Biol. 1995;15(12):6535-44. Epub 1995/12/01. doi: 10.1128/mcb.15.12.6535. PubMed PMID: 8524218; PMCID: PMC230906.

160. Parada Y, Banerji L, Glassford J, Lea NC, Collado M, Rivas C, Lewis JL, Gordon MY, Thomas NS, Lam EW. BCR-ABL and interleukin 3 promote haematopoietic cell proliferation and survival through modulation of cyclin D2 and p27Kip1 expression. J Biol Chem. 2001;276(26):23572-80. Epub 2001/04/27. doi: 10.1074/jbc.M101885200. PubMed PMID: 11323429.

161. Kaelin WG, Jr., Ratcliffe PJ. Oxygen sensing by metazoans: the central role of the HIF hydroxylase pathway. Mol Cell. 2008;30(4):393-402. Epub 2008/05/24. doi: 10.1016/j.molcel.2008.04.009. PubMed PMID: 18498744.

162. Kaelin WG, Jr. The von Hippel-Lindau tumour suppressor protein: O2 sensing and cancer. Nat Rev Cancer. 2008;8(11):865-73. Epub 2008/10/17. doi: 10.1038/nrc2502. PubMed PMID: 18923434.

163. Ivan M, Kondo K, Yang H, Kim W, Valiando J, Ohh M, Salic A, Asara JM, Lane WS, Kaelin WG, Jr. HIFalpha targeted for VHL-mediated destruction by proline hydroxylation: implications for O2 sensing. Science. 2001;292(5516):464-8. Epub 2001/04/09. doi: 10.1126/science.1059817. PubMed PMID: 11292862.

164. Jaakkola P, Mole DR, Tian YM, Wilson MI, Gielbert J, Gaskell SJ, von Kriegsheim A, Hebestreit HF, Mukherji M, Schofield CJ, Maxwell PH, Pugh CW, Ratcliffe PJ. Targeting of HIF-alpha to the von Hippel-Lindau ubiquitylation complex by O2-regulated prolyl hydroxylation. Science. 2001;292(5516):468-72. Epub 2001/04/09. doi: 10.1126/science.1059796. PubMed PMID: 11292861.

165. Masson N, Willam C, Maxwell PH, Pugh CW, Ratcliffe PJ. Independent function of two destruction domains in hypoxia-inducible factor-alpha chains activated by prolyl hydroxylation. EMBO J. 2001;20(18):5197-206. Epub 2001/09/22. doi: 10.1093/emboj/20.18.5197. PubMed PMID: 11566883; PMCID: PMC125617.

166. Lopez-Barneo J, Simon MC. Cellular adaptation to oxygen deficiency beyond the Nobel award. Nat Commun. 2020;11(1):607. Epub 2020/02/01. doi: 10.1038/s41467-020-14469-9. PubMed PMID: 32001698; PMCID: PMC6992614.

167. Lee P, Chandel NS, Simon MC. Cellular adaptation to hypoxia through hypoxia inducible factors and beyond. Nat Rev Mol Cell Biol. 2020;21(5):268-83. Epub 2020/03/08. doi: 10.1038/s41580-020-0227-y. PubMed PMID: 32144406; PMCID: PMC7222024.

168. Iommarini L, Porcelli AM, Gasparre G, Kurelac I. Non-Canonical Mechanisms Regulating Hypoxia-Inducible Factor 1 Alpha in Cancer. Front Oncol. 2017;7:286. Epub 2017/12/13. doi: 10.3389/fonc.2017.00286. PubMed PMID: 29230384; PMCID: PMC5711814.

169. Kharbanda S, Ren R, Pandey P, Shafman TD, Feller SM, Weichselbaum RR, Kufe DW. Activation of the c-Abl tyrosine kinase in the stress response to DNA-damaging agents. Nature. 1995;376(6543):785-8. Epub 1995/08/31. doi: 10.1038/376785a0. PubMed PMID: 7651539.

170. Sun X, Majumder P, Shioya H, Wu F, Kumar S, Weichselbaum R, Kharbanda S, Kufe D. Activation of the cytoplasmic c-Abl tyrosine kinase by reactive oxygen species. J Biol Chem. 2000;275(23):17237-40. Epub 2000/04/20. doi: 10.1074/jbc.C000099200. PubMed PMID: 10770918.

171. Hoj JP, Mayro B, Pendergast AM. The ABL2 kinase regulates an HSF1-dependent transcriptional program required for lung adenocarcinoma brain metastasis. Proc Natl Acad Sci U S A. 2020;117(52):33486-95. Epub 2020/12/16. doi: 10.1073/pnas.2007991117. PubMed PMID: 33318173.

172. Matsumoto Y, La Rose J, Kent OA, Wagner MJ, Narimatsu M, Levy AD, Omar MH, Tong J, Krieger JR, Riggs E, Storozhuk Y, Pasquale J, Ventura M, Yeganeh B, Post M, Moran MF, Grynpas MD, Wrana JL, Superti-Furga G, Koleske AJ, Pendergast AM, Rottapel R. Reciprocal stabilization of ABL and TAZ regulates osteoblastogenesis through transcription factor RUNX2. J Clin Invest. 2016;126(12):4482-96. Epub 2016/11/01. doi: 10.1172/JCI87802. PubMed PMID: 27797343; PMCID: PMC5127668.

173. Cavadas MA, Mesnieres M, Crifo B, Manresa MC, Selfridge AC, Scholz CC, Cummins EP, Cheong A, Taylor CT. REST mediates resolution of HIF-dependent gene expression in prolonged hypoxia. Sci Rep. 2015;5:17851. Epub 2015/12/10. doi: 10.1038/srep17851. PubMed PMID: 26647819; PMCID: PMC4673454.

174. Chen Z, Sui J, Zhang F, Zhang C. Cullin family proteins and tumorigenesis: genetic association and molecular mechanisms. J Cancer. 2015;6(3):233-42. Epub 2015/02/11. doi: 10.7150/jca.11076. PubMed PMID: 25663940; PMCID: PMC4317758.

175. Bienroth S, Wahle E, Suter-Crazzolara C, Keller W. Purification of the cleavage and polyadenylation factor involved in the 3'-processing of messenger RNA precursors. J Biol Chem. 1991;266(29):19768-76. Epub 1991/10/15. PubMed PMID: 1918081.

176. Mandel CR, Bai Y, Tong L. Protein factors in pre-mRNA 3'-end processing. Cell Mol Life Sci. 2008;65(7-8):1099-122. Epub 2007/12/26. doi: 10.1007/s00018-007-7474-3. PubMed PMID: 18158581; PMCID: PMC2742908.

177. Sun Y, Zhang Y, Hamilton K, Manley JL, Shi Y, Walz T, Tong L. Molecular basis for the recognition of the human AAUAAA polyadenylation signal. Proc Natl Acad Sci U S A. 2018;115(7):E1419-E28. Epub 2017/12/07. doi: 10.1073/pnas.1718723115. PubMed PMID: 29208711; PMCID: PMC5816196.

178. Menon S, Tsuge T, Dohmae N, Takio K, Wei N. Association of SAP130/SF3b-3 with Cullin-RING ubiquitin ligase complexes and its regulation by the COP9 signalosome. BMC Biochem. 2008;9:1. Epub 2008/01/05. doi: 10.1186/1471-2091-9-1. PubMed PMID: 18173839; PMCID: PMC2265268.

179. Oughtred R, Rust J, Chang C, Breitkreutz BJ, Stark C, Willems A, Boucher L, Leung G, Kolas N, Zhang F, Dolma S, Coulombe-Huntington J, Chatr-Aryamontri A, Dolinski K, Tyers M. The BioGRID database: A comprehensive biomedical resource of curated protein, genetic, and chemical interactions. Protein Sci. 2021;30(1):187-200. Epub 2020/10/19. doi: 10.1002/pro.3978. PubMed PMID: 33070389; PMCID: PMC7737760.

180. Perez-Perri JI, Dengler VL, Audetat KA, Pandey A, Bonner EA, Urh M, Mendez J, Daniels DL, Wappner P, Galbraith MD, Espinosa JM. The TIP60 Complex Is a Conserved Coactivator of HIF1A. Cell Rep. 2016;16(1):37-47. Epub 2016/06/21. doi: 10.1016/j.celrep.2016.05.082. PubMed PMID: 27320910; PMCID: PMC4957981.

181. Jackson S, Xiong Y. CRL4s: the CUL4-RING E3 ubiquitin ligases. Trends Biochem Sci. 2009;34(11):562-70. Epub 2009/10/13. doi: 10.1016/j.tibs.2009.07.002. PubMed PMID: 19818632; PMCID: PMC2783741.

182. Heidelberger JB, Voigt A, Borisova ME, Petrosino G, Ruf S, Wagner SA, Beli P. Proteomic profiling of VCP substrates links VCP to K6-linked ubiquitylation and c-Myc function. EMBO Rep. 2018;19(4). Epub 2018/02/23. doi: 10.15252/embr.201744754. PubMed PMID: 29467282; PMCID: PMC5891417.

183. Baluapuri A, Wolf E, Eilers M. Target gene-independent functions of MYC oncoproteins. Nat Rev Mol Cell Biol. 2020;21(5):255-67. Epub 2020/02/20. doi: 10.1038/s41580-020-0215-2. PubMed PMID: 32071436; PMCID: PMC7611238.

184. Kim Y, Nam HJ, Lee J, Park DY, Kim C, Yu YS, Kim D, Park SW, Bhin J, Hwang D, Lee H, Koh GY, Baek SH. Methylation-dependent regulation of HIF-1alpha stability restricts retinal and tumour angiogenesis. Nat Commun. 2016;7:10347. Epub 2016/01/14. doi: 10.1038/ncomms10347. PubMed PMID: 26757928; PMCID: PMC4735525.

185. Mohapatra B, Ahmad G, Nadeau S, Zutshi N, An W, Scheffe S, Dong L, Feng D, Goetz B, Arya P, Bailey TA, Palermo N, Borgstahl GE, Natarajan A, Raja SM, Naramura M, Band V, Band H. Protein tyrosine kinase regulation by ubiquitination: critical roles of Cbl-family ubiquitin ligases. Biochim Biophys Acta. 2013;1833(1):122-39. Epub 2012/10/23. doi: 10.1016/j.bbamcr.2012.10.010. PubMed PMID: 23085373; PMCID: PMC3628764.

186. Nguyen LK, Kolch W, Kholodenko BN. When ubiquitination meets phosphorylation: a systems biology perspective of EGFR/MAPK signalling. Cell Commun Signal. 2013;11:52. Epub 2013/08/02. doi: 10.1186/1478-811X-11-52. PubMed PMID: 23902637; PMCID: PMC3734146.

187. Hunter T. The age of crosstalk: phosphorylation, ubiquitination, and beyond. Mol Cell. 2007;28(5):730-8. Epub 2007/12/18. doi: 10.1016/j.molcel.2007.11.019. PubMed PMID: 18082598.

188. Chen Y, Shao X, Cao J, Zhu H, Yang B, He Q, Ying M. Phosphorylation regulates cullin-based ubiquitination in tumorigenesis. Acta Pharm Sin B. 2021;11(2):309-21. Epub 2021/03/02. doi: 10.1016/j.apsb.2020.09.007. PubMed PMID: 33643814; PMCID: PMC7893081.

189. Tanos B, Pendergast AM. Abl tyrosine kinase regulates endocytosis of the epidermal growth factor receptor. J Biol Chem. 2006;281(43):32714-23. Epub 2006/09/01. doi: 10.1074/jbc.M603126200. PubMed PMID: 16943190.

190. Chen A, Koehler AN. Transcription Factor Inhibition: Lessons Learned and Emerging Targets. Trends Mol Med. 2020;26(5):508-18. Epub 2020/05/04. doi: 10.1016/j.molmed.2020.01.004. PubMed PMID: 32359481; PMCID: PMC7198608.

191. Luttman JH, Hoj JP, Lin KH, Lin J, Gu JJ, Rouse C, Nichols AG, MacIver NJ, Wood KC, Pendergast AM. ABL allosteric inhibitors synergize with statins to enhance

apoptosis of metastatic lung cancer cells. Cell Rep. 2021;37(4):109880. Epub 2021/10/28. doi: 10.1016/j.celrep.2021.109880. PubMed PMID: 34706244; PMCID: PMC8579324.

192. Dong B, Jaeger AM, Hughes PF, Loiselle DR, Hauck JS, Fu Y, Haystead TA, Huang J, Thiele DJ. Targeting therapy-resistant prostate cancer via a direct inhibitor of the human heat shock transcription factor 1. Sci Transl Med. 2020;12(574). Epub 2020/12/18. doi: 10.1126/scitranslmed.abb5647. PubMed PMID: 33328331.

193. Skinner MK, Rawls A, Wilson-Rawls J, Roalson EH. Basic helix-loop-helix transcription factor gene family phylogenetics and nomenclature. Differentiation. 2010;80(1):1-8. Epub 2010/03/12. doi: 10.1016/j.diff.2010.02.003. PubMed PMID: 20219281; PMCID: PMC2894270.

194. Hoefflin R, Harlander S, Schafer S, Metzger P, Kuo F, Schonenberger D, Adlesic M, Peighambari A, Seidel P, Chen CY, Consenza-Contreras M, Jud A, Lahrmann B, Grabe N, Heide D, Uhl FM, Chan TA, Duyster J, Zeiser R, Schell C, Heikenwalder M, Schilling O, Hakimi AA, Boerries M, Frew IJ. HIF-1alpha and HIF-2alpha differently regulate tumour development and inflammation of clear cell renal cell carcinoma in mice. Nat Commun. 2020;11(1):4111. Epub 2020/08/19. doi: 10.1038/s41467-020-17873-3. PubMed PMID: 32807776; PMCID: PMC7431415.

195. Panea RI, Love CL, Shingleton JR, Reddy A, Bailey JA, Moormann AM, Otieno JA, Ong'echa JM, Oduor CI, Schroeder KMS, Masalu N, Chao NJ, Agajanian M, Major MB, Fedoriw Y, Richards KL, Rymkiewicz G, Miles RR, Alobeid B, Bhagat G, Flowers CR, Ondrejka SL, Hsi ED, Choi WWL, Au-Yeung RKH, Hartmann W, Lenz G, Meyerson H, Lin YY, Zhuang Y, Luftig MA, Waldrop A, Dave T, Thakkar D, Sahay H, Li G, Palus BC, Seshadri V, Kim SY, Gascoyne RD, Levy S, Mukhopadyay M, Dunson DB, Dave SS. The whole-genome landscape of Burkitt lymphoma subtypes. Blood. 2019;134(19):1598-607. Epub 2019/09/29. doi: 10.1182/blood.2019001880. PubMed PMID: 31558468; PMCID: PMC6871305.

196. Gao J, Aksoy BA, Dogrusoz U, Dresdner G, Gross B, Sumer SO, Sun Y, Jacobsen A, Sinha R, Larsson E, Cerami E, Sander C, Schultz N. Integrative analysis of complex cancer genomics and clinical profiles using the cBioPortal. Sci Signal. 2013;6(269):pl1. Epub 2013/04/04. doi: 10.1126/scisignal.2004088. PubMed PMID: 23550210; PMCID: PMC4160307.

197. Tsherniak A, Vazquez F, Montgomery PG, Weir BA, Kryukov G, Cowley GS, Gill S, Harrington WF, Pantel S, Krill-Burger JM, Meyers RM, Ali L, Goodale A, Lee Y, Jiang G, Hsiao J, Gerath WFJ, Howell S, Merkel E, Ghandi M, Garraway LA, Root DE, Golub

TR, Boehm JS, Hahn WC. Defining a Cancer Dependency Map. Cell. 2017;170(3):564-76 e16. Epub 2017/07/29. doi: 10.1016/j.cell.2017.06.010. PubMed PMID: 28753430; PMCID: PMC5667678.

198. Gluck AA, Aebersold DM, Zimmer Y, Medova M. Interplay between receptor tyrosine kinases and hypoxia signaling in cancer. Int J Biochem Cell Biol. 2015;62:101-14. Epub 2015/03/10. doi: 10.1016/j.biocel.2015.02.018. PubMed PMID: 25747905.

199. Rankin EB, Nam JM, Giaccia AJ. Hypoxia: Signaling the Metastatic Cascade. Trends Cancer. 2016;2(6):295-304. Epub 2017/07/26. doi: 10.1016/j.trecan.2016.05.006. PubMed PMID: 28741527; PMCID: PMC5808868.

200. Heun Y, Grundler Groterhorst K, Pogoda K, Kraemer BF, Pfeifer A, Pohl U, Mannell H. The Phosphatase SHP-2 Activates HIF-1alpha in Wounds In Vivo by Inhibition of 26S Proteasome Activity. Int J Mol Sci. 2019;20(18). Epub 2019/09/11. doi: 10.3390/ijms20184404. PubMed PMID: 31500245; PMCID: PMC6769879.

201. Chandel S, Manikandan A, Mehta N, Nathan AA, Tiwari RK, Mohapatra SB, Chandran M, Jaleel A, Manoj N, Dixit M. The protein tyrosine phosphatase PTP-PEST mediates hypoxia-induced endothelial autophagy and angiogenesis via AMPK activation. J Cell Sci. 2021;134(1). Epub 2020/12/17. doi: 10.1242/jcs.250274. PubMed PMID: 33323505.

202. Wang V, Davis DA, Veeranna RP, Haque M, Yarchoan R. Characterization of the activation of protein tyrosine phosphatase, receptor-type, Z polypeptide 1 (PTPRZ1) by hypoxia inducible factor-2 alpha. PLoS One. 2010;5(3):e9641. Epub 2010/03/13. doi: 10.1371/journal.pone.0009641. PubMed PMID: 20224786; PMCID: PMC2835759.

203. Maulik D, Ashraf QM, Mishra OP, Delivoria-Papadopoulos M. Effect of hypoxia on protein tyrosine phosphatase activity and expression of protein tyrosine phosphatases PTP-1B, PTP-SH1 and PTP-SH2 in the cerebral cortex of guinea pig fetus. Neurosci Lett. 2008;432(3):174-8. Epub 2008/02/06. doi: 10.1016/j.neulet.2007.11.043. PubMed PMID: 18249495.

204. Shalem O, Sanjana NE, Hartenian E, Shi X, Scott DA, Mikkelson T, Heckl D, Ebert BL, Root DE, Doench JG, Zhang F. Genome-scale CRISPR-Cas9 knockout screening in human cells. Science. 2014;343(6166):84-7. Epub 2013/12/18. doi: 10.1126/science.1247005. PubMed PMID: 24336571; PMCID: PMC4089965.

205. Lin KH, Rutter JC, Xie A, Pardieu B, Winn ET, Bello RD, Forget A, Itzykson R, Ahn YR, Dai Z, Sobhan RT, Anderson GR, Singleton KR, Decker AE, Winter PS, Locasale JW, Crawford L, Puissant A, Wood KC. Using antagonistic pleiotropy to design a chemotherapy-induced evolutionary trap to target drug resistance in cancer. Nat Genet. 2020;52(4):408-17. Epub 2020/03/24. doi: 10.1038/s41588-020-0590-9. PubMed PMID: 32203462; PMCID: PMC7398704.

206. Kim D, Paggi JM, Park C, Bennett C, Salzberg SL. Graph-based genome alignment and genotyping with HISAT2 and HISAT-genotype. Nat Biotechnol. 2019;37(8):907-15. Epub 2019/08/04. doi: 10.1038/s41587-019-0201-4. PubMed PMID: 31375807; PMCID: PMC7605509.

207. Liao Y, Smyth GK, Shi W. featureCounts: an efficient general purpose program for assigning sequence reads to genomic features. Bioinformatics. 2014;30(7):923-30. Epub 2013/11/15. doi: 10.1093/bioinformatics/btt656. PubMed PMID: 24227677.

208. Love MI, Huber W, Anders S. Moderated estimation of fold change and dispersion for RNA-seq data with DESeq2. Genome Biol. 2014;15(12):550. Epub 2014/12/18. doi: 10.1186/s13059-014-0550-8. PubMed PMID: 25516281; PMCID: PMC4302049.

209. Gyorffy B, Surowiak P, Budczies J, Lanczky A. Online survival analysis software to assess the prognostic value of biomarkers using transcriptomic data in non-small-cell lung cancer. PLoS One. 2013;8(12):e82241. Epub 2013/12/25. doi: 10.1371/journal.pone.0082241. PubMed PMID: 24367507; PMCID: PMC3867325.

210. Schneider CA, Rasband WS, Eliceiri KW. NIH Image to ImageJ: 25 years of image analysis. Nat Methods. 2012;9(7):671-5. Epub 2012/08/30. doi: 10.1038/nmeth.2089. PubMed PMID: 22930834; PMCID: PMC5554542.

Biography

Benjamin Jacob Mayro graduated *summa cum laude* from Seton Hill University in 2017 with a Bachelor of Science degree in Biochemistry with honors. As an undergraduate student at Seton Hill University, Benjamin conducted research with Dr. Jonathan Moerdyk focusing on the development of an electronically diverse and persistent indole-based Alkylaminocarbene. Further, Benjamin conducted research with Dr. Gary Thomas in the Department of Microbiology & Molecular Genetics at the University of Pittsburgh. Here, Benjamin investigated the role of the multifunctional sorting protein PACS-2 in the modulation of the Warburg effect. Benjamin began his graduate training at Duke University in August 2017 and joined the laboratory of Dr. Ann Marie Pendergast in February 2018. His graduate research focused on characterizing transcriptional networks regulated by the ABL tyrosine kinases.

Education

Duke University, PhD in Molecular Cancer Biology

Advisor: Ann Marie Pendergast

Seton Hill University, BS in Biochemistry with honors

Research Fellowships and Grants

The NCI Predoctoral to Postdoctoral Fellow Transition Award F99/K00 (F99CA264162)

NIH F31 Fellowship (F31CA243293-01A1)

Duke Proteomics and Metabolomics Grant Recipient

Academic Awards

Duke Chancellor's Scholarship

Fitzgerald Academic Achievement Award

Fitzgerald Scholars Award

The Robert and Barbara Bell Basic Science Cancer Research Award

FASEB's Protein Kinases and Protein Phosphorylation Conference Travel Award

Publications

Hoj, Jacob P; Mayro, Benjamin; Pendergast, Ann Marie. (2019). A TAZ-AXL-ABL2 feed-forward signaling axis promotes lung adenocarcinoma brain metastasis. *Cell Reports* 29, 3421-3434 e3428 (2019). PMID: 31825826 PMCID: PMC7254883

Hoj, Jacob P*; Mayro, Benjamin*; Pendergast, Ann Marie (2020). The ABL2 kinase regulates an HSF1-dependent transcriptional program required for lung adenocarcinoma brain metastasis. *Proc. Natl. Acad. Sci.,* 117 (52) 33486-33495. *- These authors contributed equally. PMID: 33318173 PMCID: PMC7777191

Luttman, Jillian; Colemon, Ashley; Mayro, Benjamin; Pendergast, Ann Marie. (2021). Role of the ABL tyrosine kinases in the epithelial–mesenchymal transition and the metastatic cascade. Cell Communication and Signaling, 19(1). PMID: 34022881 PMCID: PMC8140471

McKernan, Courtney M; Khatri, Aaditya; Child, Jessica; Chen, Qiang; Hannigan, Molly; Mayro, Benjamin; Synder, David; Nicchitta, Christopher V; Pendergast, Ann Marie (2022). ABL Kinases Regulate Translation in HER2+ Cells through Y-Box-Binding Protein 1 to Facilitate Colonization of the Brain. *Cell Reports* 40(9):111268. PMID: 36044842 PMCID: PMC9472557

Mayro, Benjamin; Hoj, Jacob P; Cerda-Smith, Christian G; Hutchinson, Haley M, Winter, Peter S; Wardell, Suzanne E; McDonnell, Donald P; Wu, Colleen; Wood, Kris C; Pendergast, Ann Marie. ABL kinases regulate the stabilization of HIF-1α and MYC through CPSF1 *Proc. Natl. Acad. Sci.,* Under Revision.